

INFORMATION TO USERS

This manuscript has been reproduced from the microfilm master. UMI films the text directly from the original or copy submitted. Thus, some thesis and dissertation copies are in typewriter face, while others may be from any type of computer printer.

The quality of this reproduction is dependent upon the quality of the copy submitted. Broken or indistinct print, colored or poor quality illustrations and photographs, print bleedthrough, substandard margins, and improper alignment can adversely affect reproduction.

In the unlikely event that the author did not send UMI a complete manuscript and there are missing pages, these will be noted. Also, if unauthorized copyright material had to be removed, a note will indicate the deletion.

Oversize materials (e.g., maps, drawings, charts) are reproduced by sectioning the original, beginning at the upper left-hand corner and continuing from left to right in equal sections with small overlaps. Each original is also photographed in one exposure and is included in reduced form at the back of the book.

Photographs included in the original manuscript have been reproduced xerographically in this copy. Higher quality 6" x 9" black and white photographic prints are available for any photographs or illustrations appearing in this copy for an additional charge. Contact UMI directly to order.

UMI

A Bell & Howell Information Company
300 North Zeeb Road, Ann Arbor MI 48106-1346 USA
313/761-4700 800/521-0600

**KINETICS AND MECHANISMS OF LEAD
SORPTION AND DESORPTION
ON SOILS AND SOIL MATERIALS**

by

Daniel G. Strawn

A dissertation submitted to the Faculty of the University of Delaware in
partial fulfillment of the requirements for the degree of Doctor of Philosophy in Plant and
Soil Sciences.

Fall 1998

© 1998 Daniel G. Strawn
All Rights Reserved

UMI Number: 9918894

UMI Microform 9918894
Copyright 1999, by UMI Company. All rights reserved.

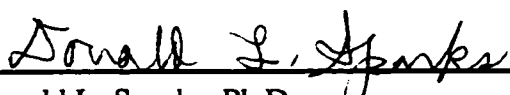
**This microform edition is protected against unauthorized
copying under Title 17, United States Code.**


UMI
300 North Zeeb Road
Ann Arbor, MI 48103

**KINETICS AND MECHANISMS OF LEAD
SORPTION AND DESORPTION
ON SOILS AND SOIL MATERIALS**

by

Daniel G. Strawn

Approved: 
Donald L. Sparks, Ph.D.
Chair of the Department of Plant and Soil Sciences

Approved: 
John C. Nye, Ph.D.
Dean of the College of Agricultural Sciences

Approved: 
John C. Cavanaugh, Ph.D.
Vice Provost for Academic Programs and Planning

I certify that I have read this dissertation and that in my opinion it meets the academic and professional standard required by the University as a dissertation for the degree of Doctor of Philosophy.

Signed: Donald L. Sparks
Donald L. Sparks, Ph.D.
Professor in charge of dissertation

I certify that I have read this dissertation and that in my opinion it meets the academic and professional standard required by the University as a dissertation for the degree of Doctor of Philosophy.

Signed: Yan Jin
Yan Jin, Ph.D.
Member of dissertation committee

I certify that I have read this dissertation and that in my opinion it meets the academic and professional standard required by the University as a dissertation for the degree of Doctor of Philosophy.

Signed: George W. Luther, III
George W. Luther, III, Ph.D.
Member of dissertation committee

I certify that I have read this dissertation and that in my opinion it meets the academic and professional standard required by the University as a dissertation for the degree of Doctor of Philosophy.

Signed: William R. Berti
William R. Berti, Ph.D.
Member of dissertation committee

ACKNOWLEDGMENTS

Donald L. Sparks, Ph.D., who has generously provided support and guidance throughout my graduate education.

Jerry Hendricks, for his assistance with all the details of conducting research.

Kathy Olson for help in analyzing ICP and soil samples.

Boyan Boyanoff for teaching me how to collect and analyze XAFS data.

John Pesek for help analyzing the stirred-flow data.

Members of my Ph.D. Advisory Committee for advice, ideas, and help in understanding my research.

Members of the University of Delaware soil chemistry research group for their help in all aspects of my graduate education, especially proofreading manuscripts, providing critical input on my research, and their friendship.

My family for their support and encouragement throughout my education.

DEDICATION

Kelly A. Strawn, Daniel D Strawn, and Sandra L. Strawn

TABLE OF CONTENTS

LIST OF TABLES	ix
LIST OF FIGURES	xi
ABSTRACT	xv
CHAPTER	
1 Introduction	1
1.1 Rationale and Scope of Research	1
1.2 Literature Review: Kinetics and Mechanisms of Sorption	7
1.2.1 Diffusion-controlled Kinetic Reactions	7
1.2.2 Kinetics and Mechanisms of Adsorption Processes	10
1.2.3 Kinetics and Mechanisms of Surface Precipitation	19
1.2.4 Sorption Mechanisms Conclusion	29
1.3 Literature Review of the Chemistry of Pb in the Environment	30
1.4 Research Justification	36
1.5 Research Objectives	38
1.6 Determining Sorption Mechanisms on Surfaces	38
1.7 Literature Cited	43
2 Kinetics and Mechanisms of Pb(II) Sorption and Desorption at the Aluminum Oxide-Water Interface	49
2.1 Abstract	49
2.2 Introduction	50
2.3 Experimental Methods	53
2.3.1 Materials.	53
2.3.2 Sorption Kinetics Experiments.	54
2.3.3 Desorption Experiments.	55
2.3.4 XAFS Analysis.	56
2.4 Results and Discussion	59

2.4.1	Lead XAFS.	59
2.4.2	Adsorption Kinetics.	65
2.4.3	Desorption Experiments.	69
2.5	Conclusion	74
2.6	Literature Cited	74
3	The Use of XAFS to Distinguish Between Inner- and Outer-Sphere Lead Adsorption Complexes on Montmorillonite	80
3.1	Abstract	80
3.2	Introduction	81
3.3	Theory	85
3.4	Experimental Methods	89
3.4.1	Materials	89
3.4.2	Adsorption Experiments.	90
3.4.3	Synchrotron XAFS Analysis	93
3.5	Results and Discussion	99
3.5.1	Adsorption Experiments	99
3.5.2	XANES Analysis.	103
3.5.3	EXAFS Analysis	108
3.6	Summary	123
3.7	Literature Cited	124
4	Effects of Soil Organic Matter on the Kinetics and Mechanisms of Pb(II) Sorption and Desorption in Soil	130
4.1	Abstract	130
4.2	Introduction	131
4.3	Methods and Materials	135
4.3.1	Batch Experiments	138
4.3.2	Stirred-flow Experiments	139
4.3.4	Data Analysis	143
4.3.5	XAFS Experiments	145
4.4	Results and Discussion	146
4.4.1	Batch Experiments	146
4.4.2	Stirred-Flow Experiments	150
4.4.3	XAFS Experiments	169

4.5	Summary	178
4.6	References	179
5	Conclusions	184
5.1	Summary of Research	184
5.2	Future Research	187
 APPENDICES		
A	Supplementary Material for Chapter 2	189
B	Supplementary Material for Chapter 3	195
C	Supplementary Material for Chapter 4	200

LIST OF TABLES

Table 2.1	Structural parameters for Pb adsorption on γ -Al ₂ O ₃ samples reacted for different lengths of time and α -PbO derived from the best-fit results of the XAFS experimental data with theoretical phase shifts and amplitude functions.	63
Table 3.1	Physicochemical properties of montmorillonite.	91
Table 3.2	Summary of XAFS sample adsorption conditions.	94
Table 3.3	Structural parameters and least squares precision (italicized in parenthesis) obtained using different fitting schemes (see text) for β -PbO and Pb(II) adsorption on montmorillonite at pH = 6.76, $I = 0.006$ M. . .	116
Table 3.4	Structural parameters derived from the XAFS experimental data using theoretical phase shift and amplitude functions for Pb(II) solutions and Pb adsorption on montmorillonite samples reacted at different I and pH	117
Table 4.1	Physicochemical and mineralogical characteristics of the soils used in this study.	137
Table 4.2	Comparison of total Pb sorbed and desorbed in stirred-flow reactor for the soil samples after 12 CV.	165
Table 4.3	Effect of residence time on Pb desorption from the Matapeake soil using the stirred-flow reactor for desorption.	168
Table 4.4	Structural parameters derived from the XAFS experimental data using theoretical phase shift and amplitude functions for Pb sorption on treated and untreated Matapeake soil samples.	174
Table A.1	Test for efficiency of resin to remove Pb from solution and for Pb recovery from resin, as well as test to make sure washing does not desorb Pb from resin.	193

Table A.2	Atoms program input file containing crystallographic data to create file for FEFF 6.0 input file.	194
Table B.1	Results from X-ray diffraction characterization	196
Table B.2	Amount of Pb recovered from resin recovered from montmorillonite samples incubated for ~200 h of adsorption, and 45 min of desorption time. $I=0.1$ M, pH=6.5, initial amount of Pb adsorbed was ~140 mmol kg^{-1}	198
Table C.1	Percentages of elements in treated and untreated Matapeake soils.	201

LIST OF FIGURES

Figure 1.1	Schematic of soil particles illustrating the different types of sorption that are possible. See text for definitions.	5
Figure 1.2	Schematic diagram of free energy (G) vs. reaction coordinate for sorption and desorption processes.	18
Figure 1.3	Schematic illustrating the theory of XAFS, and steps involved in data analysis.	41
Figure 2.1	k^3 weighted normalized χ -functions for samples incubated for different lengths of time, and α -PbO (amplitude of α -PbO spectrum is $\frac{1}{2}$ actual).	60
Figure 2.2	Fourier Transforms (RSF) of the chi-functions in Figure 2.1 (amplitude of α -PbO spectrum is $\frac{1}{2}$ actual). Vertical dashed lines are aligned at the center of the two major peaks used for fitting. The solid line is the theoretical multi-shell fit to the data, the dotted line represents the experimental data.	61
Figure 2.3	RSF of sample incubated for 6.5 h with the individual shell contributions.	64
Figure 2.4	Lead adsorption kinetics on γ -Al ₂ O ₃ at pH=6.50, I=0.1 M, and [Pb] _{initial} =2.0 mM, surface area = 100 m ² g ⁻¹ . Data points are from three separate experiments.	66
Figure 2.5	Desorption of Pb from γ -Al ₂ O ₃ by replenishing background electrolyte every 24 h. Data points are from three separate experiments.	70
Figure 2.6	Lead desorption kinetics from γ -Al ₂ O ₃ using Na-saturated resins, pH=6.50, I=0.1 M. Error bars are standard deviations of 3 samples.	72
Figure 3.1	Schematic illustrating the (010) structure of the dioctahedral montmorillonite mineral.	86

Figure 3.2	Lead adsorption on montmorillonite as function of pH. $[Pb]_{initial}=2$ mM. $[solid]=10$ g L ⁻¹ . Arrows indicate the equilibrium conditions of the montmorillonite samples used for the XAFS analysis. In the graph in the lower panel the range of the y-axis is decreased to illustrate the pH-dependent adsorption behavior of Pb-montmorillonite samples equilibrated at $I=0.006$ M.	101
Figure 3.3	XANES spectra of the Pb-montmorillonite samples equilibrated at various ionic strengths and pH, and the Pb reference samples. The spectra are normalized for step height and $E_0=13055$ eV. The dashed lines labeled A and B are aligned with the center of the peaks in the Pb ²⁺ (aq) sample (see text). "From Hesterberg et al. (1997). ^b $[Pb]=50$ mM. ^c Pb-montmorillonite samples. ^d $[Pb]=84$ mM.	106
Figure 3.4	Derivative of the XANES from Figure 3.3.	107
Figure 3.5	k^3 weighted normalized χ -functions for Pb-montmorillonite samples equilibrated at various ionic strengths and pH, and the reference samples. "From Hesterberg et al. (1997). ^b $[Pb]=50$ mM. ^c Pb-montmorillonite samples. ^d $[Pb]=84$ mM.	110
Figure 3.6	Fourier transforms (RSF) of the χ -functions in Figure 3, $\Delta k=2.3-9.6$ Å ⁻¹ . The solid line is the theoretical multishell fit to the data; the dotted line represents the experimental data. "From Hesterberg et al. (1997). ^b $[Pb]=50$ mM. ^c Pb-montmorillonite samples. ^d $[Pb]=84$ mM.	112
Figure 3.7	Back transformed Pb ²⁺ (aq) ($\Delta R=1.03-2.95$ Å) and Pb ₄ (OH) ₄ ⁴⁺ (aq) ($\Delta R=1.03-2.77$ Å) samples.	122
Figure 4.1	Schematic illustrating the experimental design of the stirred-flow experiments.	141
Figure 4.2	Sorption isotherm on the untreated Matapeake soil. The solid line is the best fit to the Freundlich equation (Equation (4.2)).	148
Figure 4.3	Sorption kinetics on Matapeake soil measured using the batch method. The solid line is the best fit to the first-order reversible equation, (Equation (4.3)).	149
Figure 4.4	Results of tracer experiment conducted at different flow rates. Chamber volumes were calculated using $V_c=8$ ml.	152

Figure 4.5	Results of tracer experiment conducted at different flow rates. Chamber volumes were calculated using the effective volume of the chamber derived from the best fit to Equation (4.1). The solid line is the fit to the data using Equation (4.1).	153
Figure 4.6	Results of sorption experiment conducted on Matapeake soil in the stirred-flow chamber, and theoretical tracers calculated using Equation (4.1).	155
Figure 4.7	Breakthrough curves for sorption on treated and untreated Matapeake soils, the St. Johns soil, and theoretical tracers.	159
Figure 4.8	Breakthrough curves for desorption from the untreated Matapeake soil and theoretical tracer.	162
Figure 4.9	Percent Pb desorbed from treated and untreated Matapeake and St. Johns soil.	164
Figure 4.10	k^3 weighted normalized χ -functions from XAFS experiments for Pb sorption on the treated and untreated Matapeake soil.	171
Figure 4.11	Fourier transforms (RSF) of the χ -functions in Figure 4.10 (dotted line), and results from multi-shell fits using theoretical backscattering phase and amplitude functions (solid line). Vertical dashed lines are aligned at the center of the two peaks used for fitting in the untreated Matapeake soil.	172
Figure 4.12	Examples of sorption complexes on the treated and untreated Matapeake soils based on the fit results of the XAFS data.	177
Figure A.1	Results from titrating Pb solution, MES (buffer) solution and a solution with both Pb and MES present. The solid line is the total base taken up by the independent Pb and MES solutions. The close match between the solid line and the Pb+MES solution indicates no change in pKa of solution when both chemicals are present in the same solution.	190
Figure A.2	pH edge for Pb adsorption on γ -Al ₂ O ₃ . [γ -Al ₂ O ₃]=10 g L ⁻¹ , I=0.1 M, [Pb] _{initial} =2.0 mM.	191
Figure A.3	Adsorption isotherm for Pb on γ -Al ₂ O ₃ . [γ -Al ₂ O ₃] = 10 g L ⁻¹ , pH=6.50, I=0.1 M. In the Langmuir equation q is the total sorption, C is the equilibrium concentration, k is the maximum sorption, and b is an adsorption coefficient.	192

Figure B.1	Adsorption kinetics of Pb on montmorillonite at two ionic strengths. [montmorillonite]=10 g L ⁻¹ , [Pb] _{initial} =2 mM, pH=6.5.	197
Figure B.2	Speciation diagram of Pb(II) in solution. These data were used to make standards for XAFS.	199

ABSTRACT

Lead is the most common contaminant found at polluted sites. In order to develop more effective risk assessment methods and remediation strategies it is critical that there be a precise understanding of the reaction pathways occurring between Pb and soils. In this study, the effects of time, pH, ionic strength, and soil organic matter on Pb sorption and desorption in soils and soil components were investigated using equilibrium, kinetic, and X-ray absorption fine structure (XAFS) spectroscopy. The use of *in situ* spectroscopic experiments together with macroscopic experiments resulted in important information about sorption and desorption reaction mechanisms.

Pb adsorption and desorption on Al_2O_3 was characterized by fast and slow reaction steps. XAFS analyses showed no change in the sorption mechanisms over a period of 1.5 h to 23 days. Based on these experiments, it was proposed that the process responsible for the slow sorption reaction is slow diffusion to sorption sites existing on the interior of the mineral, and that Pb formed an inner-sphere bidentate complex on the edges of the alumina octahedra. Desorption from the Al_2O_3 was shown to be completely reversible within 3 days.

Lead adsorption on montmorillonite was pH-dependent at high ionic strength, and pH-independent at low ionic strength. This behavior suggested two different adsorption mechanisms were occurring. XAFS results confirmed that at high

ionic strength and pH, inner-sphere complexes predominated, and at low ionic strength and pH, outer-sphere complexes predominated. However, at high ionic strength and low pH, or at low ionic strength and high pH, the XAFS data revealed that a mixture of inner- and outer-sphere Pb complexes were occurring.

Sorption and desorption behavior of Pb in soils with varying amounts of soil organic matter were measured using a stirred-flow reactor. The rate of sorption and desorption decreased as the fraction of organic matter in the soils increased. Desorption from the soils was hysteretic within the time frame of the experiments. This behavior is due to the formation of strong complexes between Pb and the ligand sites existing on SOM. Based on a comparison of the Pb desorption behavior from the aluminum oxide, the montmorillonite clay, and the soil organic matter, it was concluded that the bonds formed between Pb and soil organic matter are stronger than the the bonds formed between Pb and the soil minerals. Analysis of the extended portion of the XAFS (EXAFS) data from the soil confirms that Pb is predominantly sorbed to the SOM (C and O atoms were the only atoms present in the first and second coordination shells surrounding the Pb atoms).

Chapter 1

Introduction

1.1 Rationale and Scope of Research

Excessive exposure to Pb is toxic to many organisms, from microbes to plants and animals alike. Environmental contamination resulting from the extensive use of Pb in industrial, agricultural, building, and manufactured products has magnified the threat of Pb toxicity. Since large amounts of Pb in the environment exist in soils and sediments, an understanding of the relationship between natural materials and Pb is critical. Over the past several years many studies have been conducted to identify this relationship, and a great deal of information has been discovered. Results from these studies are used to create governmental regulations, devise cleanup strategies, and create models that predict the fate of Pb in the environment. However, in conducting these studies researchers often fail to take into account two important aspects: 1) the length of time soils are exposed to a contaminant in the laboratory is relatively short compared with the much longer contact times that exist in field contaminated soils, 2) the ionic strength and pH of the soil solution can have dramatic effects on the sorption mechanisms occurring. These discrepancies can lead to improper evaluation of Pb behavior in the environment, and result in inaccurate regulations, and models and remediation strategies that are unsuccessful. The research presented in this dissertation

investigates the effects of residence time (aging), ionic strength, and pH on Pb sorption and desorption reactions with soils, and soil components. This information will allow for a better understanding of the fate of Pb in the environment.

Lead exists in the soil as either aqueous species, as structural elements of solids, or sorbed onto soil materials. Lead is present naturally in the environment, but usually at levels that are nonthreatening. The average concentration of Pb in soils around the world is estimated to be 15 ppm (Zimdahl et al., 1977). The use of Pb by society, both past and present, has resulted in the buildup of Pb in soils to concentrations that are much higher than this average. In the United States Pb and its various compounds have been found at 635 out of 1177 sites on the National Priorities List of hazardous waste (ASTDR, 1990). The U.S. EPA has declared that there is a great need for remedial technologies for metals in Superfund programs, and that Pb is the most common metal found at hazardous waste sites (Reed et al., 1996). The following are examples of common sources of Pb contamination: disposal of batteries that contain Pb; exhaust from automobiles that burn gasoline with Pb additives; application of pesticides that contain Pb, e.g., $Pb_3(AsO_4)_2$; the use of Pb in paint; application of sewage sludge to soil that contains high levels of Pb; and the many uses of Pb in manufacturing. Scientists have made it clear that Pb is a toxic metal, and many past uses are now illegal.

Ingestion and inhalation are the predominant means of Pb contamination in humans and other animals. Ingestion is common in children who play in Pb contaminated soil, as well as in people who work in contaminated soil. Contamination can also occur from eating plants and animals that have high concentrations of Pb in them, or by

drinking contaminated water. Breathing airborne-Pb-laden dust particles is the primary source of Pb toxicity from inhalation.

Scientific studies have clearly shown that exposure to metal contaminants such as Pb at higher levels is toxic. As a result, many past uses and disposal practices for Pb are now illegal, and contamination of the environment is regulated more closely. However, due to the relatively low solubility of Pb, and its strong sorption to soils, environmental contamination persists, and the threats from Pb remain a problem that merits continued scientific investigation.

The toxicity from Pb, and its presence in the environment at dangerous levels are well established facts, however, the questions remain: how does one remediate contaminated soils effectively, and how can significant risks be accurately evaluated? Finding effective answers to these questions hinges on a clear understanding of the behavior and interactions of Pb with soils; in particular, a better understanding of the kinetics and mechanisms of Pb-soil interactions will provide scientist and engineers information to implement better strategies for dealing with Pb contaminated soil, and allow for better decisions on Pb disposal that will not cause further threats to society and the environment.

Many studies rely on an equilibrium approach to predict the retention of contaminants such as Pb on natural materials and subsequent migration through the vadose zone. Researchers often focus on determining parameters such as distribution coefficients, and the maximum amount of sorption possible. These studies are often based on the Pb-solid interactions over a short period (24 hours or less) because it is

assumed that the reaction has reached completion (Griffin et al., 1986). In addition researchers often incorrectly assume that the behavior of Pb sorption is the same at all pH values and ionic strengths. However, field soils are seldom, if ever at equilibrium, often laboratory studies are also far from equilibrium, and slow sorption, pH and ionic strength may change the distribution between solid and solution over a period of time (Smith et al., 1996; Sparks, 1998). The failure to account for these factors results in either under-predictions of the amount of contaminants retained by soils and minerals, or over-predictions of contaminant availability in the environment. A better approach is to base mobility estimates, remediation strategies, and risk assessments on the true availability of the contaminant, which is a factor of soil mineralogy, percent soil organic matter present, composition of soil solution, soil solution pH and ionic strength, and the rate of sorption and desorption.

Most soils are heterogeneous media that contain a host of different minerals, solids, and organic materials. Thus, the interaction of Pb with soils is a heterogeneous process. Several possible sorption mechanisms have been proposed (Figure 1.1): diffusion into micro-pores and solids followed by sorption onto interior surfaces; sorption to sites of variable reactivity, including sites which involve different bonding mechanisms, i.e., inner-sphere vs. outer-sphere and monodentate vs. bidentate; and surface precipitation (Fuller et al., 1993; Loehr et al., 1996; Scheidegger et al., 1996b).

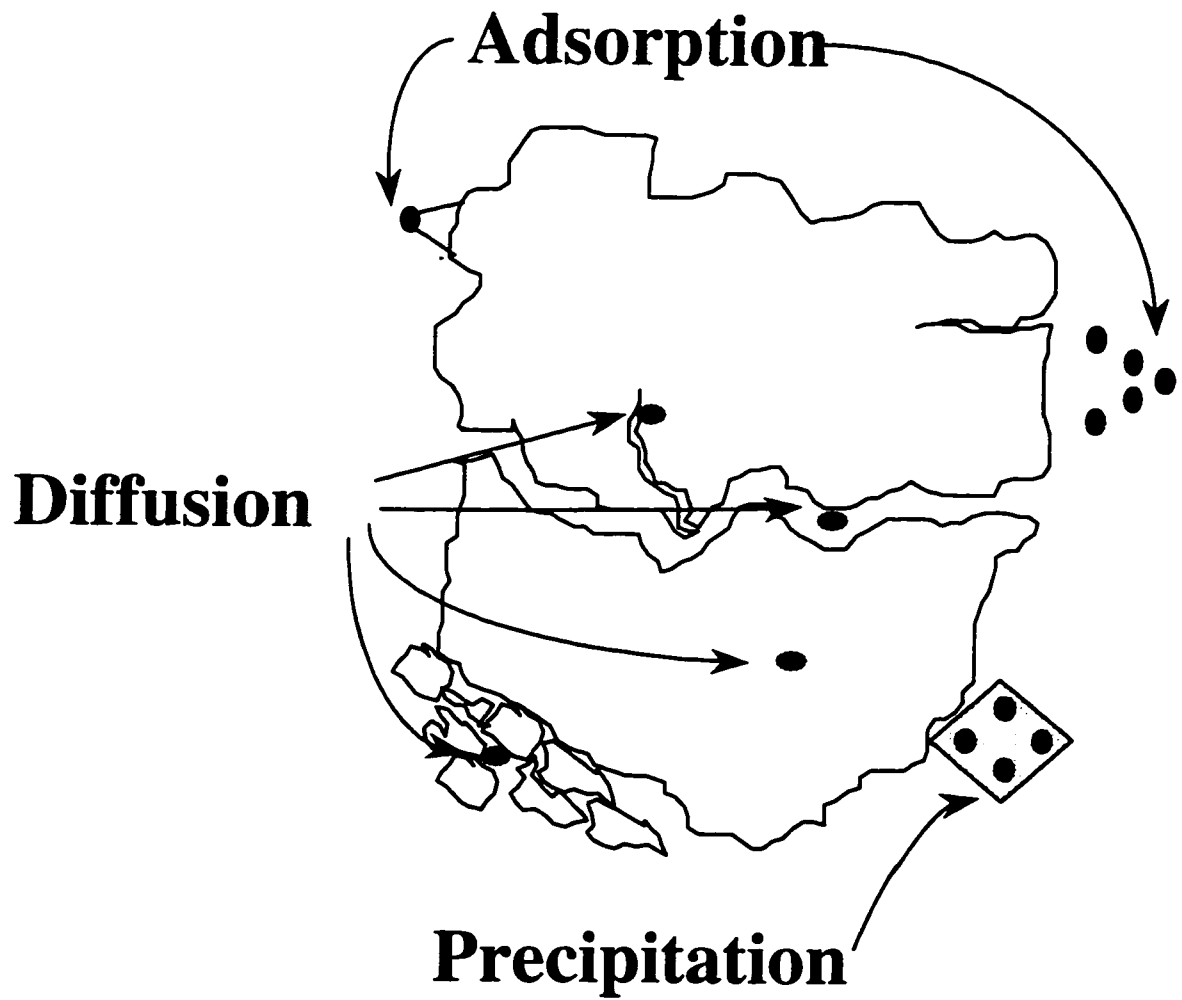


Figure 1.1 Schematic of soil particles illustrating the different types of sorption that are possible. See text for definitions.

Due to the heterogeneity of soil, these processes can occur simultaneously. A measured sorption or desorption rate often reflects a combination of all of the sorption mechanisms. However, it is possible that one mechanism may dominate at a particular time in the sorption reaction and the measured rate is an expression of primarily that reaction rate. For example, outer-sphere complexation can precede inner-sphere complexation, which can precede surface precipitation. The significance of this continuum in sorption is that while many sorption and desorption reactions may appear to have reached equilibrium, in fact the reaction can be continuous, and the slow process will not be measured if only a short reaction time is studied. In such cases, important secondary processes which are slower than the primary process may be completely overlooked. Thus, predictions on the fate of the contaminant such as Pb may be inaccurate. This can cause increased threats of toxic exposure, improper evaluation of risks, and/or misappropriation of valuable cleanup and public safety funds.

To protect human health and the environment from overexposure there must exist effective cleanup strategies, accurate risk assessment technologies, and models that correctly predict the fate of Pb in the environment. For these tasks to be accomplished time dependent reactions of trace elements with soils, and the effects of pH and ionic strength must be taken into consideration. This includes both the macroscopic effects, such as slow sorption and desorption kinetics, and the microscopic effects, such as mechanisms of sorption and the pH and ionic strength dependence of these mechanisms. Thus, the goals of the research presented in this dissertation are to investigate Pb interactions with natural materials (soil and soil components) during long exposure

periods, including the mechanisms of retention and release. This will be done by employing both macroscopic experiments and microscopic (spectroscopic) investigations.

1.2 Literature Review: Kinetics and Mechanisms of Sorption

In this section the kinetics and mechanisms of slow sorption reactions are discussed and examples from the literature are given. As illustrated in Figure 1.1, there are primarily three different sorption processes: absorption, or partitioning into the solid which is controlled by diffusion processes, and may be succeeded by sorption; adsorption which involves the formation of both inner- and outer-sphere complexes; and surface precipitation.

1.2.1 Diffusion-controlled Kinetic Reactions

Diffusion is an activated process driven by the necessity of a system to be at its lowest possible energy, i.e., uniformly distributed throughout space. Since soils are porous materials containing both macropores ($>2\text{nm}$) and micropores ($<2\text{nm}$) (Pignatello et al., 1996) diffusion is a mechanism that can control the rate of sorption of trace elements on soils. These pores can be inter-particle (between aggregates) or intra-particle (within an individual particle). Intra-particle pores can form during weathering, upon solid formation, or may be partially collapsed interlayer space between mineral sheets, i.e., vermiculite and montmorillonite. The rate of diffusion through a pore is dependent on pore size, particle size, tortuosity, chemical interactions, chemical flux through the soil, and whether the pore is continuous or discontinuous. Besides pore diffusion solid-phase diffusion is also a transport-limited process. Solid phase diffusion is dependent on

the characteristics and interactions of the chemical and the solid (Pignatello et al., 1996). Since there exists a range of diffusion rates in the soil, it follows that with increasing exposure time the fraction of contaminants in the more remote areas of soil particles (accessible via slow diffusion) will increase. This slow sorption phenomenon is often the explanation researchers use to account for the slow continuous sorption and desorption observed between metals and soil (Sparks, 1989; Burgos et al., 1996).

Bruemmer et al. (1988) measured sorption and desorption of Cd, Zn and Ni with goethite, a porous iron oxide known to have defects within the structure in which metals can be incorporated to satisfy charge imbalances. They found that the kinetics were described well with a solution to Fick's second law (a linear relation with the square root of time), and proposed that the uptake of the metal followed a three-step mechanism: "(i) adsorption of metals on external surfaces, (ii) solid-state diffusion of metals from external to internal sites, and (iii) metal binding and fixation at positions inside the goethite particle," suggesting that the second mechanism is responsible for the slow reaction (Bruemmer et al., 1988). Similar observations on sorption of divalent metal ions were made by Coughlin and Stone (1995). They suggested that the slow sorption and desorption could be a result of slow diffusion that occurred because their synthetic goethite may have had an unusually high level of pores and cavities. Axe and Anderson (1997) also found that sorption of Cd and Sr could be characterized by a model which included two steps: a rapid reversible sorption step followed by a slow, rate-limiting process involving the diffusion of the cations through small pores existing along the surface.

While the above examples have hypothesized that diffusion is the rate-limiting step based on good model fits to data and some speculation. macroscopic sorption experiments are not definitive proof of a mechanism (Sposito, 1989). To give additional support to diffusion as a mechanism for sorption onto porous media, Papelis (1995) measured surface coverages of Cd and selenite on porous aluminum oxides using X-ray photoelectron spectroscopy (XPS). Papelis (1995) calculated the expected thickness of sorbed Cd and selenite from the total metal loss from solution using both external and internal surface areas. A good agreement was found between the calculated and the measured (using XPS) surface coverage thickness when the total surface area (i.e., internal and external surface area) was used. When the surface layer thickness was calculated without considering internal surface area, then the calculated thickness exceeds the thickness observed using XPS. Therefore, the most likely sorption mechanisms were sorption to external sites, diffusion of Cd into the internal structure, and subsequent sorption. While Papelis (1995) didn't measure the kinetics of the reaction, it seems probable that the sorption to the interior sites is slower than the exterior sites, and thus a slow kinetic sorption step would exist.

Fuller et al. (1993) combined kinetic sorption and desorption experiments with spectroscopic observations (Waychunas et al., 1993) to conclude that the rate-limiting process in arsenate sorption by ferrihydrite is diffusion into the solid structure. Using X-ray absorption fine structure (XAFS) spectroscopy Waychunas et al. (1993) found that arsenate is sorbed predominantly as inner-sphere bidentate complexes, regardless of whether the arsenate was adsorbed post-mineralization of the ferrihydrite, or

present during precipitation. Thus, at the pH of their study (8.0), arsenate surface precipitates were not formed. Slow sorption and desorption were explained as slow diffusion of the arsenate to or from interior surface complexation sites that exist within disordered aggregates of crystallites. The arsenate sorption and desorption kinetics were explained well using a model which included two types of sorption sites: those easily accessible were described assuming equilibrium; while the sites which had limited accessibility were well represented by an equation which is based on Fick's second law of diffusion.

1.2.2 Kinetics and Mechanisms of Adsorption Processes

Adsorption is a phenomenon in which atoms and/or molecules accumulate at the interface between a solid phase and a solution phase, and is considered to be a two-dimensional phenomenon (Sposito, 1989). Adsorption reactions are governed by the laws of thermodynamics: energy is conserved, and the entropy of a system increases to a maximum. These two concepts can be combined to create the Gibbs free energy (G) function. For a reaction to occur the products must have a lower free energy than the reactants ($\Delta G < 0$). This can occur by either a decrease in enthalpy, an increase in entropy, or both. It is important to note that a change in enthalpy can dominate the free energy function creating a negative ΔG even when the entropy is decreased in the reaction, and visa versa. Therefore, an adsorption process leads to an association between an ion and a surface, driven by the desire of the system to achieve an overall lower free energy.

While thermodynamics can be used to determine if a reaction is favorable, it does not indicate the rate of the reaction, nor the pathways involved in arriving at the state with the lowest free energy. This information can be gained by measuring reaction kinetics. In real systems, such as soils and sediments where there exist several different types of sorption sites and reaction mechanisms, resulting in variable rates of reaction. In these systems kinetics can play an important role in the fate of trace elements since such systems are not at equilibrium, but are continuously undergoing chemical changes as they seek to produce the most stable species (Steinfeld et al., 1989). The change may be slow, resulting in the sorbate becoming less available with time (aging) (Koskinen et al., 1990), and can result in a change from one type of sorbed complex to another. This process is similar to the concept of the Ostwald-step rule: the first product in a precipitation reaction is that which has the highest solubility, followed by a slow continuous transformation to a more stable species (Stumm et al., 1996). An analogous process in adsorption would result in a multitude of adsorbed complexes, some of which may be in a metastable equilibrium state, undergoing continuous transformation to the most stable species.

Evidence for this slow, continuous change to a more stable species is commonly observed for solid materials. Upon initial precipitation the solid is in an *active* form that has a disordered lattice (amorphous), and exists in a metastable equilibrium with the solution (Stumm et al., 1996). With time the solid slowly converts to the more stable *inactive* form. The *inactive* form is more crystalline-like, and has a lower solubility. This slow kinetic phenomenon may continue for geological time spans. An example is aragonite (a polymorph of calcite), which is found in rocks < 300 million years

old. Aragonite is not thermodynamically stable, but forms under surficial temperatures and pressures, and slowly reverts to the more stable calcite (Blackburn et al., 1994). Waychunas et al. (1993), using XAFS data fitting, found that aging and continued polymerization of ferrihydrite resulted in a transformation of the number of linkages and interatomic distances to those suggesting a progression to the more ordered polymorph goethite. The slow transformation of a solid to a state with a lower free energy is often observed as an aging mechanism for precipitates, but transformations between sorption mechanisms is more difficult to distinguish, and little direct evidence exists for such processes. However, it seems reasonable to suggest that the energetics of sorption and desorption reaction processes are analogous to those of precipitation, i.e., kinetically limited by a transformation to the most stable sorption configuration (lowest ΔG).

Adsorption reactions occur via three different mechanisms: inner-sphere complexes, outer-sphere complexes, and diffuse ion (Sposito, 1989). Outer-sphere bonds consist of a solvated ion that forms a complex with a charged functional group, the primary bonding force is electrostatic. An inner-sphere complex is partially dehydrated, the ion forms a direct ionic or covalent bond with the surface functional groups. A diffuse ion exists in the water layers near the surface, and is held by electrostatic attraction from permanent charges that exist in the solid structure. A major difference between the outer-sphere complex and the diffuse ion complex is in the strength of the electrostatic force, which is directly correlated to the proximity of the ion to the surface (McBride, 1994). The type of sorption and bonding mechanism depends on several factors: 1) ionic radius, 2) electronegativity, 3) valence charge, 4) surface type, and 5)

ionic strength of the sorptive solution. There are two major types of surface sites: variable charged sites, e.g., silanol and aluminol; and permanent charge sites that result from isomorphic substitution.

To model surface complexation and understand the controlling mechanisms, scientists often assign a hypothetical bonding mechanism between an ion and a given surface. However, ions can bond to surfaces via several different mechanisms, and can undergo a continuous transition between adsorption mechanisms (Stumm et al., 1996). Waychunas et al. (1993) found that arsenate adsorbed onto ferrihydrate by both monodentate (30%) and bidentate bonding mechanisms. Bargar et al. (1996) used X-ray absorption spectroscopy (XAS) to distinguish between outer and inner-sphere sorbed Pb on α -Al₂O₃. They found that on the planar 0001 surface Pb-O-Al distances were consistent with an outer-sphere bond, while on the 1102 plane Pb was sorbed as an inner-sphere complex. Benjamin and Leckie (1981) conducted sorption experiments at several different loading levels and equilibrium pHs for Cd, Cu, Zn and Pb on amorphous iron oxyhydroxide. Their data suggested that there exist several types of bonding sites with variable bonding strengths, and that measured equilibrium constants are average values from these different types of sites. McBride (1982) found similar results on pure noncrystalline aluminum oxide using electron spin resonance (ESR) spectroscopy to study the change in Cu sorption mechanisms with time. He found that sorption involved sites of varying reactivity. The first reaction step was the rapid sorption of a low level of Cu, the second reaction occurred over several weeks and resulted in the uptake of a greater amount of Cu and ESR spectra distinct from the first reaction step. Such heterogeneity is

enhanced in natural systems that contain materials with a variety of organic and inorganic surface sites.

Adsorption reactions are often considered to form the most stable bond immediately, however, intermediates may exist that are metastable for long times. In fact, adsorption may consist of several chemical and physical reactions that limit the overall reaction rate, i.e., ion and surface dehydration, breaking of a strong bond, bond formation, and surface diffusion (McBride, 1994; Stumm et al., 1996). Hayes and Leckie (1986a) and Grossl et al. (1994) used pressure-jump relaxation to measure the kinetics of Pb sorption on aluminum oxide and Cu(II) sorption on goethite, respectively. They found that the best fit to the data was obtained with a kinetic model that included a transformation from outer-sphere to inner-sphere complexation. Their results also suggested that sorption behavior was biphasic, which they explained by suggesting that the slower reaction was a result of sites with lower affinities. This concept is similar to the high and low affinity site model proposed by Dzombak and Morel (1990). While the kinetics of these reactions are quite rapid (reactions considered on a millisecond time scale), the demonstration of a multiple step adsorption mechanism rationalizes the hypothesis that in some systems one step may be slow enough to be responsible for the slow adsorption and desorption reactions often observed in soils (Sposito, 1989).

Biphasic sorption reactions have been observed in soils. An example is the result of Lehman and Harter (1984) who measured the kinetics of chelate promoted Cu release from a soil to assess the strength of the bond formed. Their sorption/desorption data were biphasic, which they attributed to high and low energy bonding sites. They also

found that with increased residence time, 30 minutes to 24 hours, there was a transition of the Cu from low energy sites to high energy sites (as evaluated by release kinetics). Incubations for up to four days showed a continued uptake of Cu and a decrease in the fraction released within the first three minutes, which was referred to as the low energy adsorbed fraction. The results of Smith and Comans (1996), already mentioned, also showed that Cs sorption onto sediments is biphasic. They modeled exchange reactions assuming exchangeable and fixed fractions. The fixed fraction was assigned to Cs that was incorporated in the mineral lattice, i.e., predominantly specific exchange sites on illitic clay. The Cs adsorption mechanisms proposed by Smith and Comans (1996) were based on kinetic experiments, i.e., macroscopic observations. Kim et al. (1996) used nuclear magnetic resonance (NMR) spectroscopy to make microscopic observations of Cs sorption mechanisms on kaolinite, boehmite, silica gel, and illite. Their experiments coincide with those of Smith and Comans (1996), suggesting that Cs formed two distinct types of complexes on the surfaces of the minerals: inner-sphere, and outer-sphere.

The energy and stability of adsorbed species varies depending on the type of surface complex formed. It is generally accepted that surface complexes with more than one bond are more stable than complexes with a single bond (McBride, 1994; Stamm et al., 1996), and likewise for inner-sphere vs. outer-sphere sorption (McBride, 1991). One explanation for the increased stability of a multidentate bond over a monodentate bond is the increased entropy gained from a more stable configuration (steric effect) (Steinfeld et al., 1989; McBride, 1994). An analogous phenomenon is the *Chelate Effect*; for example, the ΔG for the ethylenediamine complex, a chelate ring with bidentate bonding to a

cation, is lower than ΔG of the diamine complex, which forms monodentate complexes with cations (Stumm et al., 1996). The lower ΔG for the ethylenediamine complex means it is more stable. Since the enthalpies for the complexation of cations by the two chelates are similar, the lower ΔG is a result of an increased entropy for the bidentate ring complex; as mentioned above, this phenomenon is often referred to as a steric effect or configurational entropy (Steinfeld et al., 1989; McBride, 1994). Since the reactive sites on minerals (silanol and aluminol sites) and organic matter (carboxyls and phenolic-OH) are often considered to be analogous to ligand functional groups, the steric effect is likely to be an important consideration when determining mechanisms of trace element adsorption reactions in soil. Thus, it is reasonable to conclude that if the coordination environment is appropriate, multidentate bonding will be favored (thermodynamically) over monodentate bonding. However, the formation of multiple bonds may have intermediate products that have a higher activation energy than a complex with only a single bond. As discussed below, an increase in the activation energy may limit the kinetics of complex formation.

The formation of a surface complex, or conversion of an adsorbate from one bond type to another may be thermodynamically favored but inhibited by an activation energy, which is the extra energy, beyond the difference in the free energy between the products and reactants (ΔG°), required to complete the reactions Figure 1.2. The activation energy results from the energy required to form intermediate products not accounted for in the reaction stoichiometry (Noggle, 1989). A large activation energy

will result in slower adsorption and desorption kinetics compared to sorption processes which have a lower activation energy.

Since the strength of adsorption varies depending on the surface and adsorptive being considered, the adsorbate availability (via desorption) and kinetics are variable (Pignatello et al., 1996). For many adsorbed ions it is found that the rate of adsorption is faster than desorption (Swift et al., 1991; McBride, 1994). A possible reason for the slower rate of desorption is an increase in the activation energy required to break the adsorption bonds. The activation energy for desorption can be quantified as follows: $\Delta G^{\ddagger}_{\text{desorption}} = \Delta G^{\ddagger}_{\text{adsorption}} + \Delta G^{\circ}_{\text{adsorption}}$, where $\Delta G^{\ddagger}_{\text{desorption}}$ = activation energy for desorption, $\Delta G^{\ddagger}_{\text{adsorption}}$ = activation energy for adsorption (≥ 0), and $\Delta G^{\circ}_{\text{adsorption}}$ = energy of adsorption, see Figure 1.2 (McBride, 1991). This equation indicates that desorption of chemisorbed ions yields a larger activation energy than adsorption reactions, causing desorption to be a slower process. This may be the cause of the pseudo-hysteresis that is commonly observed in sorption and desorption experiments, i.e., the forward and reverse isotherms do not overlie when given the same reaction time.

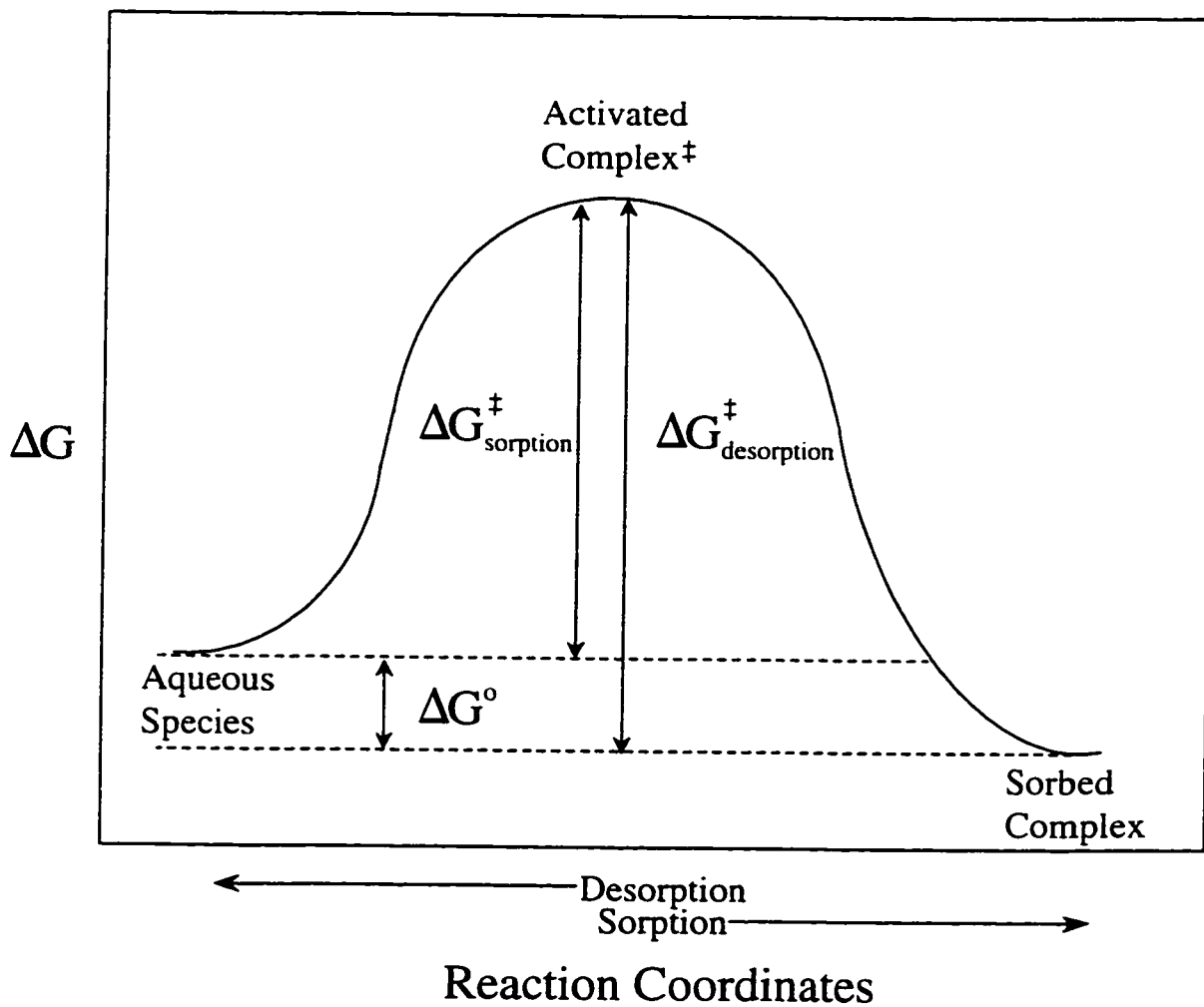


Figure 1.2 Schematic diagram of free energy (G) vs. reaction coordinate for sorption and desorption processes.

In this section we have discussed adsorption and desorption kinetics and sorbate stability. The kinetics of sorption and stability of a surface complex is a factor of both entropy (steric factors) and enthalpy (bond energetics). However, the formation of the most stable adsorbed species may be limited by intermediate complexes. Thus, if an adsorbate slowly converts from one adsorption or bonding species to a more stable complex that has a lower free energy, the result is important towards controlling the rate of uptake and affecting the availability of trace metals.

1.2.3 Kinetics and Mechanisms of Surface Precipitation

In contrast to adsorption, surface precipitation is a 3-dimensional growth phenomenon that occurs on surfaces. Classical solution chemistry defines aqueous systems in three states: undersaturated, saturated, and supersaturated, with respect to the solubility of inorganic precipitates. A system saturated or supersaturated has a negative ΔG , indicating the precipitation of a solid product is favored. Precipitation that occurs in a saturated system proceeds more slowly than a supersaturated system (Stumm et al., 1996). Surface precipitation during trace metal sorption has been observed in systems undersaturated with respect to the pure hydroxide, and below monolayer surface coverage (Fendorf et al., 1992; Fendorf et al., 1994; O'Day et al., 1994; Scheidegger et al., 1998). This means that the availability and transport of a cation or anion may be controlled by precipitation and dissolution mechanisms, as opposed to adsorption phenomena. Veith and Sposito (1977) showed that traditional sorption data are described equally well by both surface precipitate models and adsorption isotherms. In addition, it has been noted

that solubility lines of many soil solutions (logarithm of metal activity plotted as a function of pH) reveal undersaturation with respect to common precipitates, however, often have slopes paralleling those of pure precipitates (McBride, 1991). Such examples display the ambiguity of macroscopic models in describing microscopic processes, i.e., surface precipitation and adsorption models seem to describe sorption data equally well. Since precipitation and dissolution reactions exhibit slower kinetics than adsorption and desorption (Farley et al., 1985) they may be the mechanism responsible for aging and the slow kinetics of sorption and desorption often observed in experimental systems (Fendorf et al., 1992).

In this section we categorize surface precipitation into three different types that are commonly discussed in the literature. These include: formation or sorption of metal polymers (dimers, trimers, etc.) on the surface (Chisholm-Brause et al., 1990); a solid solution or coprecipitate that involves co-ions dissolved from the sorbent; and a homogeneous precipitate formed on the surface composed of ions from the bulk solution, or their hydrolysis products (Farley et al., 1985). The continuum between surface precipitation and chemisorption is controlled by several factors, including: 1) the ratio of the number of sites vs. the number of metal ions in solution, 2) the strength of the metal-oxide bond, and 3) the degree to which the bulk solution is undersaturated with respect to the metal hydroxide precipitate (McBride, 1991). The different types of surface precipitation are explained in more detail below.

Polymeric metal complexes that form at the surface, and/or the sorption of aqueous polymers, may be a mechanism that typifies surface precipitate-like complexes

(Fendorf et al., 1994). Chisholm-Brause et al. (1990) interpreted the presence of Pb in the second coordination shell of a sorbed Pb (determined using XAS) as small clusters or polynuclear structures that are analogous with hydroxy metal complexes formed in water solution. The formation of complete surface precipitates was ruled out because the number of Pb atoms in the second shell was small (0.3 to 1.5). Bargar et al. (1997) observed similar polymer formation at high loading levels for Pb on Al-oxide surfaces. Fendorf and Sparks (1994) found that Cr polymerization, and eventually Cr-hydroxide surface clusters began at surface coverages as low as 20%. It was proposed that when the structures of the sorbate and sorbent are dissimilar epitaxial growth is energetically unfavorable, and thus nucleation growth is away from the surface, i.e., surface clusters.

The formation of a homogeneous solid on a surface can occur when a solution becomes saturated and the surface acts as a nucleation site, or from a chemisorption-precipitation continuum, i.e., when adsorption reaches monolayer coverage sorption continues on the newly created sites resulting in a precipitate on the surface (multilayer surface coverage) (Farley et al., 1985; McBride, 1991). This phenomenon is analogous to the assumptions used in the classical Brunauer-Emmett-Teller (BET) isotherm model of gas sorption onto surfaces (Borg et al., 1992). The distinction between a surface precipitate and a sorbed metal complex can be subtle, and somewhat confusing, especially since polymer sorption can lead to, or preface, surface precipitation. Adding to the difficulty of distinguishing surface precipitation from sorbed metal complexes is the fact that methods for distinguishing between the two phenomena are at present in their early development, and few studies exist on this subject matter.

The solid solution concept of surface precipitation was presented in detail by Farley et al. (1985); it is described as a process similar to homogeneous coprecipitation. The composition of the surface precipitate varies, “continuously between that of the original solid and a pure precipitate of the sorbing metal (Farley et al., 1985).” The solid solution concept differs from the multilayer precipitation concept in that it includes both desorption and/or dissolution of structural ions from the sorbent and the inclusion of ions from solution. The result of coprecipitation of the solution ions with ions dissolved from the surface is a solid with isomorphic substitution, or a stable mixture of two solids (Stumm et al., 1996). An important factor controlling which ions will form a solid solution is the ionic radius. For example, Ainsworth et al. (1994) found that the extent of reversibility with aging for Co, Cd, and Pb was inversely proportional to the ionic radius of the ions, where ionic radii increase in the order $\text{Co} < \text{Cd} < \text{Pb}$. Since the ionic radius of Co is the most similar to Fe, they concluded that the hysteresis was a result of the formation of a solid solution. Solid solution formation is probably limited by the rate of mineral dissolution, rather than a lack of favorable thermodynamic conditions (McBride, 1994; Scheidegger et al., 1998). O’Day et al. (1996) observed a small amount of Si backscattering from the XAFS spectra of Co sorption on quartz ($\alpha\text{-SiO}_2$). They explained this by proposing that Co was coordinated in Si tetrahedra, which occurred by either diffusion to defect sites, or a small amount of quartz dissolution and reprecipitation of a mixed Co/Si phase (solid solution).

Surface precipitation and dissolution are slower processes than adsorption and desorption. Farley et al. (1985) noted that the rate of Cd uptake by amorphous iron

hydroxide was lower when the initial solution concentration exceeded that required for monolayer coverage. One possible reason for the slower precipitation reactions is that a precipitated ion must form several bonds, which requires more activation energy than adsorption complexes which have fewer bonds. Likewise, surface precipitates may be more stable than adsorbed species because of the formation of high energy bonds and increased coordination. Another factor that makes surface precipitates more stable is that only the surface of the precipitate is accessible to the solution for dissolution to occur (for a 3-dimensional object only the exposed surfaces are surrounded by solution).

The formation of a surface precipitate involves several reactions, including:

1) adsorption of the ion on the surface, 2) surface nucleation, and 3) crystal growth (Stumm et al., 1996). Each of these steps contains several independent reaction sequences, and the rate of precipitate formation is determined by the slowest reaction step. While the formation of surface precipitates is important for predicting the fate of trace elements in the environment, dissolution reactions are also important processes that may be the controlling mechanisms for trace element mobilization when a soil has been contaminated for long periods. For the dissolution of surface precipitates the reaction sequence is similar to the steps of dissolution of a pure solid: 1) transport of reactants from the bulk solution to the surface, 2) adsorption of solutes, 3) interlattice transfer of reacting species, 4) chemical reactions, 5) detachment of reactants from the surface, and 6) mass transport into the bulk solution (Stumm et al., 1990). These steps can be summarized as transport and surface reaction mechanisms. The mechanism controlling

the rate of dissolution is dependent on several factors, i.e., solution composition, pH, mixing, etc..

The kinetics of surface precipitate formation and dissolution has not been extensively studied. In a recent study by Scheidegger and Sparks (1996a) the rate of release of Ni from a pyrophyllite surface known to have Ni precipitates showed both a fast and slow reaction. The fast reaction was attributed to desorption of specifically sorbed Ni. The slow reaction was attributed to the slow dissolution of polynuclear Ni complexes, which were found to dissolve more slowly than pure Ni(OH)₂. In another study, Scheidegger et al. (1998) monitored the kinetics of surface precipitate formation on pyrophyllite, montmorillonite, and gibbsite using XAFS. Surface precipitate formation was initially fast on pyrophyllite and gibbsite (within minutes), but did not occur until 48 hours on montmorillonite.

O'Day et al. (1996) used XAS and kinetic experiments to hypothesize the mechanisms of surface precipitation on two different minerals. Their hypotheses were strengthened by comparing and contrasting the spectroscopic and kinetics results for different mineral surfaces. XAFS results for Co on rutile (TiO₂) showed an increase in the number of backscattering Co atoms for aging times of one day to 11 days, suggesting an increase in the size of multinuclear complexes formed on the surface. However, similar results were not seen for Co aging on quartz (α-SiO₂), which had Co(OH)₂ surface precipitates present. They hypothesized that the reason for the observed slow change in the multinuclear surface precipitate on the rutile and not on the quartz was a result of the similar radii between Co and Ti, while the radius of Si is larger than Co. As a result of

this difference in atomic radii, the Co hydroxide-like-precipitate formed on quartz was attached only to corners of select Si tetrahedra on the surface. However, Co sorption on the rutile was consistent with the formation of a precipitate that had similar lattice dimensions as the surface, effectively extending the lattice structure of the bulk solid, i.e., an epitaxial growth. The resulting Co surface precipitate was structurally strained due to charge imbalances and distortion of the CoO_6 octahedra. Thus, they proposed that the change with increasing equilibration times was due to the formation of an anatase-like structure (conclusion made based on similar octahedra bond distances between the anatase and the surface precipitate). The anatase structure, a TiO_2 polymorph, has favorable lattice dimensions for Co because of a more open structure which better accommodates the slightly larger Co ion.

There are several thermodynamic reasons for the formation of surface precipitates in unsaturated systems. For example, the solid surface may lower the energy of nucleation by providing sterically similar sites (McBride, 1991), the activity of the surface precipitate is less than unity (Sposito, 1986), and the solubility of the surface precipitate is lowered because the dielectric constant of the solution near the surface is less than that of the bulk solution (O'Day et al., 1994). It has not been established which one of these processes predominates, however, it is possible that the three phenomena simultaneously influence precipitation reactions on surfaces. To insure that precipitation is truly a surface-induced phenomenon, experimental systems should be run at conditions undersaturated with respect to known phases. However, the solubility products of many possible phases are unknown, making it difficult to determine if such phases will

precipitate in a given system. This is particularly true for mixed cation hydroxides and coprecipitation reactions on surfaces (d'Espinose de la Caillerie et al., 1995; Towle et al., 1997; Scheidegger et al., 1998). The theories on the enhancement of surface precipitation by the three mechanisms mentioned above are discussed in more detail below.

As discussed above, Farley et al. (1985) presented a solid solution model to explain the continuum between precipitation and chemisorption onto solid surfaces. The model suggests that sorption is a process that includes solid dissolution, and then reprecipitation onto the surface. Thus, the formation of a surface complex involves the coprecipitation of both the ions dissolved from the sorbent, and the ions present in the bulk solution. Therefore, assuming the solid phase is a pure crystal and has unit activity (relative to the pure macrocrystal) is an inappropriate assumption, and invalidates solubility determinations based on the law of mass action, and ion activity products that do not account for surface activity. In addition, the resulting surface complex may not be compositionally homogeneous and completely free from inclusions, causing the activity of the solid phase to be even lower (Sposito, 1986). Sposito (1986) illustrated this idea by considering the dissolution of $CdCO_3$:



$$Ion \ Activity \ Product \ (IAP) = [Cd][CO_3] = K^{so}[CdCO_3(s)] \quad (1.2)$$

Where the brackets indicate ion activity. The activity of a pure solid is often considered to be one, however, if Cd forms a mixed precipitate (coprecipitate) with another ion in

solution, such as Ca, the result is not $[\text{CdCO}_3(\text{s})] = 1$, but $\text{Cd}_x\text{Ca}_y\text{CO}_3(\text{s})$ with activity < 1 . This means that the IAP (including Ca) at the surface of the precipitate is greater than the IAP of the bulk solution. Thus, $\text{Cd}_x\text{Ca}_y\text{CO}_3(\text{s})$ will precipitate at the surface before CdCO_3 . The actual IAP of a solid solution depends on the concentration of the foreign ion (Ca in the above case) in the solid mixture phase:

$$(IAP)_i = g_i X_i K_i^{so} \quad (1.3)$$

Where g_i is the activity coefficient of solid i , X_i is the mole fraction of solid i and K_i^{so} is the solubility product of the pure mineral i (Van Riemsdijk et al., 1991). From this equation one sees that a coprecipitate with one constituent present in minor amounts has a decreased solubility product with respect to the pure mineral.

The enhancement of precipitate formation on the surface may also be due to the reduction of the energy barrier necessary for nucleation processes to occur in an aqueous solution. This is a factor of the lattice dimensions of the solid, and those of the precipitate to be formed, i.e., a steric interaction (McBride, 1991). The result of surface nucleation sites is that the extent of supersaturation required for precipitation is decreased. However, there may be other important factors contributing to surface nucleation interactions. For example Fendorf et al. (1992) observed Al surface precipitates on MnO_2 using high resolution transmission electron microscopy (HRTEM), but not on TiO_2 under the same conditions (undersaturated with respect to the most likely Al hydroxide precipitates, and equivalent surface coverages). If promotion of surface precipitation below saturation was a result of the presence of nucleation sites then one

would expect to see precipitates on both surfaces. Thus, another factor inhibited surface precipitate formation on the TiO_2 , i.e., steric hindrances between the two surfaces.

The dielectric constant of the solution at the interface of a solid is much less than it would be in the bulk solution (Hiemenz, 1986). This is a result of the surface charge aligning the dipoles of the water layers nearest the surface. This phenomenon is called dielectric saturation, and results in a dielectric constant an order of magnitude or less in the first few angstroms of the surface (McBride, 1994). The activity of individual ions in solution is inversely proportional to the dielectric constant of water.

Consequently, near the surface the lowered dielectric constant of the water causes an increased ion activity, and the IAP near the surface will exceed that of the bulk solution. O'Day et al. (1994) used a more direct approach to this concept that calculates the change in the free energy near the surface as a function of the dielectric constant using the Born charging equation for a spherical ion. However, calculations for sorption of Co on kaolinite revealed that the average surface dielectric constant is not low enough to account for surface precipitation of a pure hydroxide phase as the predominant mechanism of sorption. Thus, if surface precipitation was the mechanism of sorption, then either the value of the dielectric constant near the surface was incorrect (possible since dielectric constants near surfaces are difficult to determine), or precipitation was enhanced by one of the aforementioned mechanisms (O'Day et al., 1994).

Regardless of the mechanism, surface precipitation is an important process affecting trace metal reactions with natural materials. Since surface precipitation kinetics can be slow, the extent of precipitation and subsequent dissolution of surface precipitates

are affected by residence time; thus, they are important slow kinetic mechanisms which can control the fate of trace elements in the environment.

1.2.4 Sorption Mechanisms Conclusion

In section 1.2 three sorption mechanisms have been discussed: diffusion, adsorption processes, and precipitation reactions on surfaces. While evidence exists that suggests all three mechanisms occur, the slow sorption mechanism occurring in a particular system is highly dependent on the prevailing environmental conditions, e.g., solution pH, sorbent characteristics, ionic strength, trace metal characteristics, dissolution rate of the solid, and the microporosity of the solid.

When predicting the transport of trace elements in the vadose zone researchers must know the kinetics of sorption and desorption behavior. If slow kinetics are controlling these mechanisms then reaction-transport models should include such chemical processes. This will result in more accurate predictions and improved management of existing and potential risks. In addition, if the mechanism responsible for slow sorption or desorption is known, researchers can design remediation strategies more efficiently. This may include mobilizing or immobilizing contaminants based on the pH of the soil solution, treating the soil with chelating ligands, or creating treatments for specific exposure times based on the kinetics of the reactions.

In section 1.2 several methods used for the determination of mechanisms have been presented. With the rapid advancement of technology the future should bring an even better understanding of soil sorption mechanisms and kinetic processes. It is critical

that researchers combine their efforts with those in related fields so that the most contemporary, and valid models can be developed and employed to predict the fate of contaminants in the environment.

1.3 Literature Review of the Chemistry of Pb in the Environment

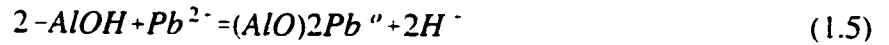
Lead is a heavy metal with an atomic weight of 207.2, in its neutral state it contains 82, neutrons, protons and electrons. In aquatic systems Pb usually loses two of the 6p electrons giving it a net charge of +2. The remaining $6s^2$ electrons are the outer shell electrons that exist as a lone pair of electrons. This lone pair has significant influences on the reactivity and coordination of Pb^{2+} ions. Lead can also lose both 6s electrons under severe oxidizing conditions giving it a net positive charge of +4. Lead (IV) is not very stable in most environments, thus, the divalent form usually controls the fate of Pb in aqueous geochemical conditions. Since Pb is a strongly sorbed atom, and its solubility is low at relevant pH values, most natural waters have low concentrations of aqueous Pb. In fact, a significant fraction of Pb in waterways may exist in an undissolved state, and is being transported as colloidal particles (Hem, 1976). Thus an understanding of the interactions between aqueous Pb species and solid surfaces is critical.

The solution concentration of Pb in natural waters with pH near seven is normally less than 10 $\mu\text{g/L}$ (Hem, 1976). The common species of aqueous Pb in acid soils are Pb^{2+} , organic-Pb, $PbSO_4^0$ and $PbHCO^{3+}$, and for alkaline soils $PbCO_3^0$, $PbHCO^{3+}$, organic-Pb, $Pb(CO_3)_2^{2-}$, and $PbOH^+$ (Sposito, 1989). The behavior of Pb in solution is largely governed by the size (ionic radius = 1.2 Å), valence and electronegativity of the ion. These characteristics contribute to the strength and number of water molecules

surrounding the Pb atom (the hydration number for Pb is between five and 8)(Burgess, 1978). Lead is considered a type B ion, or a soft sphere ion, which means that the electron sheath is easily deformed by external charges making it more polarizable than type A ions. Another classification scheme (Sparks, 1995) considers Pb a soft acid, which corresponds to most type B ions. The hard and soft acid classification scheme predicts that a particular acid will have a strong affinity for its respective hard or soft base. This means that Pb will have a strong affinity to form covalent bonds with soft bases. Soft bases are atoms and molecules that have a low electronegativity, are Lewis bases, easily polarized, and easily oxidized.

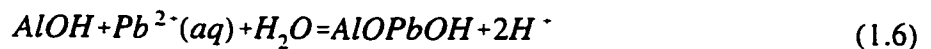
Many experiments have been conducted showing that soils form strong complexes with Pb (Zimdahl et al., 1977). This strong sorption is a result of Pb forming specific bonds with functional groups on oxides, edges of clay minerals, and organic matter. In addition Pb may form precipitates with inorganic C, Cl, P, and S anions. Since oxides and organic matter are common in soils, and have high surface areas, the fraction of Pb sorbed to these components is likely large. Hohl and Stumm (1976) observed that the ratio of protons released to the number of Pb atoms sorbed was between one and two for the oxide surface $\gamma\text{-Al}_2\text{O}_3$. They hypothesized that Pb sorption on surfaces could be modeled by treating the sorption sites similar to amphoteric functional groups in polyelectrolyte solutions. The production of protons was a result of Pb forming either a monodentate or bidentate sorption reaction, and equilibrium between these two reactions resulted in a non-integer value for the ratio of protons released to the number of Pb atoms

sorbed. Modeling the reaction and determining reaction constants required the proposal of two equations:



While their data were well represented by the proposed equations, their results were ambiguous because they suggested that the value of $H^+/(Pb \text{ consumed})$ was approximately 1.5 but the number of ligands used per Pb atom consumed was 1.1. The latter value indicates that very few bidentate complexes were formed. Thus, the accuracy of the complexation models was not completely accurate.

Davis and Leckie (1978) revamped the model of Hohl and Stumm (1976) and presented a complexation mechanism for Pb on oxides, which they claimed was more accurate. The mechanisms of sorption were represented by the triple layer model that accounts for specific protonation and deprotonation reactions on the surface (σ_o), outersphere chemisorption of cations and anions (σ_p), and diffuse layer co-ions attracted to the surface by the electrostatic potential of the surface (σ_d). Their modeling approach also included two equations, the first one was the same as that used by Hohl and Stumm (1976), but they replaced the bidentate forming reaction with another monodentate reaction that releases two protons:

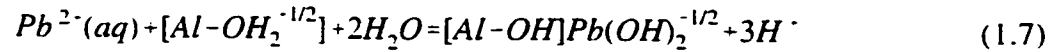


This complexation mechanism involves both the hydrolysis of the surface reactant site and a water from the Pb hydration sphere, i.e., one proton released from the surface (σ_o) and one from the hydration sheath of the Pb (σ_p or σ_d). The net effect is the sorption of an aquo-hydroxy-Pb species. This model improved the previously proposed model of Hohl and Stumm (1976) because it allowed for the ratio H^+/Pb consumed to be between one and two, and avoided the discrepancy encountered by the previous researchers, i.e., the bidentate sorption mechanism. The model fits to the data were good in both instances.; however, the mass balance for the Davis and Leckie (1978) approach was much better.

As already stated, solution chemistry fails to uniquely identify the sorption reactions occurring on solids. To gain a better understanding of the sorption mechanism Chisholm-Brause et al. (1990) performed XAS measurements of Pb sorption on $\gamma\text{-Al}_2\text{O}_3$. The lack of surface precipitates, or diffusion into the solid was indicated by minimal second neighbor metal atoms. This was determined by a weak beat pattern in the EXAFS spectra, and theoretical fits that require 0.3-1.5 second-neighbor Pb atoms, and 0.3-1.5 second-neighbor Al atoms. The authors' conclusions were based on the proposal that both surface precipitation and intra-particle diffusion would require several second-neighbor metal atoms. Thus, they concluded that the Pb must be adsorbed onto the mineral surface.

Bargar et al. (1997) analyzed the XAFS spectrum of Pb adsorbed on different surfaces of $\alpha\text{-Al}_2\text{O}_3$ at different pH values. From this analysis they concluded that Pb adsorption is primarily bidentate complexation on the edges of Al-octahedra and outer-

sphere complexation on the 0001 surface. Bargar et al. (1997) predicted that the predominant reaction for Pb adsorption on α -Al₂O₃ can be described by as follows:



Lead XAFS experiments have also been presented by Chisholm-Brause et al. (1990) and Roe et al. (1991). However, none of this research has investigated the effects of time and ionic strength on sorption mechanism; two critical aspects of metal sorption reactions that should be taken into account

To date no research has reported surface precipitation as a major mechanism controlling Pb sorption. One reason for this may be that the radius of Pb is much larger than that of Si and Al, the predominant atoms in many minerals (McBride, 1994). This means that a Pb-solid solution surface precipitate is not favorable for many minerals. The basis for the ionic radius being the controlling factor for solid solution formation is somewhat confusing since Pb sorption on calcite is not very strong despite the similar radius of Ca. On the other hand, Pb associates readily with hydroxy apatite in nature because it fits well into the Ca site of the mineral lattice (McBride, 1994). Experimental evidence for the ionic radius dependency for the lack of formation of a Pb solid solution was presented by Coughlin and Stone (1995). They noted that while Cu, Ni, and Co all experienced an increase in sorption onto goethite upon the addition of 1000 μ M Fe(II), Pb showed no change. They hypothesized that Pb did not fit into the Fe(II)/Fe(III) structure formed on the surface. As discussed earlier, this is similar to the hypothesis that

Ainsworth et al. (1994) presented for the lack of hysteresis in Pb sorption/desorption reactions on HFO.

While performing experiments on a pure mineral allows one to control the experimental system and elucidate mechanisms more easily, such mechanisms may or may not predominate in a soil, which is far from pure. Since XAS detects an average of all of the Pb neighbors and coordinations its applicability to real soils is limited. Nevertheless, Manceau et al. (1996) used EXAFS to speciate Pb in three different industrially contaminated soils. They proposed that the shape of the spectra was directly dependent on the nearest-neighbor and coordination geometry of the Pb atom within three to four angstroms. Thus, the spectra of known compounds can be used as a fingerprint to compare with the spectra of the soil. While interpretations made from this type of analysis are useful, care should be taken in making too many conclusions since analysis of spectra alone can be misleading in terms of the species present. In a soil contaminated from a gasoline manufacturer they proposed that most of the Pb was complexed to salicylate and catechol-type functional groups. In the soil collected from a battery manufacturing plant they suggested PbSO_4 and silica bound Pb were the predominant species present. Near a Pb-Zn smelter the soil-Pb was present in several different forms, preventing it from being identified.

Due to the low solubility of Pb minerals or salts, discrete particles of Pb are often found in soils. This is enhanced by the limited moisture found in many environments, or drying and wetting cycles. Lead contaminated soils can also arise from the application of Pb solids to the soil, e.g., Pb paint, batteries, or mining of Pb minerals.

Such minerals and solids can be the controlling phases in the solubilization of Pb and eventual toxicity to plants and animals. Link et al. (1994) used electron microprobe analysis to analyze two yard soils from Aspen, Colorado and Butte Montana. In the Aspen yard soil they detected that most of the Pb was present as liberated particles of PbCO_3 (cerussite). The Butte yard soil contained a complex mix of Pb-metal oxides, and some Pb phosphate or sulphate salts. Cotter-Howells et al. (1994) combined analytical transmission electron microscopy, X-ray diffraction, and EXAFS to determine the predominant mineralogy of a mine waste soil from the United Kingdom. They found that a large amount of the Pb was present as discrete particles of pyromorphite ($\text{Pb}_5(\text{PO})_3\text{Cl}$). Thus, while sorption/desorption reactions are important in controlling the fate of Pb in many soils, the presence of Pb solids may predominate as the source and sink of Pb in a particular soil. There are several controlling factors that determine the phase of the Pb present: moisture status or climate, origination of Pb in soil, native soil mineralogy, soil biological activity, and human influences.

1.4 Research Justification

Harmful chemicals such as Pb have been present in the environment at higher than natural levels for many years. However, often the toxicity and behavior of a particular chemical are evaluated based on short term experiments using a single ionic strength. From such experiments distribution coefficients and kinetic behavior are measured. The discrepancy in equilibrium conditions, and length of time a pollutant is in the environment, and the time experiments are conducted in the laboratory leads to inaccuracies in soil management and protection. This results in misguided expenditures

of both time and money on remediation and regulation. Thus, the objectives of this research are to investigate the kinetics and mechanisms of Pb sorption and desorption as a function of time, pH and ionic strength on natural minerals.

Hysteresis and slow desorption are often observed in soils and mineral studies. These phenomena are enhanced by aging. While many researchers have proposed likely mechanisms for such behavior, few have done little more than speculate a logical reason for their observations. In addition, most research is conducted on sorption reactions, ignoring the desorption reactions. This is surprising since once a soil is contaminated the controlling mechanism for its potential toxicity is either desorption, or dissolution. An understanding of the mechanisms responsible for behaviors such as hysteresis or slow sorption/desorption would be valuable information that would help explain the aging phenomenon, and provide a better understanding of the factors important for studying desorption reactions.

This research will provide fresh insights into the kinetics and mechanisms of metal sorption. With this information, researchers will better be able to predict the availability of a pollutant for transport, degradation, and possible remediation. In addition, this research will enhance the ability to make predictions and measurements of distribution coefficients and the kinetics of uptake and release will be improved. This information will save government, industry, and agriculture tremendous amounts of time and money, as well as make regulations more precise. In the long run, results from this research will contribute to the protection and health of the public, plants, animals, soils, and waterways.

1.5 Research Objectives

The objectives of the research presented in this dissertation are to:

1. Perform Pb sorption and desorption kinetics experiments on soils and soil minerals to determine the effects of residence time on sorption and release.
2. Monitor the change in Pb surface complexes on soil minerals as a function of incubation time using X-ray absorption fine structure (XAFS) spectroscopy to determine mechanistic information on slow sorption reactions.
3. Determine the effects of ionic strength and pH on Pb adsorption on clay minerals.
4. Determine if XAFS can be used to distinguish between sorption mechanisms such as inner- and outer-sphere complexes on the surfaces of clay minerals.
5. Measure the effects of soil organic matter on Pb sorption kinetic mechanisms using a stirred-flow reactor and XAFS.

1.6 Determining Sorption Mechanisms on Surfaces

There are two major approaches used to elucidate surface complexation mechanisms: macroscopic analysis by solution chemistry followed by interpretation of the data using predictive models, and microscopic observations of the surface complexes formed using advanced instrumentation techniques, i.e., microscopy or spectroscopy. From these two approaches has been borne a third technique: monitoring reactions as they are occurring on a microscopic level, e.g., time resolved spectroscopy. While these three techniques are all beneficial for predicting sorbate-sorbent interactions, none offers a definitive answer with respect to determining a mechanism. Thus, it is necessary to use several different methods of analysis to prove mechanisms, and understand sorption reactions.

Most sorption models used today are based on mechanistic assumptions, however, certain parameters for the models are usually unknown. Therefore, they must be estimated or circumvented by placing a fitting parameter into the equation. The problem with this approach is that the model is often no better than an empirical equation (an empirical equation provides little evidence that a particular mechanism is occurring). Despite this problem, many sorption models provide useful insight into complexation mechanisms, and cautious interpretations and conclusions are justified. Examples of such models are the modified triple layer, constant capacitance, and models used to predict diffusion limited processes (Hayes et al., 1986b; Ball et al., 1991; Goldberg, 1992). In a recent study by Manning and Goldberg (1996) the constant capacitance model was used to predict As(V), P, and Mo sorption reactions on goethite and gibbsite. In oxyanion competitive sorption studies they found that P and As(V) had similar affinities, while Mo had a lower relative affinity. The model they used represented the data well, however, it was indiscriminate in that it predicted both monodentate and bidentate sorption mechanisms equally well. Thus, mechanistic conclusions based on the model are uncertain, and should be validated using molecular scale techniques.

Spectroscopy offers scientists an opportunity to probe molecular and atomic structures, and determine details of the local environment. One popular spectroscopy used by soil and environmental scientists is X-ray absorption spectroscopy (XAS). This technique uses high energy x-rays to excite the electrons of a particular atom. The emission of energy from the atom is then detected using a fluorescence detector. The resulting spectra are divided into three regions: pre-edge, near-edge (X-ray absorption

near edge structure: XANES), and far-edge (extended X-ray absorption fine structure: EXAFS). Figure 1.3 illustrates the concepts behind XAFS theory. One of the unique features of the EXAFS technique is that ab-initio calculations of the theoretical backscattering off of atoms surrounding the central atom can be fit to the raw data. The equation describing this backscattering includes factors for the coordination number, backscatterer distance from the central atom, thermal and physical disorder, and phase shift. With such information speciation of the sorbed complex can be predicted and mechanisms hypothesized. An important advantage of XAS over many other spectroscopic methods is that samples can be analyzed without drying, which allows *in-situ* analysis of surface reactants. However, it is important to realize that XAS spectra do not provide precise measurements of an atom's local environment, but averages from all atoms within the sample (O'Day et al., 1994). Thus, careful sample preparations are critical if a reasonable level of certainty is to be achieved in XAS experiments.

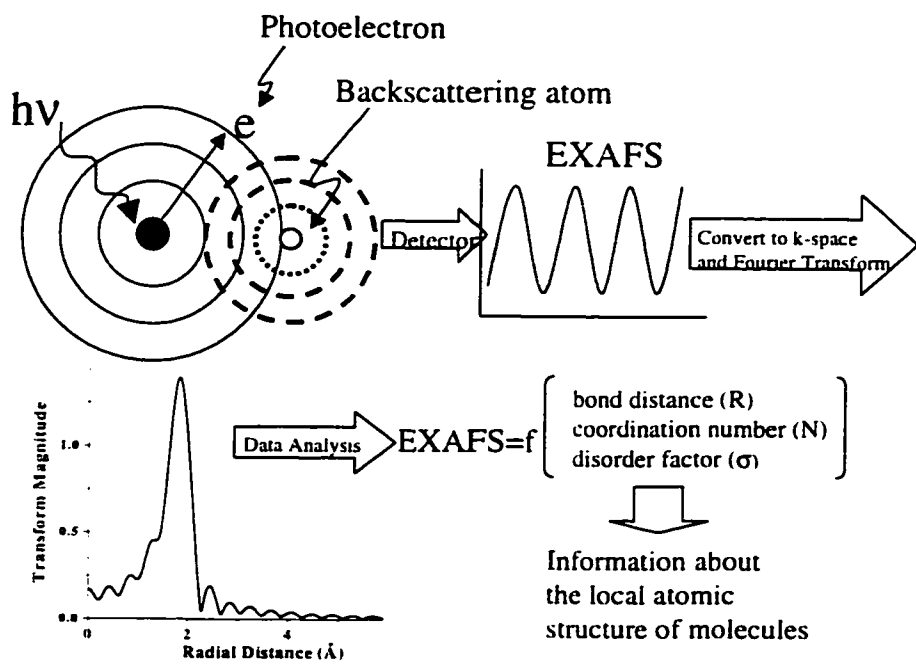


Figure 1.3 Schematic illustrating the theory of XAFS, and steps involved in data analysis.

A good example of carefully controlled experiments to elucidate sorption mechanisms is the work of Papelis and Hayes (1996) who studied Co sorption on montmorillonite using XAS. Because montmorillonite has both permanent charge sites and variable charge sites, and the sorption mechanism on each site is different, it was necessary for them to carefully control pH and ionic strength of the sorption samples to selectively sorb Co on the surfaces. The XAS spectra indicated that at neutral pH, and high ionic strength (0.1 M), the second neighbor of Co was another Co atom. This suggests that a polynuclear Co species is present at the surface hydroxyl sites, and that the high concentration of Na ions had displaced the Co ions from the permanent charged sites. This was confirmed by analyzing the XAS spectra at the same pH but lower ionic strength (0.001 M); results suggested that most of the Co was surrounded by waters in an octahedral coordination, as expected for outer-sphere complexes of Co.

The combination of kinetics and spectroscopy to do real time studies (time-resolved) is ideal since spectroscopy can provide information about the species type present on the surface, and kinetics can provide insight into the process over time that the sorbate and sorbent undergo to arrive at a particular surface product. As mentioned above, XAS is a particularly useful tool for such research since studies can be conducted under ambient experimental conditions, i.e., a high vacuum is not necessary, and samples do not have to be dried. To date, only a few time resolved spectroscopic studies have been reported in the literature (Waychunas et al., 1993; O'Day et al., 1996; Scheidegger et al., 1998).

The use of XAS has benefitted soil and environmental sciences tremendously, and resulted in many great advances in understanding the mechanisms by which metals interact with surfaces. The research presented in this dissertation uses XAS extensively as a tool to provide new information on the interactions occurring between Pb and soil mineral surfaces.

1.7 Literature Cited

- Ainsworth, C. C., J. L. Pilon, P. L. Gassman and W. G. Van Der Sluys. 1994. Cobalt, cadmium, and lead sorption to hydrous iron oxide: Residence time effect. *Soil Sci. Soc. Am. J.* 58: 1615.
- ASTDR. 1990. Lead.. Agency for Toxic Substance Disease Registry, Division of Toxicology. Atlanta, GA .
- Axe, L. and P. R. Anderson. 1997. Experimental and theoretical diffusivities of Cd and Sr in hydrous ferric oxide. *J. Colloid Interface Sci.* 185 (2): 436.
- Ball, W. P. and P. V. Roberts. 1991. Long-term sorption of halogenated organic chemicals by aquifer material. 2. Intraparticle diffusion. *Environ. Sci. Technol.* 25 (7): 1237.
- Bargar, J. R., G. E. Brown, Jr. and G. A. Parks. 1997. Surface complexation of Pb(II) at oxide-water interfaces: I. XAFS and bond-valence determination of mono- and polynuclear Pb(II) sorption products on Al-oxides. *Geoch. Cosmochim. Acta* 61 (13): 2617.
- Benjamin, M. M. and J. O. Leckie. 1981. Multiple-site adsorption of Cd, Cu, Zn, and Pb on amorphous iron oxyhydroxides. *J. Colloid Interface Sci.* 79 (1): 209.
- Blackburn, W. H. and W. H. Dennen. 1994. Principles of mineralogy. Wm. C. Brown Publishers, Dubuque, IA.
- Borg, R. J. and G. J. Dienes. 1992. The physical chemistry of solids. 1. Academic Press, Inc., London.
- Bruemmer, G. W., J. Gerth and K. G. Tiller. 1988. Reaction kinetics of the adsorption and desorption of nickel, zinc and goethite. I. Adsorption and diffusion of metals. *J. Soil Sci.* 39: 37.

- Burgess, J. 1978. Metal ions in solution. John Wiley and Sons, Chinchester, England.
- Burgos, W. D., J. T. Novak and D. F. Berry. 1996. Reversible sorption and irreversible binding of naphthalene and α -naphthol to soil: Elucidation of processes. *Environ. Sci. Technol.* 30 (4): 1205.
- Chisholm-Brause, C. J., K. F. Hayes, A. L. Roe, G. E. Brown, Jr., G. A. Parks and J. O. Leckie. 1990. Spectroscopic investigation of Pb(II) complexes at the γ -Al₂O₃/water interface. *Geoch. Cosmochim. Acta* 54: 1897.
- Cotter-Howells, J. D., P. E. Champness, J. M. Charnock and R. A. D. Patrick. 1994. Identification of pyromorphite in mine-waste contaminated soils by ATEM and EXAFS. *Eur. J. Soil Sci.* 45: 393.
- Coughlin, B. R. and A. T. Stone. 1995. Nonreversible adsorption of divalent metal ions (Mn, Co, Ni, Cu, and Pb) onto goethite: Effects of acidification, Fe addition, and picolinic acid addition. *Environ. Sci. Technol.* 29 (9): 2445.
- Davis, J. A. and J. O. Leckie. 1978. Surface ionization and complexation at the oxide/water interface. *J. Colloid Interface Sci.* 67: 90.
- d'Espinose de la Caillerie, J. B., M. Kermarec and O. Clause. 1995. Impregnation of γ -alumina with Ni(II) and Co(II) ions at neutral pH: Hydrotalcite-type coprecipitate formation and characterization. *J. Am. Chem. Soc.* 117: 11471.
- Dzombak, D. A. and F. M. M. Morel. 1990. Surface complexation modeling: Hydrous ferric oxide. 1. John Wiley & Sons, New York, NY.
- Farley, K. J., D. A. Dzombak and F. M. M. Morel. 1985. A surface precipitation model for the sorption of cations on metal oxides. *J. Colloid Interface Sci.* 106 (1): 226.
- Fendorf, S. E., G. M. Lamble, M. G. Stapleton, M. J. Kelley and D. L. Sparks. 1994. Mechanisms of chromium (III) sorption on silica. 1. Cr(III) surface structure derived by extended X-ray absorption fine structure spectroscopy. *Environ. Sci. Technol.* 28 (2): 284.
- Fendorf, S. E., D. L. Sparks and M. Fendorf. 1992. Surface precipitation reactions on oxide surfaces. *J. Colloid Interface Sci.* 148 (1): 295.
- Fuller, C. C., J. A. Davis and G. A. Waychunas. 1993. Surface chemistry of ferrihydrite: Part 2. Kinetics of arsenate adsorption and coprecipitation. *Geoch. Cosmochim. Acta* 57: 2271.

- Goldberg, S. 1992. Complexation models in soil chemical systems. D. L. Sparks (ed.) *Advances in agronomy*. Vol. 47. Academic Press, San Diego, CA.
- Griffin, R. A., W. A. Sack, W. R. Roy, C. C. Ainsworth and I. G. Krapac. 1986. Batch type 24-h distribution ratio for contaminant adsorption by soil materials. p. 390. *In* D. Lorenzen (ed.) *Hazardous and industrial solid waste testing and disposal*. Vol. 6. American Society for Testing and Materials, Philadelphia, PA.
- Grossl, P. R., D. L. Sparks and C. C. Ainsworth. 1994. Rapid kinetics of Cu(II) adsorption/desorption on goethite. *Environ. Sci. Technol.* 28 (8): 1422.
- Hayes, K. F. and J. O. Leckie. 1986a. Mechanism of lead ion adsorption at the goethite-water interface. p. 115. *In* J. A. Davis and K. F. Hayes (eds.) *Geochemical processes at mineral surfaces*. Vol. 323. American Chemical Society, Washington D.C.
- Hayes, K. F. and J. O. Leckie. 1986b. Mechanisms of lead ion adsorption at the goethite-water interface. p. 115. *In* J. A. Davis and K. F. Hayes (eds.) *Geochemical processes at mineral surfaces*. Vol. 323. American Chemical Society, Washington D.C.
- Hem, J. D. 1976. *Inorganic chemistry of Pb in water*. U. S. Department of the Interior, Washington.
- Hiemenz, P. C. 1986. *Principles of colloid and surface chemistry*. Marcel Dekker, Inc., New York, NY.
- Hohl, H. and W. Stumm. 1976. Interaction of Pb^{2+} with hydrous $\gamma-Al_2O_3$. *J. Colloid Interface Sci.* 55 (2): 281.
- Kim, Y., R. J. Kirkpatrick and R. T. Cygan. 1996. ^{133}Cs NMR study of cesium on the surfaces of kaolinite and illite. *Geoch. Cosmochim. Acta* 60 (21): 4059.
- Koskinen, W. C. and S. S. Harper. 1990. The retention process: mechanisms. p. 51. *In* H. H. Cheng (ed.) *Pesticides in the soil environment: processes, impacts, and modeling*. Soil Science Society of America, Madison, WI.
- Lehman, R. G. and R. D. Harter. 1984. Assessment of copper soil bond strength by desorption kinetics. *Soil Sci. Soc. Am. J.* 48: 769.

- Link, T. E., M. V. Ruby, A. Davis and A. D. Nicholson. 1994. Soil lead mineralogy by microprobe: an interlaboratory comparison. *Environ. Sci. Technol.* 28 (5): 965.
- Loehr, R. C. and M. T. Webster. 1996. Behavior of fresh vs. aged chemicals in soils. *J. Soil Cont.* 5 (4): 361.
- Manceau, A., M.-C. Bosset, G. Sarret, J.-L. Hazemann, M. Mench, P. Cambier and R. Prost. 1996. Direct determination of lead speciation in contaminated soils by EXAFS spectroscopy. *Environ. Sci. Technol.* 30 (5): 1540.
- Manning, B. A. and S. Goldberg. 1996. Modeling competitive adsorption of arsenate with phosphate and molybdate on oxide minerals. *Soil Sci. Soc. Am. J.* 60: 121.
- McBride, M. B. 1982. Cu^{2+} characteristics of aluminum hydroxide and oxyhydroxides. *Clays Clay Miner.* 30 (1): 21.
- McBride, M. M. 1991. Processes of heavy and transition metal sorption by soil minerals. p. 149. *In* G. H. Bolt, M. F. D. Boodt, M. H. B. Hayes and M. B. McBride (eds.) *Interactions at the soil colloid-soil solution interface*. Vol. 190. Kluwer Academic Publishers, Dordrecht, Netherlands.
- McBride, M. M. 1994. *Environmental chemistry of soils*. Oxford University Press, New York, NY.
- McLaren, R. G., D. M. Lawson and R. S. Swift. 1986. Sorption and desorption of cobalt by soils and soil components. *J. Soil Sci.* 37: 413.
- Noggle, J. H. 1989. *Physical chemistry*. Harper Collins, New York, NY.
- O'Day, P., G. A. Parks and G. E. Brown, Jr. 1994. Molecular structure and binding sites of cobalt (II) surface complexes on kaolinite from X-ray absorption spectroscopy. *Clays Clay Miner.* 42 (3): 337.
- O'Day, P. A., C. Chisholm-Brause, S. N. Towle, G. A. Parks and G. E. Brown, Jr. 1996. X-ray absorption spectroscopy of Co(II) sorption complexes on quartz ($\alpha\text{-SiO}_2$) and rutile (TiO_2). *Geoch. Cosmochim. Acta* 60 (14): 2515.
- Papelis, C. 1995. X-ray photoelectron spectroscopic studies of cadmium and selenite adsorption on aluminum oxides. *Environ. Sci. Technol.* 29: 1526.

- Papelis, C. and K. F. Hayes. 1996. Distinguishing between interlayer and external sorption sites of clay minerals using X-ray absorption spectroscopy. *Colloids and Surfaces* 107: 89.
- Pignatello, J. J. and B. Xing. 1996. Mechanisms of slow sorption of organic chemicals to natural particles. *Environ. Sci. Technol.* 30 (1): 1.
- Reed, B. E., P. C. Carriere and R. Moore. 1996. Flushing of Pb(II) contaminated soils using HCl, EDTA, and CaCl₂. *J. Env. Eng.* 122: 48.
- Roe, A. L., K. F. Hayes, C. Chisholm-Brause, G. E. Brown, Jr., G. A. Parks, K. O. Hodgson and J. O. Leckie. 1991. In situ X-ray absorption study of lead ion surface complexes at the goethite-water interface. *Langmuir* 7: 367.
- Scheidegger, A. M., G. M. Lamble and D. L. Sparks. 1996a. Investigation of Ni sorption on pyrophyllite: An XAFS study. *Environ. Sci. Technol.* 30 (2): 548.
- Scheidegger, A. M. and D. L. Sparks. 1996b. Kinetics of the formation and the dissolution of nickel surface precipitates on pyrophyllite. *Chem. Geol.* 132 (1-4): 157.
- Scheidegger, A. M., D. G. Strawn, G. M. Lamble and D. L. Sparks. 1998. The kinetics of mixed Ni-Al hydroxide formation on clays and aluminum oxides: A time-resolved XAFS study. *Geoch. Cosmochim. Acta* 62 (13): 2233.
- Smith, J. T. and R. N. J. Comans. 1996. Modeling the diffusive transport and remobilization of ¹³⁷Cs in sediments: The effects of sorption kinetics and reversibility. *Geoch. Cosmochim. Acta* 60 (6): 995.
- Sparks, D. L. 1989. *Kinetics of soil chemical processes*. Academic Press, Inc., San Diego, CA.
- Sparks, D. L. 1995. *Environmental soil chemistry*. Academic Press, San Diego, CA.
- Sparks, D. L. 1998. Kinetics of soil chemical phenomena: Future directions. P. M. Huang, D. L. Sparks and S. A. Boyd (eds.) *Future prospects for soil chemistry*. Soil Science Society of America, Special Publication, Madison, WI.
- Sposito, G. 1986. Distinguishing adsorption from surface precipitation. p. 217. *In* J. A. Davis and K. F. Hayes (eds.) *Geochemical processes at mineral surfaces*. Vol. 323. American Chemical Society, Washington D.C.
- Sposito, G. 1989. *The chemistry of soils*. Oxford University Press, New York, NY.

- Steinfeld, J. I., J. S. Francisco and W. L. Hase. 1989. Chemical kinetics and dynamics. Prentice Hall. Englewood Cliffs, NJ.
- Stumm, W. and J. J. Morgan. 1996. Aquatic chemistry, chemical equilibria and rates in natural waters. John Wiley & Sons, Inc., New York, NY.
- Stumm, W. and R. Wollast. 1990. Coordination chemistry of weathering: Kinetics of the surface-controlled dissolution of oxide minerals. *Reviews of Geophysics* 28 (1): 53.
- Swift, R. S. and R. G. McLaren. 1991. Micronutrient adsorption by soils and soil colloids. p. 257. *In* G. H. Bolt, M. F. D. Boodt, M. H. B. Hayes and M. B. McBride (eds.) *Interactions at the soil colloid-soil solution interface*. Vol. 190. Kluwer Academic Publishers, Dordrecht, Netherlands.
- Towle, S. N., J. R. Bargar, G. E. Brown, Jr. and G. A. Parks. 1997. Surface precipitation of Co(II)(aq) on Al₂O₃. *J. Colloid Interface Sci.* 187: 62.
- Van Riemsdijk, W. H. and S. E. A. T. M. Van der Zee. 1991. Comparison of models for adsorption, solid solution and surface precipitation. p. 241. *In* G. H. Bolt, M. F. D. Boodt, M. H. B. Hayes and M. B. McBride (eds.) *Interactions at the soil colloid-soil solution interface*. Vol. 190. Kluwer Academic Publishers, Dordrecht, Netherlands.
- Veith, J. A. and G. Sposito. 1977. On the use of the Langmuir equation in the interpretation of "adsorption" phenomena. *Soil Sci. Soc. Am. J.* 41: 697.
- Waychunas, G. A., B. A. Rea, C. C. Fuller and J. A. Davis. 1993. Surface chemistry of ferrihydrite: Part I. EXAFS studies of the geometry of coprecipitated and adsorbed arsenate. *Geoch. Cosmochim. Acta* 57: 2251.
- Zimdahl, R. L. and R. K. Skogerboe. 1977. Behavior of lead in the soil. *Environ. Sci. Technol.* 11: 1202.

Chapter 2

Kinetics and Mechanisms of Pb(II) Sorption and Desorption at the Aluminum Oxide-Water Interface

2.1 Abstract

The fate of Pb in the environment is highly dependent on sorption and desorption reactions onto solid surfaces. In this study Pb sorption and desorption kinetics on γ -Al₂O₃ at pH=6.50, I=0.1 M, and [Pb]_{initial}=2mM were investigated using both macroscopic and spectroscopic measurements. X-ray absorption fine structure (XAFS) spectroscopy revealed a Pb-Al bond distance of 3.40 Å, consistent with an inner-sphere bidentate bonding mechanism. XAFS results show no change with time in the average local atomic structure surrounding the Pb, and no indication of the formation of Pb surface precipitates. Adsorption kinetics were initially fast resulting in 76% of the total sorption occurring within 15 min, followed by a slow continuous sorption reaction likely resulting from diffusion through micropores. Desorption at I=0.1 M, and pH=6.50, was studied using a cation exchange resin as a sink for Pb (aq). Under these conditions Pb desorption was 98% reversible within 3 days of incubation time. Furthermore, desorption and adsorption kinetics demonstrated similar trends, a fast reaction followed by a slow reaction. The use of spectroscopy combined with adsorption and desorption kinetic studies has revealed important information on the interaction between Pb and Al

(hydr)oxides. This information is valuable for predicting the fate of Pb in the environment.

2.2 Introduction

The reaction of metals at the solid-solution interface plays an important role in determining their fate in the environment. In the past, researchers have focused on determining adsorption distribution coefficients (K_d), sorption capacity, and the pH dependence of metal sorption. Often these studies were based on short reaction periods, for example, 24 h. However, in natural systems reactions can continue for days, months, or years (Sposito, 1989; Steinfeld et al., 1989; Papelis et al., 1995; Sparks, 1995). In addition, researchers often neglect desorption reactions, assuming that sorption and desorption rates are the same. However, desorption can often be much slower, and sorption reactions are often nonreversible (Harter, 1991). This may be a reason for the commonly observed hysteresis (Verburg et al., 1994).

Metal sorption at the mineral/water interface is often initially fast followed by a decrease in the sorption rate (Lehman et al., 1984; Sparks, 1989; Harter, 1991; Fuller et al., 1993; Papelis et al., 1995; Smith et al., 1996; Axe et al., 1997; Scheidegger et al., 1998). Three possible mechanisms for the slow reactions have been proposed: diffusion into micro-pores of solids, followed by sorption onto interior sites; sorption to sites of lower reactivity; and surface precipitation (Fuller et al., 1993; Papelis et al., 1995; Loehr et al., 1996; Scheidegger et al., 1996; Axe et al., 1997; Towle et al., 1997). Distinguishing between these mechanisms based on macroscopic experiments alone is

difficult. One approach used to address these difficulties is to investigate sorption mechanisms using spectroscopy which allows reactions to be studied at a molecular level.

In the past several years the use of X-ray absorption spectroscopy (XAS) to study Pb sorption reactions has provided important mechanistic information (Chisholm-Brause et al., 1990; Roe et al., 1991; Bargar et al., 1996; Manceau et al., 1996; Bargar et al., 1997a; Hesterberg et al., 1997). Bargar et al. (1997a) studied Pb sorption onto α -Al₂O₃ (corundum). They concluded that the Pb sorption mechanism was primarily bidentate edge-sharing complexes (inner-sphere). Bargar et al. (1996) also used grazing incident XAS and found that Pb formed outer-sphere bonds on the 0001 plane of α -Al₂O₃. This research has provided evidence that Pb sorption is heterogeneous, and involves several different mechanisms. Since the sorption mechanisms vary, it is likely that the rates of the sorption mechanisms are different, and there may be slow reactions which are not measured under short reaction periods. Thus, in this study we have expanded the investigation of Pb sorption mechanisms on Al (hydr)oxides by combining kinetic and spectroscopic measurements so that possible changes in reaction mechanisms can be distinguished.

The combination of kinetics and spectroscopy to do real time sorption studies (time-resolved) is ideal, since spectroscopy can provide direct information on the type of species present at the surface, and kinetics can provide insight into the processes that the sorbate and sorbent undergo to reach equilibrium (Waychunas et al., 1993; Hunter et al., 1994; O'Day et al., 1994; Sparks, 1995; O'Day et al., 1996; Scheidegger et al., 1998). Scheidegger et al. (1998) combined kinetics and XAS and showed that the formation of

mixed Ni/Al-hydroxide surface precipitates was one of the mechanisms responsible for slow Ni sorption on montmorillonite. To date, the formation of mixed precipitates has not been observed as a sorption mechanism for Pb sorption on Al (hydr)oxides over relatively short time periods. The formation of a solid solution is not likely since the radius of Pb is too large to substitute for Al in a mineral structure (Valcheva et al., 1995; Bargar et al., 1997a). However, surface precipitates may occur in systems that are undersaturated with respect to the (hydr)oxide species (Towle et al., 1997). Since precipitation is a slower process than adsorption, and the surface can affect solubility constants, precipitation has not been ruled out as a possible sorption mechanism for Pb on γ -Al₂O₃ in samples incubated for extended times.

The objectives of this study were to investigate the kinetics and mechanisms of Pb sorption and desorption on γ -Al₂O₃ over incubation periods longer than the traditional 24 h, including sorption reversibility, and the stability of sorbed Pb. Both macroscopic kinetic experiments, and time resolved XAFS measurements were conducted. The information presented in this study will provide insights into the mechanisms of Pb sorption on γ -Al₂O₃ that are relevant to the long exposure times that exist in the environment, and will help with modeling Pb sorption reactions on mineral surfaces.

Aluminum minerals play an important role in the sequestration and immobilization of trace elements in the environment (Goldberg et al., 1995). They possess amphoteric surface aluminol functional groups that form chemical bonds with many heavy metals, including Pb (Hohl et al., 1976; Kinniburgh, 1976; Davis, 1978;

Goldberg et al., 1995). In nature γ - Al_2O_3 is found only under high pressure and high temperature conditions. However, the surface of this mineral completely hydrates when exposed to moisture, creating a layer of chemisorbed water along the basal plane of the mineral (Knozinger et al., 1985; Goldberg et al., 1995; Bargar et al., 1997b). Thus, the hydrated surface of γ - Al_2O_3 is similar to Al hydroxide minerals commonly found in soils, such as, gibbsite, bayerite and boehmite. Therefore, γ - Al_2O_3 is a useful mineral for simulating reactive surfaces occurring in the environment.

2.3 Experimental Methods

2.3.1 Materials.

The mineral γ - Al_2O_3 was obtained from Degussa Inc. (Akron, OH). Other than freeze drying for accurate weight measurements, the γ - Al_2O_3 was used as received. The γ polymorph of Al_2O_3 is a synthetic mineral. It is ideal for experimental work since it is well characterized, it can be commercially obtained in a relatively pure state (greater than 99.6% is Al_2O_3 , structure confirmed by X-ray diffraction) and it has a large surface area ($\sim 100 \text{ m}^2 \text{ g}^{-1}$) allowing for a high metal loading level that is necessary for spectroscopic (XAFS) measurements.

All solutions were made with ACS reagent grade chemicals and distilled deionized (D.I.) H_2O . In order to eliminate CO_2 all experiments were conducted in a glove box with an N_2 atmosphere. Temperature was maintained at 25°C .

2.3.2 Sorption Kinetics Experiments.

Prior to the addition of the Pb solution, a suspension of 13.3 g L^{-1} of the $\gamma\text{-Al}_2\text{O}_3$ was preequilibrated for 24 h at $\text{pH}=6.50$ in background electrolyte (stirring at 350 rpm). The background electrolyte solution consisted of a mixture of NaNO_3 and 0.075 M MES (2-[N-Morpholino] ethane sulphonic acid) adjusted to $\text{pH}=6.50$ and total $I=0.1 \text{ M}$. MES is an organic buffer with a pK_a of 6.10. It has been shown that this buffer does not significantly complex with metals or interfere with metal sorption (Good et al., 1966; Baeyens et al., 1997). At the start of the kinetic experiment 10 mL aliquots from an 8 mM Pb stock solution ($I=0.1$ adjusted with NaNO_3) were added every 30 s until the $[\text{Pb}]=2 \text{ mM}$ and the $[\gamma\text{-Al}_2\text{O}_3]=10 \text{ g L}^{-1}$ (total suspension volume $=0.180 \text{ L}$). The suspension pH was then readjusted to $\text{pH}=6.50$ with $\sim 20 \mu\text{L}$ drops of 10 M NaOH . In order to avoid local oversaturation the very small drops were added while the suspension was being rapidly stirred. Periodically 5 mL samples were removed and immediately centrifuged at 11950 g for 3 min. The supernatant was filtered through a $0.2 \mu\text{m}$ filter and acidified with one drop ($\sim 20 \mu\text{L}$) of concentrated HNO_3 . The solution was then analyzed by inductively coupled plasma emission spectrometry (ICP) for total Pb. The amount of Pb sorbed was calculated from the difference between the initial and the final Pb concentration. During the first 24 h of the sorption experiment the suspension was stirred at 350 rpm with a Teflon stir bar, and subsequently the suspension was placed on an orbital shaker operating at a speed of $150 \text{ orbits min}^{-1}$. The sorption kinetics results represent data points from three separate experiments.

2.3.3 Desorption Experiments.

Desorption experiments were carried out using two different methods. In both methods desorption was started after 48 hours of sorption incubation time. This reaction time was chosen because the sorption reaction is >97% complete within this time. For the first method, 10 mL of the reacted suspension was centrifuged at 26890 g for 5 min. The supernatant was removed and replaced with 9.5 mL of buffered background electrolyte (I=0.1 M, NaNO₃ + MES, pH=6.50). The supernatant was collected and analyzed for total Pb. The total amount of desorbed Pb was calculated by subtracting the non-sorbed Pb entrapped in the paste (left over from the previous replenishment) from the total amount of Pb in solution. This replenishment was carried out every 24 h for 9 days. For the second method, a 5 mL aliquot of the reacted suspension was placed in a 10 mL centrifuge tube with 0.25 g of Dowex-HCR-42 Na saturated (16-40 mesh) cation exchange resin. The exchange capacity of the resin was 2.4 times greater than the total amount of Pb present in solution and on the sorbent. Periodically, samples were centrifuged and the supernatant was collected. Analysis of the supernatant solutions indicated that [Pb] was less than 5 μM (0.5% initial [Pb]). The resin was separated from the γ-Al₂O₃ by rinsing with D.I. H₂O over an 80 mesh sieve until the resin returned to its translucent color, suggesting that all of the solid (white color) had been removed from the resin. Finally the resin was placed in a centrifuge tube with 5 mL of 7 M HCl for 24 h to recover the Pb. The amount of Pb remaining on the surface at a given time was calculated as the difference between the initial amount of Pb added to the suspension minus the amount of Pb recovered from the resin. The following

observations were made regarding the reliability of the resin desorption method from independent experiments on a 2 mM Pb solution: 1) the resin removed >99% of the Pb from solution; 2) the acid recovered 97% of the total Pb; and 3) the amount of Pb removed from the resin by washing with D.I. H₂O was below detection limits. Corrections were made to the desorption samples for observation 2.

2.3.4 XAFS Analysis.

Samples analyzed by XAS were prepared independently of the sorption kinetic studies. All experimental conditions were the same except that pH was maintained at 6.50 by addition of 0.1 M base, rather than MES. Samples incubated for 1.5 and 6.5 h were prepared adjacent to the beamline with N₂ rapidly bubbling through the samples to eliminate CO₂. The wet γ -Al₂O₃ pastes were loaded into an Al sample holder and sealed in front and back with Kapton tape (CHR Industries). All samples were immediately cooled to 77 K by placing them in liquid N₂.

XAFS data acquisition of the Pb L_{III}-edge (13055) was conducted on beamline X-11A at the National Synchrotron Light Source (NSLS), Brookhaven National Laboratory, Upton, New York. The electron beam energy was 2.5 GeV and the maximum beam current was 300 mA. The monochromator used in this case consisted of two parallel Si(111) crystals with an entrance slit of 1 mm. The parallel crystal monochromator was detuned by reducing I₀ 25% at the Pb-edge. The XAS data were collected in fluorescence mode using a Stern-Heald type detector filled with Kr and equipped with an As filter (Lytle et al., 1984).

The XAFS data analysis was accomplished using the program MacXAFS 4.0 (Bouldin et al., 1995). The XAFS spectra were processed using the following procedure: 1) Multiple scans were merged and normalized relative to E_0 (determined from the inflection point of the derivative of the spectra) and step height; 2) the chi-function was extracted from the raw data using a linear pre-edge and a cubic spline post-edge consisting of 3 knots set at unequal distances, and converting the data from energy to k space; 3) the chi-function was then weighted by k^3 in order to compensate for dampening of the XAFS amplitude with increasing k ; 4) the data were Fourier transformed ($\Delta k=3.6-11.3 \text{ \AA}^{-1}$) to yield a radial structure function (RSF). For background removal (step 2) the positions of the knots were selected using the following criteria: 1) minimization of peaks in the region prior to the first major peak in the RSF, 2) minimization of oscillations in the spline derivative, and insuring nonconformity in oscillation phase between the spline derivative and spectra, and 3) maximizing the height of the primary O peak in the RSF without significantly dampening any other peaks. Once an optimum set of parameters was determined all sample spectra were processed in the same manner.

The XAFS k^3 weighted spectra were fit in R-space using the fitting routine in MacXAFS 4.0 (Bouldin et al., 1995). Background on the theories and procedures for fitting XAFS data can be found elsewhere (Stern, 1988). The particular details used in fitting the data are listed below. Single scattering theoretical spectra and phase shifts for Pb-Pb backscatterers, Pb-O backscatterers, and Pb-Al backscatterers were calculated using the FEFF6.0 code (Zabinski et al., 1997), with an input file based on a model of α -PbO (tetrahedral) (Leciejewicz, 1961) (generated with the program ATOMS) with two of

the Pb atoms at 3.69 Å replaced by Al. The values of the Debye Waller (σ^2) term for the second shell were fixed at 0.009 Å², which is the average of the σ^2 values from all sorption samples when they were allowed to vary on their own. This is justified by the following observations: when allowed to vary the standard deviation of the σ^2 was small (0.003 Å²) for all samples; there was no trend in the σ^2 for the samples incubated for different times; fixing the σ^2 reduced the number of free parameters in the fitting routine, and thus the uncertainties in the coordination number (N); and, 0.009 Å² is consistent with the value used by other researchers to fit Pb sorption data (Chisholm-Brause et al., 1990; Bargar et al., 1997a). The edge shift (E_0) for all shells was constrained to be equal. All other parameters were allowed to vary. An amplitude reduction factor was determined by fitting the theoretical single scattering O-shell to the same shell of the experimental spectra of a well characterized α -PbO. For both the experimental and theoretical spectra square windows were cut at equal values in the RSF. Based on a comparison of the theoretical α -PbO (Leciejewicz, 1961) and the experimental α -PbO (Table 2.1 and Figure 2.2) the accuracies of the interatomic distances (R) and N between Pb and the first shell O backscatterers can be estimated. In this case the accuracies are smaller than the confidence limits of the least-squares non-linear fitting procedure. Thus, the accuracies can be inferred from the precision values given in Table 2.1. Similarly, the accuracies of R and N for second shell Al backscatterers can be inferred from the precision of the fits of the second shell Pb atoms in the α -PbO (Bargar et al., 1997a).

2.4 Results and Discussion

2.4.1 Lead XAFS.

Figure 2.1 shows the background subtracted k^3 weighted chi-functions for the samples incubated for times of 1.5 h to 23 days, and the α -PbO. A strong sinusoidal beat pattern typical of first neighbor O-shell backscattering is observed for all sorption samples. The existence of multiple frequencies due to second shell backscattering would result in dampening or additive amplitude effects on the peaks, or the development of shoulders due to a distinct frequency from the major frequency. However, these characteristics are difficult to distinguish in the chi-function when their contributions are small.

The characteristic frequencies of the individual components that exist in the chi-function are more easily observed by Fourier transforming the spectra into radial structure functions (RSF). Figure 2.2 shows the RSF (uncorrected for phase shift) for the different samples, and the respective best fits that resulted from multiple shell fitting. Qualitative analysis of the chi-structure, and the RSF for the different samples does not reveal any significant differences between the samples incubated for different lengths of time. The lack of the development of any major second shells in the region between 3.0 and 4.0 Å in the RSF (based on the position of Pb-Pb shells in the RSF of α -PbO in Figure 2.2) suggests that a Pb surface precipitate is not occurring.

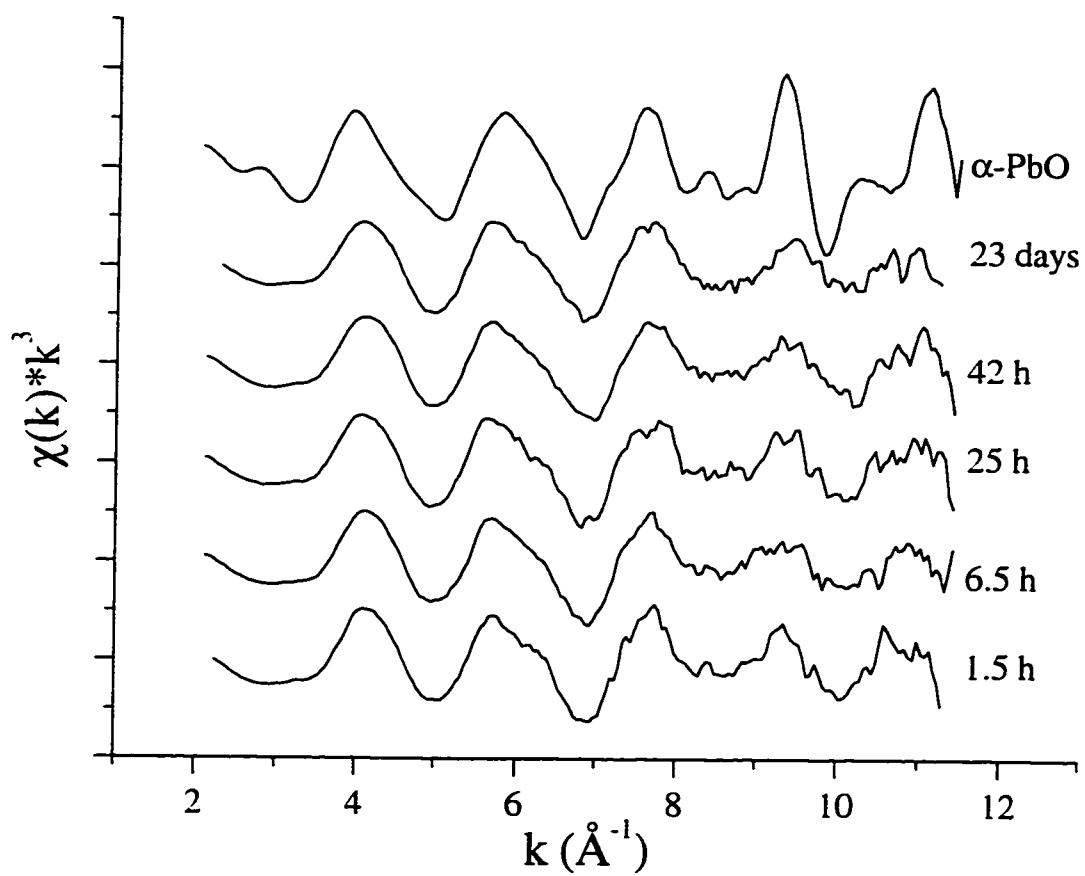


Figure 2.1 k^3 weighted normalized χ -functions for samples incubated for different lengths of time, and α -PbO (amplitude of α -PbO spectrum is $\frac{1}{2}$ actual).

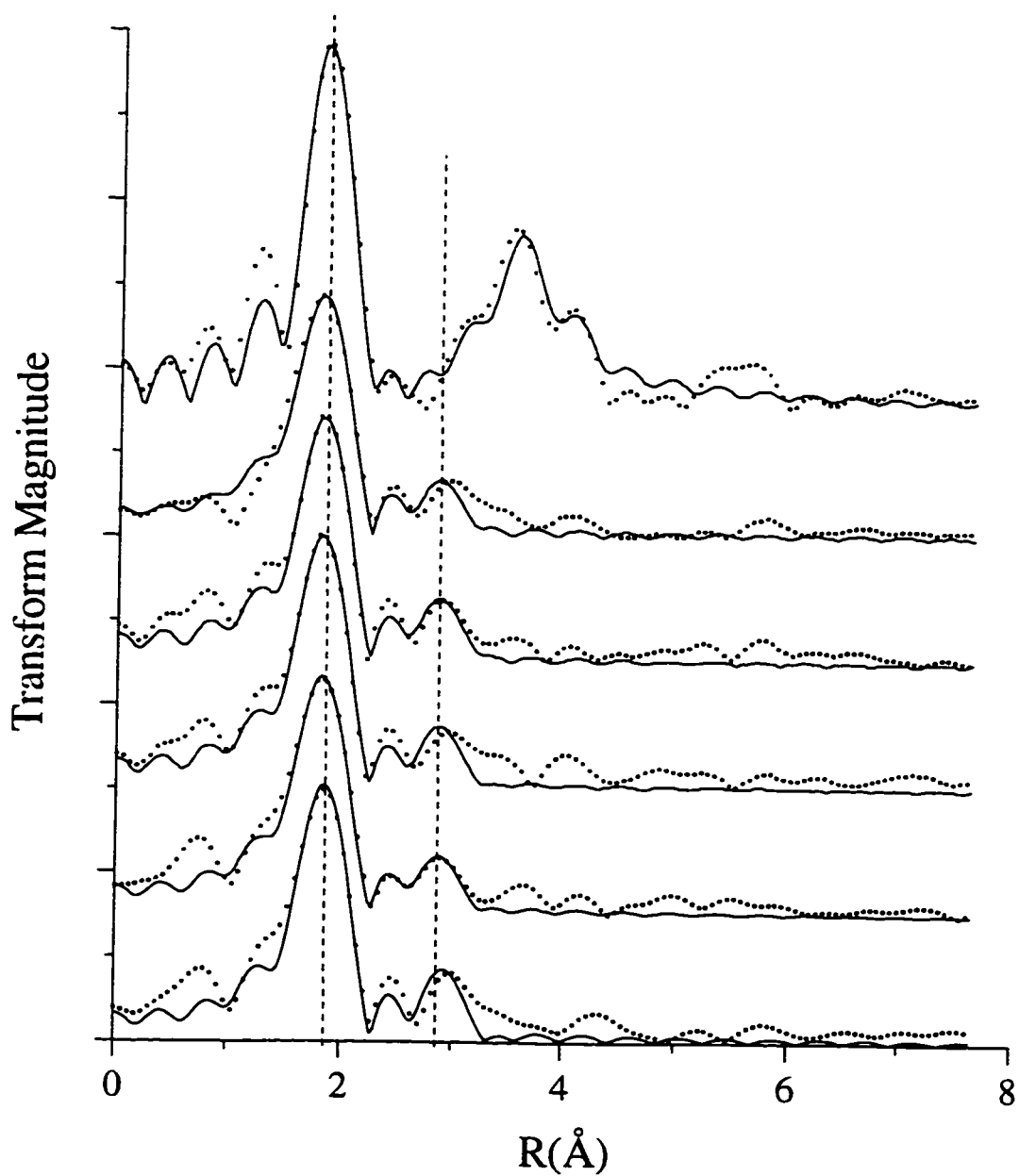


Figure 2.2 Fourier Transforms (RSF) of the chi-functions in Figure 2.1 (amplitude of α -PbO spectrum is $\frac{1}{2}$ actual). Vertical dashed lines are aligned at the center of the two major peaks used for fitting. The solid line is the theoretical multi-shell fit to the data, the dotted line represents the experimental data.

The best fits of the data were obtained by fitting two shells, the first shell containing an O atom and the second an Al atom. Attempts to fit Pb in the second shell, both with and without the Al atom, were unsuccessful. The fit of the theoretical RSF to the experimental RSF for $\Delta k(\text{\AA}^{-1})=3.6-11.3$ and $\Delta R(\text{\AA})=1.01-3.35$ is shown in Figure 1b for the different sorption samples. The results of the fit are presented in Table 2.1. The peak centered at $\sim 1.80 \text{\AA}$ in the RSF can be fit with 1.86-2.23 O backscatterers at $R=2.28-2.30 \text{\AA}$. The second peak centered at $\sim 2.90 \text{\AA}$ can be fit with 0.91-1.11 Al backscatterers at $R=3.38-3.43 \text{\AA}$. The RSF and best fit for the α -PbO are included for comparison.

Individual contributions to the two shells for the sample incubated for 6.5 h are shown in Figure 2.3. Three important points can be made from Figure 2.3: 1) the two major peaks in the RSF of the raw data are reasonably modeled by backscattering from first shell O and a second shell Al; 2) the small peak centered at $\sim 2.45 \text{\AA}$ in the raw spectra is not necessarily a contribution from another backscattering atom since it can be explained by the combined contributions from side lobes of the O and the Al backscatterers; and 3) various other small peaks located after the primary backscattering peak in the RSF exist that are most likely due to scattering from additional atoms present in small amounts in the second shell (e.g., Pb), combinations of side lobes from the two dominant peaks, noise in the data, and/or frequencies that exist in the spectra due to multiple scattering paths. Attempts to resolve point three by fitting were unsuccessful due to the low amplitude of the peaks, and the limited capabilities of fitting routines when too many free variables are introduced.

Table 2.1 Structural parameters for Pb adsorption on γ -Al₂O₃ samples reacted for different lengths of time and α -PbO derived from the best-fit results of the XAFS experimental data with theoretical phase shifts and amplitude functions.

Reaction Time	Pb-O shell			Pb-Al shell			E ^o eV
	R (Å) ^{b,c}	N ^{e,f}	σ^2 (Å ²) ^d	R (Å) ^c	N ^e	σ^2 (Å ²) ^h	
1.5 h	2.30	1.9	0.0051	3.43	1.1	0.009	0.61
6.5 h	2.29	2.1	0.0069	3.39	0.9	0.009	2.75
25 h	2.29	2.0	0.0056	3.40	1.0	0.009	4.28
42 h	2.28	1.9	0.0052	3.38	1.1	0.009	4.25
23 days	2.28	2.2	0.0069	3.38	0.9	0.009	5.71
α -PbO'	2.28	4.1	0.0030	3.67/ 3.90'	6.2/ 4.0'	0.006 ^k	2.70

^a Phase shift; ^b Interatomic distance; ^c Coordination number; ^d Debye Waller factor; Fit quality confidence limits for parameters: ^e $\pm 1\%$, ^f $\pm 20\%$, ^g $\pm 40\%$; ^h Fixed; ⁱ Fit with 3 backscattering atoms: O, Pb, Pb; ^j Slash is a demarcation between Pb backscatterers; ^k Constrained to be equal for both Pb atoms.

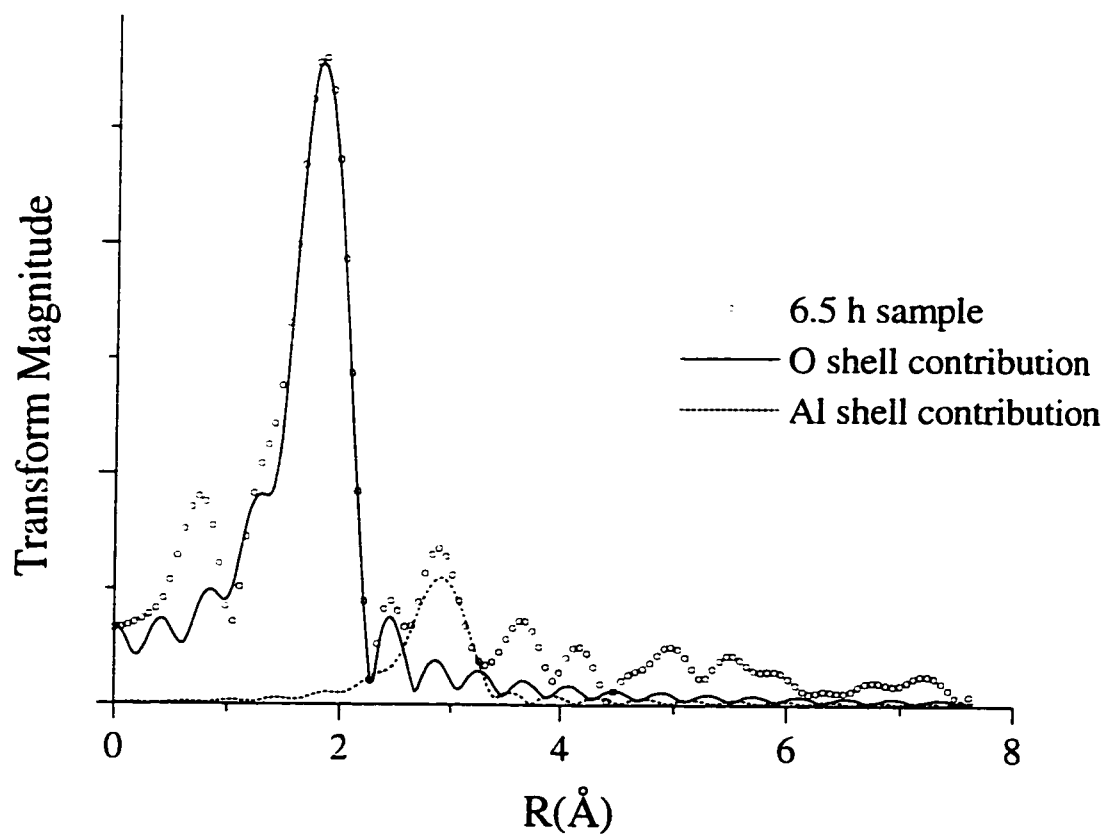


Figure 2.3 RSF of sample incubated for 6.5 h with the individual shell contributions.

The structural parameters obtained from the XAFS are similar to those presented by Bargar et al. (1997a), who hypothesized that the bonding coordination environment for Pb consisted of three hydroxyls arranged in a distorted trigonal pyramid (Bargar et al., 1997a). Using known Al-O bond distances (average from the literature=1.91 Å (Bargar et al., 1997a)) and experimental Pb-O distances (average R=2.29 Å), the calculated maximum Pb-Al bond distance should be 3.42 Å when Pb is sorbed as an inner-sphere complex sharing hydroxyl ligands on the edge of an octahedral complex (Bargar et al., 1997a). The average Pb-Al bond distance of all of the samples in these experiments is 3.40 Å. Thus, we conclude that the majority of Pb in our experiments is adsorbed as an inner-sphere bidentate edge complex. Increasing incubation time had no noticeable effect on the local atomic structure of the sorbed Pb. The possibility of surface precipitation at pH=6.50 and surface loadings of 1.10 to 1.27 $\mu\text{mole m}^{-2}$ can be ruled out since a significant peak was not observed in the RSF, nor were we able to successfully fit Pb as a backscattering atom using the multi-shell fitting procedure.

2.4.2 Adsorption Kinetics.

The results of the adsorption kinetics experiment are presented in Figure 2.4. Within 15 min a very fast adsorption reaction occurred accounting for 76% of total adsorbed Pb. Following the initial fast reaction the adsorption reaction continued for ~30 h, after which only a small amount of additional sorption occurred (~2.5%). After 600 h ~63% of the Pb initially added to the suspension had been adsorbed.

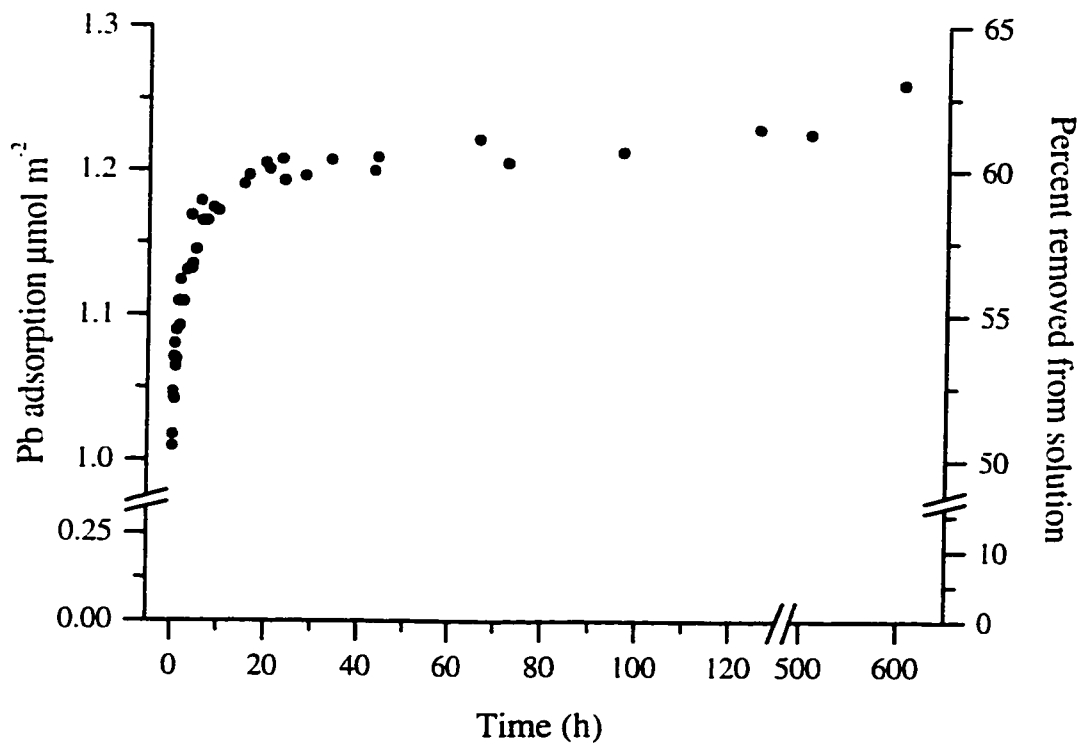


Figure 2.4 Lead adsorption kinetics on $\gamma\text{-Al}_2\text{O}_3$ at $\text{pH}=6.50$, $I=0.1\text{ M}$, and $[\text{Pb}]_{\text{initial}}=2.0\text{ mM}$, surface area = $100\text{ m}^2\text{ g}^{-1}$. Data points are from three separate experiments.

Attempts to fit the data with a linear form of the steady-state first-order reaction equation were unsuccessful, providing evidence that the reaction kinetics data represent separate reaction mechanisms. Fast Pb adsorption reactions on $\gamma\text{-Al}_2\text{O}_3$ have been studied using relaxation kinetic methods (reaction times on the order of seconds) (Hayes et al., 1986; Yasunaga et al., 1986). Results of these studies suggest that fast reactions are most likely a chemical reaction with surface sites on $\gamma\text{-Al}_2\text{O}_3$ that are readily accessible (Hayes et al., 1986; Yasunaga et al., 1986). Secondary slow reactions have been observed for metal sorption on many different (hydr)oxides (Fuller et al., 1993; Papelis et al., 1995; Loehr et al., 1996; Scheidegger et al., 1996; Axe et al., 1997; Towle et al., 1997). Hayes and Leckie (1986) reported that sorption of Pb on goethite continued for times as long as hours to days. Similarly, Benjamin and Leckie (1981) observed that sorption of several heavy metals (including Pb) on amorphous iron oxyhydroxide was initially fast followed by a much slower second step.

As mentioned above, there are three possible explanations for the slow reaction: diffusion to internal sites, surface precipitation, or adsorption to sites that have a slower reaction rate due to low affinity (Fuller et al., 1993; Loehr et al., 1996; Scheidegger et al., 1996; Axe et al., 1997; Towle et al., 1997). In this experiment a third possibility for the slow sorption reaction is the formation of additional sorption sites due to the slow transformation of $\gamma\text{-Al}_2\text{O}_3$ into a lower energy solid phase (Dyer et al., 1993). Surface precipitation can be ruled out based on the XAFS results presented earlier. However, the other two slow sorption mechanisms are difficult to isolate.

Diffusion-limited sorption is likely occurring since the γ - Al_2O_3 structure is a microcrystalline material consisting of small connected particles with a large internal surface (Kinniburgh et al., 1981; Shriver et al., 1994). In addition the formation of stable aggregates during preequilibration can occur, creating physical barriers that restrict access to adsorption sites. The Schultze-Hardy rule predicts that for monovalent ions in a suspension of Al-hydrous oxide the critical coagulation constant is 0.05 M (Sposito, 1984). Since the γ - Al_2O_3 suspension was preequilibrated with an anion concentration well above this value (~ 0.1 M), coagulation is likely. Diffusion as a rate-limiting sorption mechanism was observed in the experiments of Papelis and colleagues (Papelis, 1995; Papelis et al., 1995) who employed kinetic experiments and X-ray photon spectroscopy (XPS) to show that the slow adsorption reaction of Cd and selenite onto porous alumina is a diffusion-controlled reaction.

In addition to slow diffusion occurring, slow reactions with aluminol sites may also occur. Lead hydrolysis and association reactions are generally thought to be fast (Hayes et al., 1986; Yasunaga et al., 1986). However, several different types of ligand sites exist on γ - Al_2O_3 (Bargar et al., 1997a), and sorption onto sites with large activation energies is possible (resulting in slower kinetics).

It can be concluded that Pb adsorption kinetics are biphasic, that is, an initially fast reaction is followed by a slow reaction. In this paper we have provided evidence that the slow sorption reaction is not a result of surface precipitation. However, the distinction between the other three mechanisms mentioned above would require additional experiments. The kinetic data in this paper does suggest that there exist a

significant slow Pb adsorption reaction on $\gamma\text{-Al}_2\text{O}_3$. Thus, when making predictions based on equilibrium this slow reaction step should be considered.

2.4.3 Desorption Experiments.

The desorption behavior of Pb from $\gamma\text{-Al}_2\text{O}_3$ using the replenishment method is presented in Figure 2.5. The results show that the Pb is steadily removed from the surface with each replenishment. After four replenishments the slope of the percent removed versus the number of replenishments decreases. This is likely due to the increased affinity by the surface for Pb as the adsorbed concentration decreases (nonlinear isotherm behavior). The replenishment experiments provide an indication of the strength of the Pb-surface bond. If the Pb is held strongly by the surface, little desorption would be expected over the time scale of the measurements due to an increased activation energy requirement. However, in this experiment 69% of the sorbed Pb was removed after 9 replenishments. It is likely that with additional replenishments all of the adsorbed Pb would be removed from the surface. Thus, we hypothesize that Pb is not forming strong bonds with $\gamma\text{-Al}_2\text{O}_3$ that would require large activation energies to break.

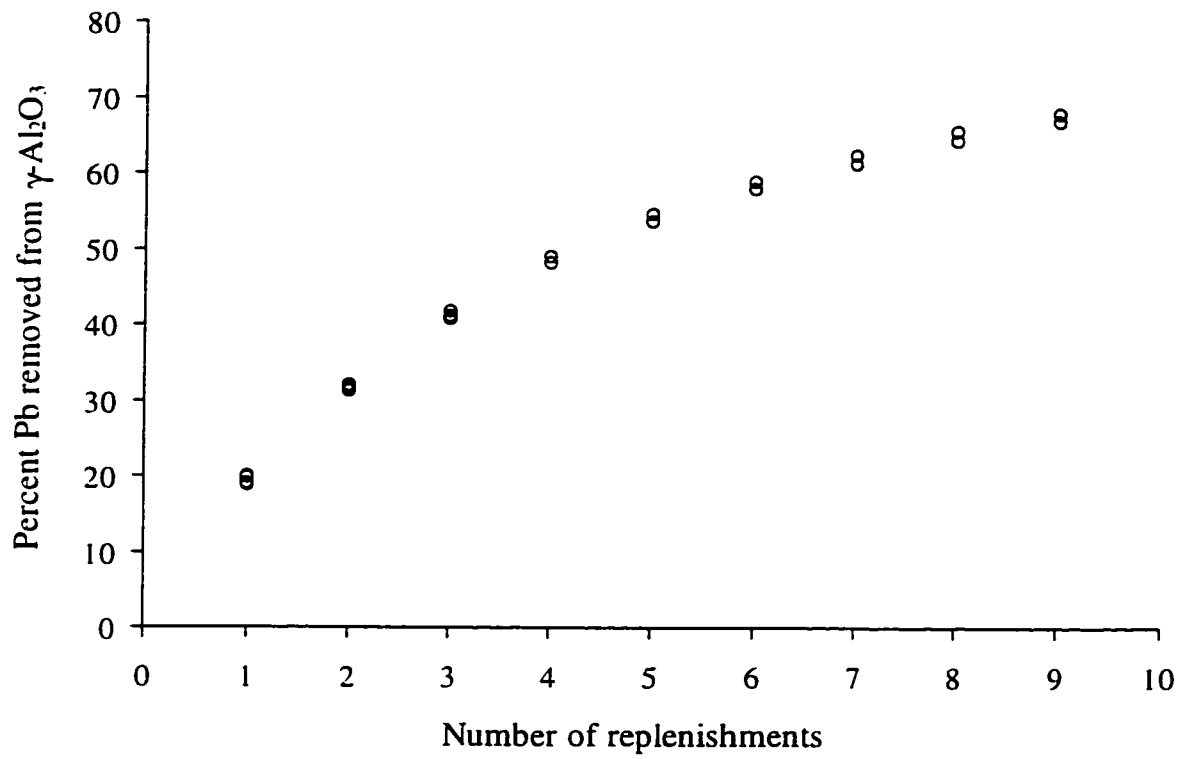


Figure 2.5 Desorption of Pb from $\gamma\text{-Al}_2\text{O}_3$ by replenishing background electrolyte every 24 h. Data points are from three separate experiments.

It is important to note that the data in Figure 2.5 do not necessarily represent the actual Pb desorption behavior. If equilibrium was reached in each replenishment then the results from the experiment would represent a reverse isotherm. If the system were far from equilibrium, so that back reactions were insignificant, the data would represent the desorption kinetic behavior. Neither of these conditions is present in this experimental system, but this experiment does show that Pb is readily released from the surface, suggesting that the activation energy for this process is small.

One useful technique for evaluating desorption kinetics is to drive the desorption forward by removing the products to avoid back reactions, for example, removing Pb^{2+} from the simplified desorption reaction $=SPb + 2H^+ \rightleftharpoons =SH_2 + Pb^{2+}$ (where $=S$ is a surface site). This simplifies the desorption kinetics since back reactions are eliminated (Amacher, 1991). The desorbed Pb can be removed from solution by using cation exchange resins that have a high affinity for the ion being desorbed. Figure 2.6 shows the results of the desorption kinetics using a Na-saturated resin as a sink for Pb (aq) to eliminate back reactions.

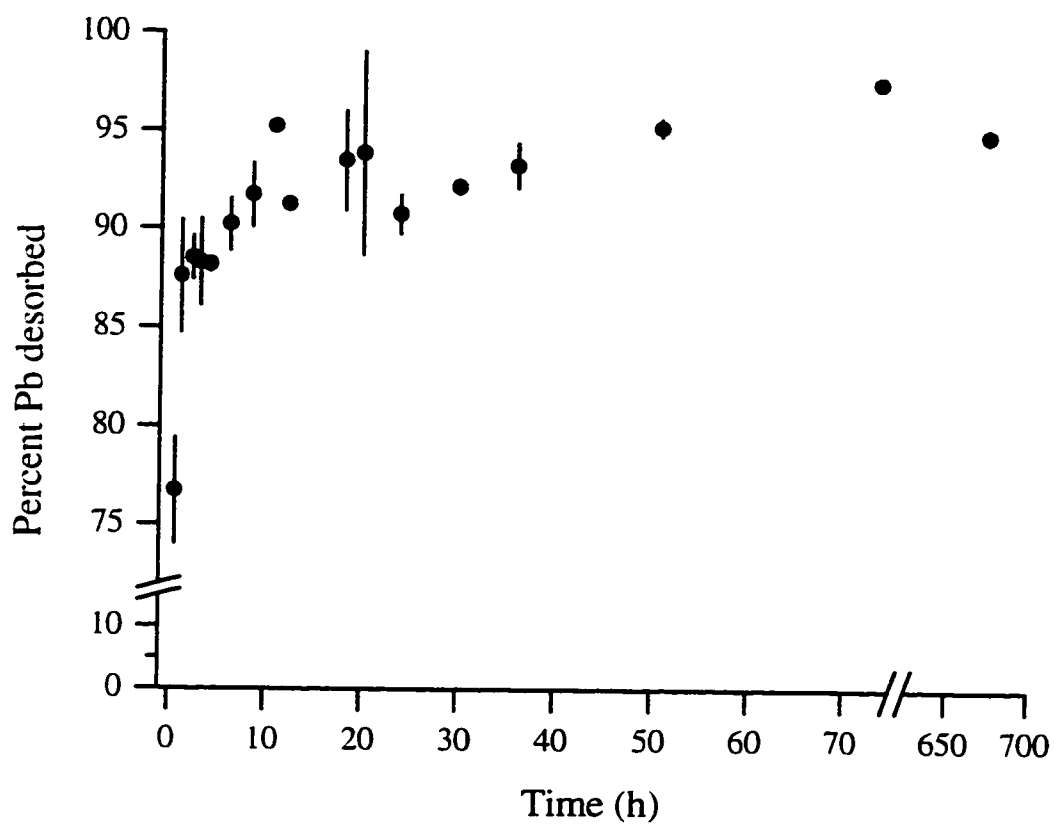


Figure 2.6 Lead desorption kinetics from γ - Al_2O_3 using Na-saturated resins, pH=6.50, I=0.1 M. Error bars are standard deviations of 3 samples.

Similar to the adsorption kinetics, the desorption kinetics show a biphasic type behavior: within 30 min 78% of the Pb is desorbed from the surface, followed by slow desorption continuing for 70 h, resulting in a recovery of 98% of the sorbed Pb. The mechanisms responsible for the fast and slow desorption kinetic behavior are likely the reverse reactions of the adsorption mechanisms: initially a fast desorption from sites readily available followed by a slow release from sites on the interior of the solid. This behavior suggests that diffusion limited sorption is responsible for the slow sorption reaction.

Resins are often used in studies to examine the availability, and potential leachability of ions in soils since they remove aqueous cations from solution (Sadusky et al., 1987; Skogley et al., 1996). In our experiments the resin was able to remove all of the aqueous Pb, causing the surface to release all of the sorbed Pb in an attempt to reestablish equilibrium. The ease with which the Pb was removed from the surface of the $\gamma\text{-Al}_2\text{O}_3$ suggests that the bond between Pb and aluminol sites is weak compared to the bond formed between Pb and the functional groups of the resin. Therefore, we hypothesize that adsorption onto Al-(hydr)oxide minerals may not be a significant mechanism for Pb retention in systems where other sorbents exist that can complex Pb more strongly (e.g., organic matter, clays, and carbonates).

The complete desorption of Pb from the surface is surprising since it is commonly thought that the bonds formed in inner-sphere sorption are relatively strong, and irreversible due to the higher activation energy required for desorption as compared to adsorption (McBride, 1991; McBride, 1994; Strawn et al., 1998, In Press). However,

these desorption experiments show that Pb is readily released from a surface with which it has formed a direct chemical bond. Gunneriusson et al. (1994) and Ainsworth et al. (1994) also found that Pb adsorbed onto goethite and hydrous iron oxide, respectively, is reversible with respect to pH.

2.5 Conclusion

The results of this study suggest three important points that will improve the capabilities of researchers to predict the fate of Pb in the environment: 1) the molecular environment of Pb sorbed onto γ -Al₂O₃ is stable when allowed to incubate for long periods, and does not involve the formation of Pb surface precipitates; 2) Pb adsorption is characterized by fast and slow reaction steps (after 30 h the reaction has slowed down considerably); and 3) Pb adsorption appears to be reversible provided that Pb desorption is carried out for a long enough time (~3 d in this case).

2.6 Literature Cited

- Ainsworth, C. C., J. L. Pilon, P. L. Gassman and W. G. Van Der Sluys. 1994. Cobalt, cadmium, and lead sorption to hydrous iron oxide: Residence time effect. *Soil Sci. Soc. Am. J.* 58: 1615.
- Amacher, M. C. 1991. Methods of obtaining and analyzing kinetic data. p. 19. *In* D. L. Sparks and D. L. Suarez (eds.) *Rates of soil chemical processes*. Vol. 27. Soil Science Society of America, Madison, WI.
- Axe, L. and P. R. Anderson. 1997. Experimental and theoretical diffusivities of Cd and Sr in hydrous ferric oxide. *J. Colloid Interface Sci.* 185 (2): 436.
- Baeyens, B. and M. H. Bradbury. 1997. A mechanistic description of Ni and Zn sorption on Na-montmorillonite. Part I: Titration and sorption measurements. *J. Cont. Hyd.* 27: 199.

- Bargar, J. R., G. E. Brown, Jr. and G. A. Parks. 1997a. Surface complexation of Pb(II) at oxide-water interfaces: I. XAFS and bond-valence determination of mono- and polynuclear Pb(II) sorption products on Al-oxides. *Geoch. Cosmochim. Acta* 61 (13): 2617.
- Bargar, J. R., S. N. Towle, G. E. Brown, Jr. and G. A. Parks. 1996. Outer-sphere Pb(II) adsorbed at specific surface sites on single crystal α -alumina. *Geoch. Cosmochim. Acta* 60 (18): 3541.
- Bargar, J. R., S. N. Towle, G. E. Brown, Jr. and G. A. Parks. 1997b. XAFS and bond-valence determination of the structures and compositions of surface functional groups and Pb(II) and Co(II) sorption products on single-crystal α -Al₂O₃. *J. Colloid Interface Sci.* 185: 473.
- Benjamin, M. M. and J. O. Leckie. 1981. Multiple-site adsorption of Cd, Cu, Zn, and Pb on amorphous iron oxyhydroxides. *J. Colloid Interface Sci.* 79 (1): 209.
- Bouldin, C., L. Furenlid and T. Elam. 1995. MacXAFS: An EXAFS analysis package for the Macintosh. *Phys. B* 208/209: 190.
- Chisholm-Brause, C. J., K. F. Hayes, A. L. Roe, G. E. Brown, Jr., G. A. Parks and J. O. Leckie. 1990. Spectroscopic investigation of Pb(II) complexes at the γ -Al₂O₃/water interface. *Geoch. Cosmochim. Acta* 54: 1897.
- Davis, J. A. 1978. Surface ionization and complexation at the oxide/water interface. *J. Colloid Interface Sci.* 67 (1): 90.
- Dyer, C. and P. J. Hendra. 1993. Surface hydration of aqueous γ -Al₂O₃ studied by fourier transform raman and infrared spectroscopy--I. initial results. *Spectrochim. Acta* 49A (5/6): 691.
- Fuller, C. C., J. A. Davis and G. A. Waychunas. 1993. Surface chemistry of ferrihydrite: Part 2. Kinetics of arsenate adsorption and coprecipitation. *Geoch. Cosmochim. Acta* 57: 2271.
- Goldberg, S., J. A. Davis and J. D. Hem. 1995. The surface chemistry of aluminum oxides and hydroxides. p. 271. *In* G. Sposito (ed.) *The environmental chemistry of aluminum*. CRC Press, Boca Raton, FL.
- Good, M. E., G. D. Winget, W. Winter, T. N. Connolly, S. Izawa and R. M. M. Singh. 1966. Hydrogen ion buffers for biological research. *Biochemistry* 5 (2): 467.

- Gunneriusson, L., L. Lovgren and S. Sjoberg. 1994. Complexation of Pb(II) at the goethite (α -FeOOH)/water interface: The influence of chloride. *Geoch. Cosmochim. Acta* 58 (22): 4973.
- Harter, R. D. 1991. Kinetics of sorption/desorption processes in soil. p. 135. *In* D. L. Sparks and D. L. Suarez (eds.) Rates of soil chemical processes. Vol. 27. Soil Science Society of America, Madison, WI.
- Hayes, K. F. and J. O. Leckie. 1986. Mechanism of lead ion adsorption at the goethite-water interface. p. 115. *In* J. A. Davis and K. F. Hayes (eds.) Geochemical processes at mineral surfaces. Vol. 323. American Chemical Society, Washington D.C.
- Hesterberg, D., D. E. Sayers, W. Zhou, G. M. Plummer and W. P. Robarge. 1997. X-ray absorption spectroscopy of lead and zinc speciation in a contaminated groundwater aquifer. *Environ. Sci. Technol.* 31: 2840.
- Hohl, H. and W. Stumm. 1976. Interaction of Pb^{2+} with hydrous γ - Al_2O_3 . *J. Colloid Interface Sci.* 55 (2): 281.
- Hunter, D. B. and P. M. Berch. 1994. In situ measurements of tetraphenylboron degradation kinetics on clay mineral surfaces. *Environ. Sci. Technol.* 28: 686.
- Kinniburgh, D. G. 1976. Adsorption of alkaline earth, transition, and heavy metal cations by hydrous oxide gels of iron and aluminum. *Soil Sci. Soc. Am. J.* 40: 796.
- Kinniburgh, D. G. and M. L. Jackson. 1981. Cation adsorption by hydrous metal oxides and clay. p. 91. *In* M. A. Anderson and A. J. Rubin (eds.) Adsorption of inorganics at solid-liquid interfaces. Ann Arbor Science, Ann Arbor, MI.
- Knozinger, H. and P. Ratnasamy. 1985. Catalytic aluminas: surface models and characterization of surface sites. *Catal. Rev.--Sci. Eng.* 17: 31.
- Leciejewicz, J. 1961. On the crystal structure of tetragonal (red) PbO. *Acta Crystallogr.* 14 (12): 1304.
- Lehman, R. G. and R. D. Harter. 1984. Assessment of copper-soil bond strength by desorption kinetics. *Soil Sci. Soc. Am. J.* 48: 769.
- Loehr, R. C. and M. T. Webster. 1996. Behavior of fresh vs. aged chemicals in soils. *J. Soil Cont.* 5 (4): 361.

- Lytle, F. W., R. B. Gregor, D. R. Sandstorm, E. C. Marques, J. Wong, C. L. Spiro, G. P. Huffman and F. E. Huggins. 1984. Measurement of soft X-ray absorption spectra with a fluorescent ion chamber detector. *Nucl. Instrum. Methods Phys. Res.* 226: 542.
- Manceau, A., M.-C. Bosset, G. Sarret, J.-L. Hazemann, M. Mench, P. Cambier and R. Prost. 1996. Direct determination of lead speciation in contaminated soils by EXAFS spectroscopy. *Environ. Sci. Technol.* 30 (5): 1540.
- McBride, M. M. 1991. Processes of heavy and transition metal sorption by soil minerals. p. 149. *In* G. H. Bolt, M. F. D. Boodt, M. H. B. Hayes and M. B. McBride (eds.) *Interactions at the soil colloid-soil solution interface*. Vol. 190. Kluwer Academic Publishers, Dordrecht, Netherlands.
- McBride, M. M. 1994. *Environmental chemistry of soils*. Oxford University Press, New York, NY.
- O'Day, P., G. E. Brown, Jr. and G. A. Parks. 1994. X-ray absorption spectroscopy of cobalt (II) multinuclear surface complexes and surface precipitates on kaolinite. *J. Colloid Interface Sci.* 165: 269.
- O'Day, P. A., C. Chisholm-Brause, S. N. Towle, G. A. Parks and G. E. Brown, Jr. 1996. X-ray absorption spectroscopy of Co(II) sorption complexes on quartz (α -SiO₂) and rutile (TiO₂). *Geoch. Cosmochim. Acta* 60 (14): 2515.
- Papelis, C. 1995. X-ray photoelectron spectroscopic studies of cadmium and selenite adsorption on aluminum oxides. *Environ. Sci. Technol.* 29: 1526.
- Papelis, C., P. V. Roberts and J. O. Leckie. 1995. Modeling the rate of cadmium and selenite adsorption on micro- and mesoporous transition aluminas. *Environ. Sci. Technol.* 29: 1099.
- Roe, A. L., K. F. Hayes, C. Chisholm-Brause, G. E. Brown, Jr., G. A. Parks, K. O. Hodgson and J. O. Leckie. 1991. In situ X-ray absorption study of lead ion surface complexes at the goethite-water interface. *Langmuir* 7: 367.
- Sadusky, M. C., D. L. Sparks, M. R. Noll and G. J. Hendricks. 1987. Kinetics and mechanisms of potassium release from sandy middle Atlantic coastal plain soils. *Soil Sci. Soc. Am. J.* 51: 1460.
- Scheidegger, A. M. and D. L. Sparks. 1996. Kinetics of the formation and the dissolution of nickel surface precipitates on pyrophyllite. *Chem. Geol.* 132 (1-4): 157.

- Scheidegger, A. M., D. G. Strawn, G. M. Lamble and D. L. Sparks. 1998. The kinetics of mixed Ni-Al hydroxide formation on clays and aluminum oxides: A time-resolved XAFS study. *Geoch. Cosmochim. Acta* 62 (13): 2233.
- Shriver, D. F., P. Atkins and C. H. Langford. 1994. *Inorganic chemistry*. W. H. Freeman and Company, New York, NY.
- Skogley, E. O. and A. Dobermann. 1996. Synthetic ion-exchange resins: soil and environmental studies. *J. Environ. Qual.* 25: 13.
- Smith, J. T. and R. N. J. Comans. 1996. Modeling the diffusive transport and remobilization of ^{137}Cs in sediments: The effects of sorption kinetics and reversibility. *Geoch. Cosmochim. Acta* 60 (6): 995.
- Sparks, D. L. 1989. *Kinetics of soil chemical processes*. Academic Press, Inc., San Diego, CA.
- Sparks, D. L. 1995. *Environmental soil chemistry*. Academic Press, San Diego, CA.
- Sposito, G. 1984. *The Surface Chemistry of Soils*. Oxford University Press, New York, NY.
- Sposito, G. 1989. *The chemistry of soils*. Oxford University Press, New York, NY.
- Steinfeld, J. I., J. S. Francisco and W. L. Hase. 1989. *Chemical kinetics and dynamics*. Prentice Hall, Englewood Cliffs, NJ.
- Stern, E. A. 1988. Theory of EXAFS. p. 3. *In* D. C. Koningsberger and R. Prins (eds.) *X-ray absorption: Principles, applications, and techniques of EXAFS, SEXAFS, and XANES*. Wiley, New York, NY.
- Strawn, D. G. and D. L. Sparks. 1998, In Press. Sorption kinetics of trace elements in soils and soil materials. H. M. Selim and A. Iskandar (eds.) *The fate and transport of trace metals in the environment*. Ann Arbor Press, Ann Arbor, MI.
- Towle, S. N., J. R. Bargar, G. E. Brown, Jr. and G. A. Parks. 1997. Surface precipitation of cobalt on Al_2O_3 . *J. Colloid Interface Sci.* 187: 62.
- Valcheva, M. L., N. Davidova and A. H. Weiss. 1995. Thermal Decomposition of the Pb, Al-hydrotralcite Material. *J. Mater. Sci.* 30: 737.

- Verburg, K. and P. Baveye. 1994. Hysteresis in the binary exchange of cations on 2:1 clay minerals: A critical review. *Clays Clay Miner.* 42 (2): 207.
- Waychunas, G. A., B. A. Rea, C. C. Fuller and J. A. Davis. 1993. Surface chemistry of ferrihydrite: Part 1. EXAFS studies of the geometry of coprecipitated and adsorbed arsenate. *Geoch. Cosmochim. Acta* 57: 2251.
- Yasunaga, T. and T. Ikeda. 1986. Adsorption-desorption kinetics at the metal-oxide-solution interface studied by relaxation kinetics. p. 231. *In* J. A. Davis and K. F. Hayes (eds.) *Geochemical processes at mineral surfaces*. Vol. 323. American Chemical Society, Washington D. C.
- Zabinski, S. I., J. J. Rehr and A. Ankudinov. 1997. Multiple-scattering calculations of X-ray absorption spectra. *Phys. Rev. B* 52: 2995.

Chapter 3

The Use of XAFS to Distinguish Between Inner- and Outer-Sphere Lead Adsorption Complexes on Montmorillonite

3.1 Abstract

Adsorption mechanisms of Pb on montmorillonite were investigated by conducting equilibrium and X-ray absorption fine structure (XAFS) spectroscopy studies. Data from the batch equilibrium studies indicate that Pb is adsorbing via two mechanisms. At $I=0.1$ M 43% of the available Pb was removed from the solution at pH=4.11, and 98.9% at pH=7.83. At $I=0.006$ M 97% of the available Pb was removed from solution at pH=4.42, and 100% at pH=8.06. These results show that at the lower ionic strength Pb adsorption is pH-independent. This type of behavior is consistent with an outer-sphere complexation mechanism (electrostatic attraction). However, in the system equilibrated at higher ionic strength Pb adsorption is pH-dependent, suggesting inner-sphere complexation as the mechanism of adsorption since the edge sites of the montmorillonite are amphoteric and can form covalent bonds with Pb. The X-ray absorption near edge structure (XANES) and extended X-ray absorption fine structure spectroscopy (EXAFS) results reveal that in the sample equilibrated at $I=0.006$ M, pH=4.48-6.4 the local atomic structure (LAS) surrounding the adsorbed Pb is similar to the LAS surrounding Pb^{2+} (aq). Since Pb^{2+} (aq) is surrounded by water molecules, and the

adsorbed Pb has a similar coordination environment, then the adsorption mechanism for Pb on the montmorillonite at the lower ionic strength and pH must be outer-sphere complexation. In the system equilibrated at $I=0.1$ M, $\text{pH}=6.77$ the XANES and EXAFS results indicate that the LAS surrounding the adsorbed Pb atom is similar to the LAS surrounding the $\text{Pb}_4(\text{OH})_4^{4+}$ (aq) complex (covalent bonds between the Pb atoms and the hydroxide ligands), and a sample of $\gamma\text{-Al}_2\text{O}_3$ with Pb adsorbed via inner-sphere complexes. These similarities indicate that at this ionic strength and pH, Pb is forming inner-sphere complexes on the montmorillonite, and some Pb polymerization is occurring. In samples equilibrated at $I=0.006$ M, $\text{pH}=6.77$ and $I=0.1$ M, $\text{pH}=6.31$ the XAFS results suggest that Pb is forming both inner- and outer-sphere adsorption complexes. The results of this study reveal that adsorption on clays is not only an electrostatic cation exchange reaction, but involves the formation of chemical bonds, depending on I and pH. This information is important for accurate prediction of the distribution of cations on clay minerals.

3.2 Introduction

Since clay minerals are major components of soils, industrial processes, and waste remediation efforts, it is important to understand how metals such as Pb interact with their surfaces. One of the primary interactions between metals and clay minerals is adsorption. There are two distinct adsorption mechanisms. These are outer-sphere adsorption, which occurs primarily on the basal planes existing in the interlayer of the clay minerals, and inner-sphere adsorption, which occurs at the amphoteric ligand sites existing on the edges of clay minerals (Sposito, 1989; Sparks, 1995).

Historically, adsorption on clay minerals has been considered to be primarily cation exchange (outer-sphere) resulting from an electrostatic attraction between a cation and the permanent charge associated with the mineral due to isomorphic substitution (Marshall, 1935). The cation exchange capacity (CEC) of clay minerals is determined by measuring the uptake of cations that do not form chemical bonds with the functional groups existing on the clay mineral, such as Na. This value is often used as an indication of the amount of metals that can be adsorbed. However, CEC does not represent inner-sphere adsorption sites that exist at the edges of clays. In order to describe cation exchange mechanisms, scientists developed the Gouy-Chapman theory (Sparks, 1995). This theory describes the ions as existing in a diffuse layer adjacent to a charged surface. The double-layer theory assumes that all interactions between adsorbed ions and surfaces are electrostatic (coulombic).

pH-dependent charge behavior has been recognized as an important characteristic in soils since the beginning of the 20th century (Thomas, 1977). In soils that have high concentrations of iron and/or aluminum oxides, inner-sphere adsorption was considered to be an important adsorption mechanism (Hingston et al., 1967; Huang et al., 1973; Thomas, 1977). Inner-sphere adsorption on clay mineral edges has long been considered to be negligible compared to outer-sphere adsorption on the basal planes. Evidence for adsorption onto the edges of clays was provided by Shoefield and Samson (1953) who showed that kaolinite could adsorb Cl^- on its edges, but had a net negative overall charge due to the permanent charge sites (Thomas, 1977). Recent research has suggested that inner-sphere adsorption of metals on the edges of clay minerals can be

significant (White et al., 1988; Schulthess et al., 1990; Zachara et al., 1993; Keren et al., 1995). Zachara and Smith (1993) investigated the effects that adsorption sites existing on the edges of smectites had on cadmium adsorption. They used a multiple site model that included fixed charged sites (outer-sphere) and variable charged sites (inner-sphere). They found that as pH and ionic strength increased, adsorption on AlOH sites existing at the edges of the clay became increasingly important.

Modeling has provided important insights into adsorption mechanisms. However, in order to provide more definitive information about adsorption mechanisms it is necessary to combine microscopic and macroscopic experiments (Sposito, 1989). A useful spectroscopic technique that has provided important insights into the mechanisms of metal sorption to mineral surfaces is X-ray absorption spectroscopy (XAS). The fine structure of the X-ray absorption (XAFS) consists of the near-edge (XANES), and the extended portions (EXAFS) (Fendorf et al., 1996). From XAFS data it is possible to obtain important information about the LAS of adsorbed ions, such as, the type of atoms surrounding the central atom (atom being probed), the coordination number (N), interatomic distances (R), and oxidation state (Teo et al., 1981). Bargar et al. (1996) used grazing incidence XAFS to show that Pb forms inner-sphere complexes on the (002) plane of α -Al₂O₃, and outer-sphere complexes on the (001) plane. Papelis and Hayes (1996) used XAFS to study the pH and ionic strength dependence of Co adsorption on montmorillonite. They found that at high ionic strength sorption was pH-dependent, while at lower ionic strength sorption was less pH-dependent. XAFS analysis of the samples suggested that adsorption at low ionic strength and low pH consisted of

predominantly outer-sphere adsorption complexes, while adsorption at high ionic strength and higher pH consisted of the formation of Pb-polymer complexes at the edge sites. Kim et al. (1996) used nuclear magnetic resonance (NMR) to show that adsorption of cesium on illite involved both inner-sphere adsorption on the edges of clay, and outer-sphere adsorption on the basal plane of the clay. Similar findings have been found for adsorption of organic molecules on amorphous oxides (Person et al., 1998). These studies have shown that the mechanisms of adsorption on clay minerals and oxides are variable, and that the use of macroscopic methods in conjunction with microscopic methods is important to elucidate adsorption mechanisms. In this study we continue this theme of research by presenting an in depth analysis of the pH and ionic strength dependence of Pb adsorption at the montmorillonite-water interface. Results from this study will allow for the development of better models to describe the ion distribution and mechanisms of metal sorption on mineral surfaces.

The objective of this study is to characterize the pH and ionic strength dependence of Pb(II) adsorption mechanisms on montmorillonite. To accomplish these objectives we used both batch adsorption studies and XAFS studies. In addition, this study will demonstrate the usefulness of XAFS for distinguishing between multiple adsorption mechanisms in a single system. A better understanding of how Pb interacts with surfaces is crucial since Pb is an important element in industrial processes, and is one of the most common contaminants in the environment (Reed et al., 1996). In the environment Pb is usually associated with organic and inorganic colloids and minerals (Hem, 1976; Zimdahl et al., 1977). An understanding of the nature of these interactions is

critical for improving remediation strategies, risk assessment, and disposal practices. Furthermore, the LAS of Pb and its chemical behavior are complex and varied (Manceau et al., 1996; Richens, 1997), intensifying the need for research on this toxic heavy metal.

3.3 Theory

The clay mineral montmorillonite has a high surface area and CEC, and is present throughout soil and aquatic systems (Borchardt, 1989). It is a dioctahedral smectite mineral having a half cell chemical formula $M_{0.33} H_2O Si_4 (Al_{1.67} (Fe^{2+}, Mg)_{0.33}) O_{10} (OH)_2$ (Sparks, 1995), where M is a monovalent interlayer cation (2). Figure 3.1 shows the montmorillonite structure, which consists of silica tetrahedra above and below an aluminum octahedron. Substitution of Fe^{2+} and Mg^{2+} atoms for Al^{3+} in the octahedral layer creates a positive charge deficit, giving the overall structure a net negative charge. Since the charge deficit arises in the octahedral layer, the net charge at the surface (basal O ligands surrounding the Si-tetrahedra, see Figure 3.1) is delocalized. The isomorphic substitution is the origin of the permanent charges that exist on montmorillonite. Metal adsorption at the basal plane of the montmorillonite is largely due to coulombic interactions between the positively charged metal ions and the negatively charged surface, and involves at least one layer of water between the metal ion and the surface.

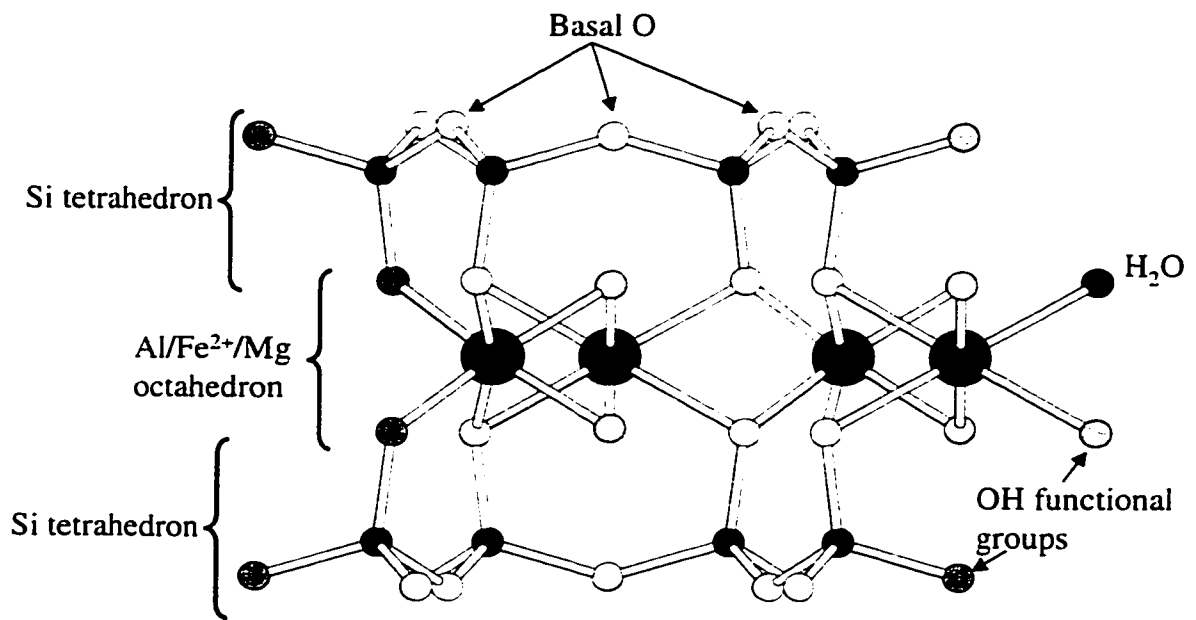


Figure 3.1 Schematic illustrating the (010) structure of the dioctahedral montmorillonite mineral.

The broken edges of the montmorillonite consist of OH and O atoms which have unsatisfied bonds (White et al., 1988). These form Lewis acid or Lewis base functional groups depending on pH (amphoterism). Cation adsorption at these sites involves the formation of covalent bonds between the cations and the Lewis base functional groups, either silanol or aluminol sites (see Figure 3.1) (Sparks, 1995). Therefore, based on the molecular structure of the montmorillonite, both inner- and outer-sphere adsorption complexes can be formed.

The distribution of cations in a montmorillonite system is dependent on ionic strength and pH. Adsorption on the planar sites of montmorillonite is considered to behave according to the rules of electrostatic interactions; ion size, concentration, and valence determine the distribution within a diffuse double layer (Babcock, 1963; Sparks, 1995; Stumm et al., 1996). At high ionic strength the background electrolyte ions (commonly Na⁺ ions) will out compete other adsorptive ions for the planar sites. Thus, adsorption of cations on the basal plane of clay minerals will be small when the cation concentration is much lower than the concentration of background electrolyte ions.

Adsorption on the edge sites depends on ionic strength, pH, and the type of ion adsorbing. pH is important since the functional groups existing at the edge sites are amphoteric. The point of zero net proton charge (PZNPC) is a measurement that is often used to speciate the pH-dependent surface, for example:



Where =S is a surface functional group. From this equation it is clear that as pH changes the speciation of the surface functional group changes. The pH where the net charge on the surface is zero is called the PZNPC. The PZNPC for montmorillonite is reported in Table 3.1. Since the speciation of the edge site functional groups changes with pH, the complexation of metal cations with these functional groups is also pH-dependent.

The reaction of cations such as Pb with the amphoteric functional groups includes both electrostatic and chemical forces. The contributions of electrostatic attraction and chemisorption to the overall free energy of reaction ($\Delta G^{\circ}_{\text{adsorption}}$) are represented in the following equation (James et al., 1972; Westall, 1986):

$$\Delta G^{\circ}_{\text{adsorption}} = \Delta G^{\circ}_{\text{electrostatic}} + \Delta G^{\circ}_{\text{chemical}} + \Delta G^{\circ}_{\text{solvation}} \quad (3.2)$$

Where $\Delta G^{\circ}_{\text{electrostatic}}$ is the free energy due to coulombic interactions, $\Delta G^{\circ}_{\text{chemical}}$ is the free energy involved in making and breaking chemical bonds between the surface functional groups and the metal, and $\Delta G^{\circ}_{\text{solvation}}$ is the free energy involved in dehydrating the metal. The magnitude of $\Delta G^{\circ}_{\text{chemical}}$ is dependent on the protonated state of the functional groups. As pH increases, the number of deprotonated functional groups increases. The increase in deprotonated functional groups with pH causes a decrease in the energy required for the formation of bonds between cations and surface hydroxyl groups since protons do not need to be displaced from the surface prior to adsorption. Alternatively, the increase in pH causes a decrease in protons in solution causing less competition between cations and protons for the surface functional groups (i.e., law of mass action). The magnitude of

$\Delta G_{\text{electrostatic}}^{\circ}$ for adsorption on edge sites is also a function of the pH with respect to the PZNPC; as pH increases the potential existing at the edge sites becomes more negative, resulting in a stronger electrostatic interaction and a more negative free energy.

The ability to form chemical bonds with the functional groups is a key factor that determines the distribution of metal ions as a function of ionic strength and pH. For example, Pb^{2+} is a large cation that is highly polarizable and readily forms complexes with hydroxide-type functional groups, while Na^{+} is a small more electronegative ion (less likely to share its electrons) that does not readily form complexes with ligands. Thus, in systems in which the background electrolyte cations do not form covalent bonds, but the metal cations do, adsorption onto the pH-dependent edge sites will favor the metal ions; even though the concentration of the background electrolyte cations is higher (Zachara et al., 1993; McKinley et al., 1995; Papelis et al., 1996).

3.4 Experimental Methods

3.4.1 Materials

The smectite used was a montmorillonite from Crook County, Wy (SWy-2, Clay Minerals Society). The montmorillonite was treated to remove organic matter and carbonates using procedures described in Amonette and Zelazny (1994): traces of organic matter were oxidized by treating with a solution of 3% H_2O_2 at 333 K; carbonates were removed by reacting the suspension for 4 h in Na-acetate buffer at 333 K, pH=4.74. Next the clay was Na-saturated, and the less than 2 μm fraction was separated by collecting the supernatant of a suspension of the clay in deionized (D.I.) H_2O that was centrifuged until

all but the less than 2 μm fraction was settled; this step was repeated several times. Excess salts were removed by dialysis, and the final suspension was freeze dried to remove the bulk water. Some of the physicochemical properties of montmorillonite are listed in Table 3.1. X-ray diffraction and thermogravimetric analysis showed that the final mineral phase was montmorillonite, and contained no detectable impurities.

3.4.2 Adsorption Experiments.

All solutions were made in a glovebox with ACS reagent grade chemicals and D.I. H_2O that had been boiled, cooled with purified N_2 and stored in a CO_2 -free glovebox. All experiments were conducted in the glovebox containing a N_2 atmosphere to eliminate effects of CO_2 contamination. The temperature was maintained at 298 K throughout the experiment.

Table 3.1 Physicochemical properties of montmorillonite.

Particle size	<2.0 microns
Specific surface area	
EGME	697 m ² /g
N ₂ -BET	15.2 m ² /g
pH at zero point of charge ^a	~7.5-8.5
Theoretical coordination	2:1 clay: Si-tetrahedra: Al-octahedra with some Mg ²⁺ and Fe ²⁺ substitution
Cation exchange capacity ^b	~820 mmol/kg (measured at pH=6.0)
≡SOH site capacity ^c	~80 mmol/kg

^a From Avena et al. (1998) and Helmy et al. (1994). ^b From Zachara et al. (1993). ^c From Baeyens and Bradbury (1997).

Two montmorillonite suspensions of 13.3 g L^{-1} were preequilibrated for 24 h in either 0.001 M or 0.1 M NaClO_4 solution. After preequilibration 5-ml aliquots from $\sim 8 \text{ mM Pb}(\text{ClO}_4)_2$ stock solutions were added every 1 min to the suspensions until the total Pb concentration in the reaction vessel was $\sim 2 \text{ mM}$ and the total suspension volume = 0.1 L. Following the Pb additions the final ionic strengths of the suspensions were 0.006 M and 0.1 M. The actual $\text{Pb}(\text{ClO}_4)_2$ stock solution concentrations were measured on an inductively coupled plasma emission (ICP) spectrometer; for the $I=0.006 \text{ M}$ system $[\text{Pb}]_{\text{stock}}=7.83 \text{ mM}$, and for the $I=0.1 \text{ M}$ system $[\text{Pb}]_{\text{stock}}=8.10 \text{ mM}$, thus, initial concentrations in the montmorillonite suspensions were 1.96 mM and 2.03 mM, respectively. Following the addition of the Pb solution the pH for the $I=0.1 \text{ M}$ suspension was 4.32, and for the $I=0.006 \text{ M}$ suspension pH=4.70. The pH of the suspension was then adjusted by adding dilute HClO_4 or NaOH to the rapidly stirring suspensions in $\sim 10\text{-}\mu\text{L}$ aliquots. Starting at the lowest pH, the suspension pH was raised by 0.1-0.25 pH units. After each pH increment, 6-mL aliquots of the suspension were removed and put in 10 mL polycarbonate centrifuge tubes and placed on an end-over-end rotator (4 rpm). The samples were allowed to equilibrate for 24 h. This time was established as sufficient since samples incubated for longer periods (up to 3 wks) had an undetectable amount of additional Pb uptake. At the end of equilibration time the pH of the samples was measured, and the samples were centrifuged for 15 min at 19,000 rpm. The supernatant was filtered through $0.2\text{-}\mu\text{m}$ filters, acidified, and measured for total Pb concentration using an ICP spectrometer. The total amount of Pb removed from solution was calculated from the difference between the initial and final Pb concentrations.

3.4.3 Synchrotron XAFS Analysis

Montmorillonite samples analyzed by XAS were prepared using the same procedures as described above, except that the suspensions were centrifuged for an additional 30 min at 19,000 rpm. The additional centrifuging was necessary to reduce the volume of entrained solution. In the XAFS samples the amount of Pb sorbed to the montmorillonite surface was at least 300 times higher than the amount of non-sorbed Pb in the entrained solution. Thus, the contribution of non-sorbed Pb to the XAFS spectra is negligible. The equilibrium conditions of the XAFS samples are listed in Table 3.2. The samples used for XAFS experiments are also indicated with arrows on the pH-edge in Figure 3.2.

Table 3.2 Summary of XAFS sample adsorption conditions.

<i>I</i> (M)	pH	Removal from solution (%)	Adsorbed Pb(II) (mmol kg ⁻¹)	Primary adsorption mechanisms ^a
0.1	6.77	86.7	171	inner-sphere
0.1	6.31	71.2	140	mixed
0.006	6.76	99.0	201	mixed
0.006	6.40	98.5	200	outer-sphere
0.006	5.83	98.0	199	outer-sphere
0.006	4.48	96.8	197	outer-sphere

^aBased on results from XAFS data analysis.

Two $\text{Pb}(\text{ClO}_4)_2$ solutions were prepared and used as $\text{Pb}(\text{II})$ reference materials. One solution contained primarily the Pb polymer $\text{Pb}_4(\text{OH})_4^{4+}$ (aq) (total $[\text{Pb}] = 84$ mM, $\text{pH} = 6.46$, and $I = 1.16$ M NaClO_4). The speciation of this solution based on the hydrolysis constants given by Baes and Mesmer (1986) is 70% $\text{Pb}_4(\text{OH})_4^{4+}$ (aq), 19% Pb^{2+} (aq), 9.1% $\text{Pb}_6(\text{OH})_8^{4+}$ (aq), and 1.9% other Pb-OH complexes. Another solution (total $[\text{Pb}] = 50$ mM, $\text{pH} = 4.10$, and $I = 0.15$ M) was prepared that contained primarily Pb^{2+} (aq) (99.9%). All solutions and pastes were loaded in the glovebox into polycarbonate or Teflon sample cell holders, sealed with Kapton tape (CHR industries), and placed in airtight containers with an N_2 (g) atmosphere until XAS analysis. The samples were stored for no longer than 24 h before analysis.

XAS data acquisition of the Pb L_{III} -edge (13055) was conducted on beamline X-11A at the National Synchrotron Light Source (NSLS), Brookhaven National Laboratory, Upton, New York. The electron beam energy was 2.5 or 2.8 GeV and the maximum beam current was 300 mA. The monochromator consisted of two parallel Si(111) crystals with an entrance slit of 0.5 mm. The parallel crystal monochromator was detuned by reducing I_0 25% at the Pb-edge. The XAS data were collected in fluorescence mode using a Stern-Heald type detector filled with Kr and equipped with an As filter (Lytle et al., 1984). The spectrum of the 0.05 M $\text{Pb}(\text{ClO}_4)_2$ reference solution was collected in transmission mode. A Pb-foil was used as an internal standard in all experiments as an internal standard of the beam energy. The spectra were collected at room temperature (~ 298 K).

The XAFS data analysis was accomplished using the program MacXAFS 4.0 (Bouldin et al., 1995). The spectra were processed using the following procedure: 1) Multiple scans were merged and normalized relative to E_0 (determined from the inflection point of the derivative of the spectra) and step height; 2) the χ -function was extracted from the raw data using a linear pre-edge and a cubic spline post-edge consisting of 3 knots set at unequal distances, and converting the data from energy to k space; 3) the χ -function was then weighted by k^3 to compensate for dampening of the XAFS amplitude with increasing k ; and 4) the data were Fourier transformed to yield a radial structure function (RSF). For background removal (step 2) the positions of the knots were selected using the following criteria: 1) minimization of peaks in the region before the first major peak in the RSF, 2) minimization of oscillations in the spline derivative, and insuring nonconformity in the oscillation phase between the spline derivative and spectra, 3) maximizing the height of the primary O peak in the RSF without significantly dampening any other peaks, and 4) a decrease in the widths of the peaks in the RSF at half maximum height.

The XAFS k^3 weighted spectra were fit in R-space using the fitting routine in MacXAFS 4.0 (Bouldin et al., 1995). Background on the theories and procedures for fitting XAFS data can be found elsewhere (Stern, 1988). The particular details used in fitting the data are listed below. Single scattering theoretical spectra and phase shifts for Pb-Pb backscatterers and Pb-O backscatterers were calculated using the FEFF6.0 code (Zabinski et al., 1997), with an input file based on a model of α -PbO (tetrahedral) (Leciejewicz, 1961) (generated with the program ATOMS). When more than one O was

fit, the position of the second O atom backscatterer was fixed at 2.47 Å. This value was used since it is the distance obtained from the Pb²⁺ (aq) sample and is the same as the value obtained when only a single O shell was fit to Pb-montmorillonite samples believed to have similar interatomic distances as the Pb²⁺ (aq) sample. In addition this is the value that previous researchers have reported as the bond distance between Pb(II) and water ligands in the primary solvation shell (Bargar et al., 1996). The value of the Debye Waller (σ^2) term for the second shell Pb backscatterer was fixed at 0.01 Å². This is justified by the following observations: there was no trend in the σ^2 for the samples at different *I* or pH; fixing the σ^2 reduced the number of free parameters in the fitting routine, and thus the uncertainties in the coordination number; and, 0.01 Å² is consistent with the value used by other researchers to fit Pb sorption data (Chisholm-Brause et al., 1990; Bargar et al., 1997; Strawn et al., 1998). The edge shift (E_0) for all shells was constrained to be equal. An amplitude reduction factor was determined by fitting the theoretical single scattering O-shell to the same shell of the experimental spectra of a well-characterized α -PbO. For both the experimental and theoretical spectra square windows were cut at equal values in the χ -structure and the RSF. In all cases the number of independent variables in the fitting routine was less than the degrees of freedom as calculated by $N_{\text{free}} = 2 \cdot \Delta k \cdot \Delta R / \pi$, where Δk is the width of the window cut in k-space (χ -structure), and ΔR is the width of the window cut in R-space (Fourier transform) (Stern, 1988). To determine if the contribution from a particular shell was significant two factors were considered: 1) a reduction in the residual, and 2) the error in the accuracy of the N for a given shell was not greater than ~75%. The bond distances of all shells were

corrected by adding the factor $2\sigma^2/R$, which is a systematic correction to bond distances not accounted for by the fitting program (significant when σ^2 is high or R is low) (personal communication. B. Boyanoff, 1998).

Based on the accuracies of the $R_{\text{Pb-O}}$ and $N_{\text{Pb-O}}$ between Pb and the first shell O backscatterers ($R_{\text{Pb-O}} < 2.31 \text{ \AA}$) can be estimated by comparing the theoretical β -PbO (Hill, 1985) and the experimental β -PbO. In this case the accuracies were smaller than the confidence limits of the least-squares non-linear fitting procedure. Thus, the accuracies reported in the "Results and Discussion" section can be used as estimates of the errors in the absolute values. Similarly, the absolute accuracies of $R_{\text{Pb-Pb}}$ and $N_{\text{Pb-Pb}}$ for second shell Pb backscatterers can be inferred from the confidence limits derived from the fits of the second shell Pb atoms in experimental α -PbO data (Strawn et al., 1998).

The absolute accuracies of $R_{\text{Pb-O}}$ and $N_{\text{Pb-O}}$ for the O backscatterers at $R > 2.30 \text{ \AA}$ in this system were more difficult to estimate for the following reasons: 1) σ^2 for this shell is high since the H_2O ligands form weak bonds with the Pb^{2+} ions, the XAFS data were collected at room temperature (thermal disorder is high), and the coordination environment of Pb^{2+} ions is highly distorted (Manceau et al., 1996); 2) in cases where there were strong second O shell contributions, fitting both shells resulted in high correlations between the $R_{\text{Pb-O}}$ and $N_{\text{Pb-O}}$ of the first and second O shells; and 3) EXAFS fitting gives average bond distances (Bunker, 1984), which, in this case, had a high standard deviation (represented by a large value of σ^2) resulting from the large variance in $R_{\text{Pb-O}}$ between the Pb atoms and the H_2O ligands. To address point 3 we attempted to fit the longer O backscatterer atom by fitting an additional atom within the peak, and/or a

cummulant. Cummulants attempt to correct for the effects that non-gaussian disorder have on R (Bunker, 1984). However, use of either of these strategies resulted in extremely high correlations between R, N, and the cummulant variable. In addition, the results obtained when fitting using cummulants were dependent on the Δk region used. The strong correlations that existed are likely due to over-parameterization of the fitting procedure, and/or limitations of fitting when two identical atoms have distances that are too close. Due to these limitations there may be significant differences between the actual and observed Pb-O interatomic distances when Pb is coordinated by H₂O ligands. Unfortunately, good reference materials do not exist for Pb²⁺ (aq), making assessment of absolute errors difficult. Regardless of these limitations, the fitting of the data did result in consistent $R_{\text{Pb-O}}$ and $N_{\text{Pb-O}}$ values for the O shells occurring at $R_{\text{Pb-O}} > 2.31 \text{ \AA}$. In addition the $R_{\text{Pb-O}}$ and $N_{\text{Pb-O}}$ values obtained from the Pb²⁺ (aq) standard make good references to detect the contributions of similarly coordinated Pb in the Pb-montmorillonite samples.

3.5 Results and Discussion

3.5.1 Adsorption Experiments

The effects of ionic strength and pH on the adsorption behavior of Pb on montmorillonite are shown in Figure 3.2. At $I=0.006 \text{ M}$ the montmorillonite removed nearly all of the Pb from solution, regardless of pH; 97% of the available Pb was adsorbed at pH=4.42 (adsorption=197 mmol kg⁻¹) and ~100% at pH=8.06 (adsorption=203 mmol kg⁻¹). The pH-independent behavior of Pb adsorption at $I=0.006 \text{ M}$ suggests that at this low ionic strength the vast majority of the Pb was adsorbed on planar sites via outer-

sphere adsorption mechanisms. A small degree of pH-dependent Pb adsorption behavior at $I=0.006$ M occurred (lower panel Figure 3.2). This suggests that at low ionic strength minor amounts of Pb were adsorbed on edge sites via inner-sphere mechanisms.

In the Pb-montmorillonite samples equilibrated at high ionic strength ($I=0.1$ M) uptake of Pb was strongly pH-dependent; at pH=4.11 only 43% of the available Pb was removed from solution resulting in a loading level of $85.3 \text{ mmol kg}^{-1}$, where as at pH=7.83, 99% of the available Pb had been removed from solution resulting in a loading level of 195 mmol kg^{-1} . This pH-dependent Pb adsorption behavior suggests that at high ionic strength Pb forms inner-sphere complexes with the functional groups existing on the montmorillonite edges. Similar pH-dependent adsorption behavior has been observed for several other metal/mineral systems (Schindler et al., 1987; Wang et al., 1987; Goldberg et al., 1988; Sparks, 1995; Stumm et al., 1996).

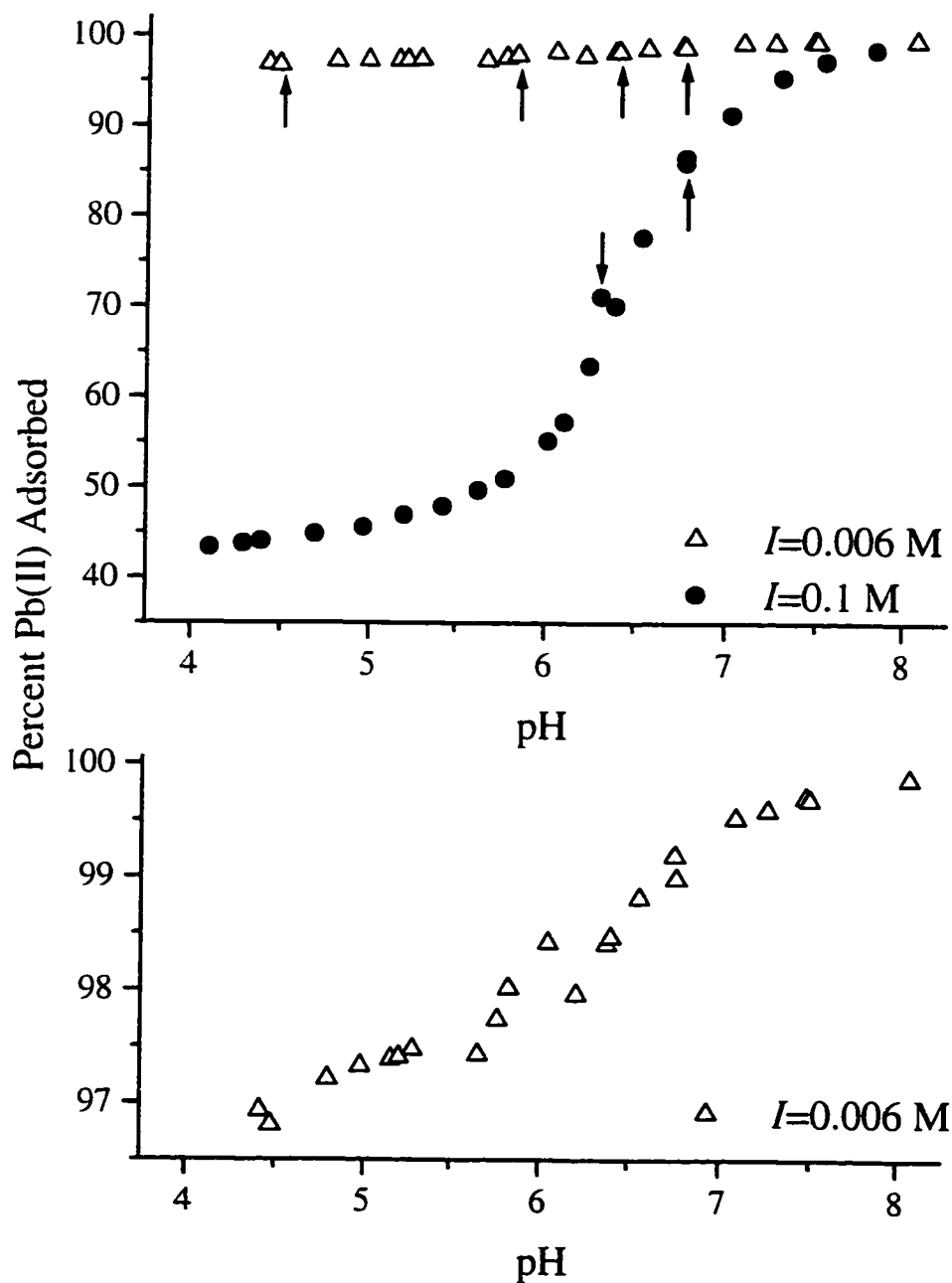


Figure 3.2 Lead adsorption on montmorillonite as function of pH, $[Pb]_{\text{initial}}=2$ mM, $[\text{solid}]=10$ g L⁻¹. Arrows indicate the equilibrium conditions of the montmorillonite samples used for the XAFS analysis. In the graph in the lower panel the range of the y-axis is decreased to illustrate the pH-dependent adsorption behavior of Pb-montmorillonite samples equilibrated at $I=0.006$ M.

The steep increase in adsorption between pH~6 and 7 in the $I=0.1$ M system, with an inflection point at pH~6.5 (based on the derivative of the data, not shown) is a result of the increase in the surface potential, and an increase in the number of deprotonated functional groups that occurs as the pH approaches the PZNPC (Avena et al., 1998). The PZNPC reported in Table 3.1 is based on proton adsorption experiments conducted using two different methods at various ionic strengths (Helmy et al., 1994; Avena et al., 1998). Avena et al. (1998) predicted that H^+ adsorption on the edge sites of montmorillonite is significant below pH=6; conversely, the number of deprotonated sites is significant above pH=6. Therefore, the $\Delta G_{\text{chemical}}$ and $\Delta G_{\text{electrostatic}}$ would become more negative as pH increases above pH=6, causing the $\Delta G_{\text{adsorption}}$ to decrease (become more favorable). This would result in increased adsorption above pH=6. Thus, the steep increase in Pb adsorption between pH 6 and 7 is characteristic of Pb adsorption on the amphoteric silanol and aluminol functional groups existing on the edges of the montmorillonite mineral. Outer-sphere adsorption of Pb on the basal planes of montmorillonite at this ionic strength is inhibited by the high concentration of Na^+ ions that are able to satisfy the electrostatic charge that exists.

Based on the Pb adsorption behavior at high ionic strength it can be concluded that the pH-dependent adsorption behavior associated with the edges of the clays is significant. Taking the difference between the values from the minimum and maximum adsorption at $I=0.1$ M, the total pH-dependent adsorption capacity is ~ 110 mmol kg^{-1} . This is 54% of the total amount of Pb that was adsorbed in the $I=0.006$ M system at pH=8.06. However, this value is not an absolute edge site adsorption capacity

since several other factors contribute to pH-dependent adsorption. For example, the formation of Pb-polymers would cause multiple Pb atoms to sorb to edge sites without each Pb forming a bond to a surface functional group. Since the formation of Pb-OH (aq) polymers is directly correlated to pH and ionic strength, the occurrence of Pb-polymer sorption complexes is expected to increase as pH and/or ionic strength increases. In addition, there could be some contribution of pH-dependent charge to the overall surface potential (edge charge spill over) (Chang et al., 1996). This behavior would cause the surface potential to decrease (become more negative) as pH increases, resulting in additional outer-sphere adsorption. Therefore, the prediction of the distribution of Pb based solely on adsorption behavior as a function of ionic strength and pH is problematic. However, the data does indicate that two distinct sorption mechanisms are occurring.

3.5.2 XANES Analysis.

The Pb-L_{III} XANES is very sensitive to the first shell coordination environment (Rao et al., 1984; Bargar et al., 1996; Bargar et al., 1997). To gain information about the LAS of Pb in the montmorillonite samples the energy and shape of the XANES spectral features can be compared to reference materials. In addition changes in the LAS in the Pb-montmorillonite samples equilibrated at different ionic strengths and pH can be detected by comparing the XANES spectra to each other.

The XANES spectra of the Pb-montmorillonite samples and the model compounds are presented in Figure 3.3. In order to illustrate the differences in the spectra of the samples and the reference compounds the first derivatives of the spectra are shown

in Figure 3.4. Two main characteristics in the spectra of the samples, and the reference compounds, exist that can be used for comparisons: 1) the size and shape of the peaks occurring between ~5-25 eV and ~30-70 eV, and 2) the position of the center of the peaks lying in these regions. The first peak in the Pb^{2+} (aq) sample is sharper (smaller full width half maximum) than the first peak in the $\text{Pb}_4(\text{OH})_4^{4+}$ (aq) sample. In the Pb^{2+} (aq) sample the center lies at ~11 eV (dashed line A in Figure 3.3). The center of the peak in the same region in the $\text{Pb}_4(\text{OH})_4^{4+}$ (aq) sample lies at ~14 eV. The 3 eV shift is considered significant since the scanning step size was much smaller (0.5 eV). In the Pb^{2+} (aq) sample the second peak that occurs in the region between ~30 and 70 eV has a center at ~46 eV (dashed line B in Figure 3.3). The center of the second peak in the $\text{Pb}_4(\text{OH})_4^{4+}$ (aq) sample lies at ~58 eV. In addition the size of the second peak is much smaller in the $\text{Pb}_4(\text{OH})_4^{4+}$ (aq) sample. The peak positions in these samples are similar to those found by Bargar et al. (1997) for the same Pb(II) reference materials. Bargar et al. (1997) also showed that the XANES structure of other common Pb compounds with different LAS are distinctly different from these two reference compounds. The β -PbO XANES spectrum in Figure 3.4 is included to further demonstrate the sensitivity and distinctiveness of Pb XANES spectra. From the data in Figures 3.3 and 3.4 it is evident that distinct differences occur in the XANES when bond distances and coordination numbers of the LAS surrounding Pb atoms are different.

Comparison of the position, shape and size of the XANES spectra from the Pb-montmorillonite samples (Figure 3.3 and 3.4) suggests that at low ionic strength and low pH ($I=0.006$ M, $\text{pH}=4.48$) the LAS of adsorbed Pb is similar to Pb^{2+} (aq). The

similarities in these spectra suggests that at this ionic strength and pH adsorbed Pb is surrounded by water molecules similar to the Pb^{2+} (aq) sample, and forms outer-sphere complexes. At high ionic strength and high pH ($I=0.1$ M, $\text{pH}=6.77$) the LAS of adsorbed Pb is similar to $\text{Pb}_4(\text{OH})_4^{4+}$ (aq). This suggests that Pb is forming bonds to hydroxide ligands with similar distances and coordination environments as $\text{Pb}_4(\text{OH})_4^{4+}$ (aq) (inner-sphere bonds).

In addition to using the Pb^{2+} (aq) and $\text{Pb}_4(\text{OH})_4^{4+}$ (aq) samples as references, the first derivative of a sample of Pb adsorbed on $\gamma\text{-Al}_2\text{O}_3$ from a previous study is included in Figure 3.4 (Strawn et al., 1998). The similarities in the XANES structure of the Pb adsorbed on $\gamma\text{-Al}_2\text{O}_3$ and the Pb adsorbed on the montmorillonite at high ionic strength and pH suggests that the LAS of the first shells of O surrounding the Pb atoms are similar. It has been shown using EXAFS that the LAS of Pb complexed with $\gamma\text{-Al}_2\text{O}_3$ consists of predominantly structural O ligands, and that the Pb was adsorbed as bidentate inner-sphere complexes on the edges of octahedrally coordinated structural aluminum atoms (Strawn et al., 1998). The structure of this complex is a distorted trigonal pyramid with an inert lone pair of electrons ($6s^2$) on one side, and three hydroxide ligands on the other side (hemidirected) (Bargar et al., 1997; Shimon Livny et al., 1998). Based on the similarities in the XANES spectra it can be concluded that the Pb adsorbed to the edges of the montmorillonite are forming similar types of complexes.

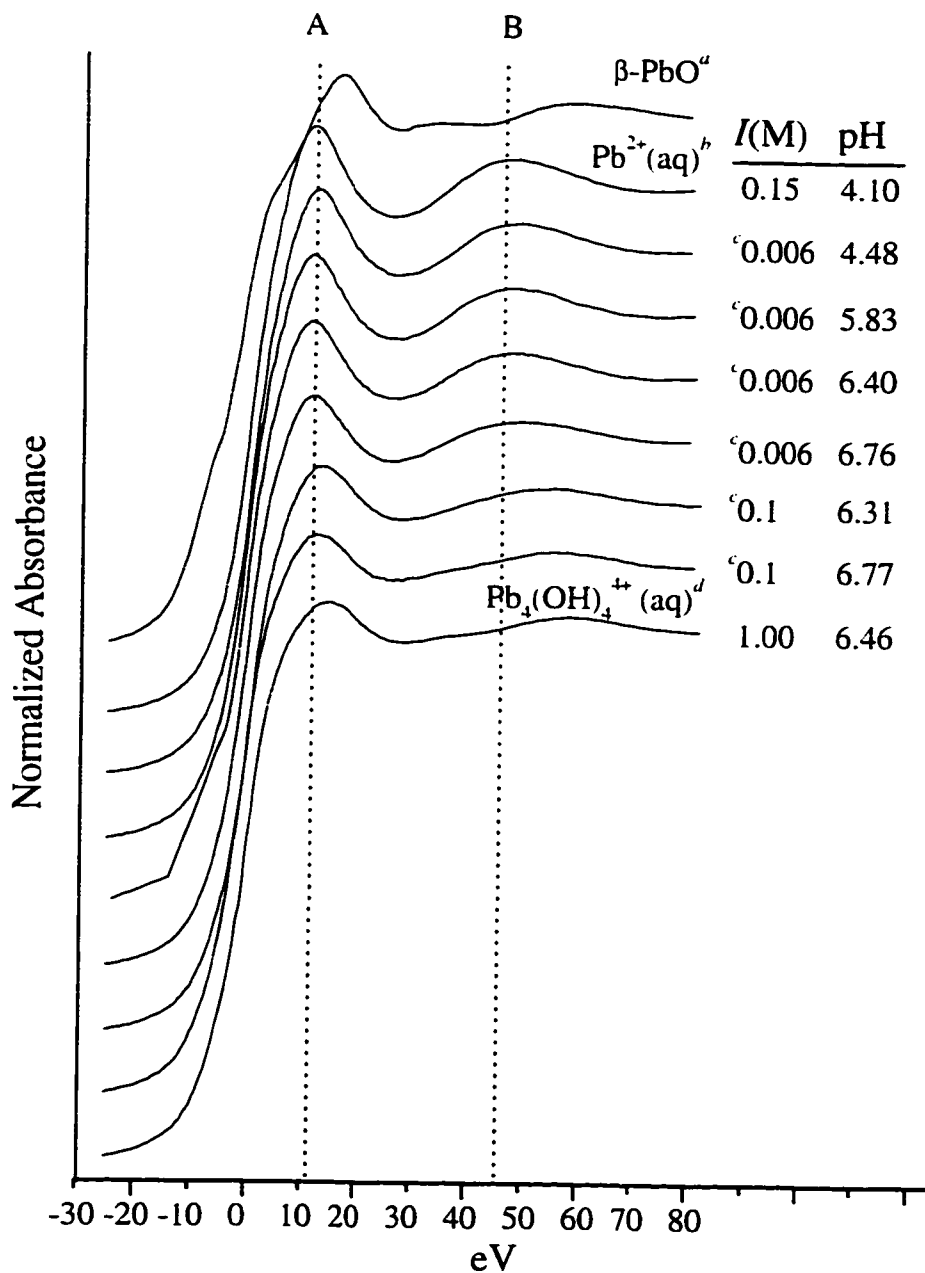


Figure 3.3 XANES spectra of the Pb-montmorillonite samples equilibrated at various ionic strengths and pH, and the Pb reference samples. The spectra are normalized for step height and $E_0=13055$ eV. The dashed lines labeled A and B are aligned with the center of the peaks in the $\text{Pb}^{2+}(\text{aq})$ sample (see text). ^aFrom Hesterberg et al. (1997). ^b[Pb]=50 mM. ^cPb-montmorillonite samples. ^d[Pb]=84 mM.

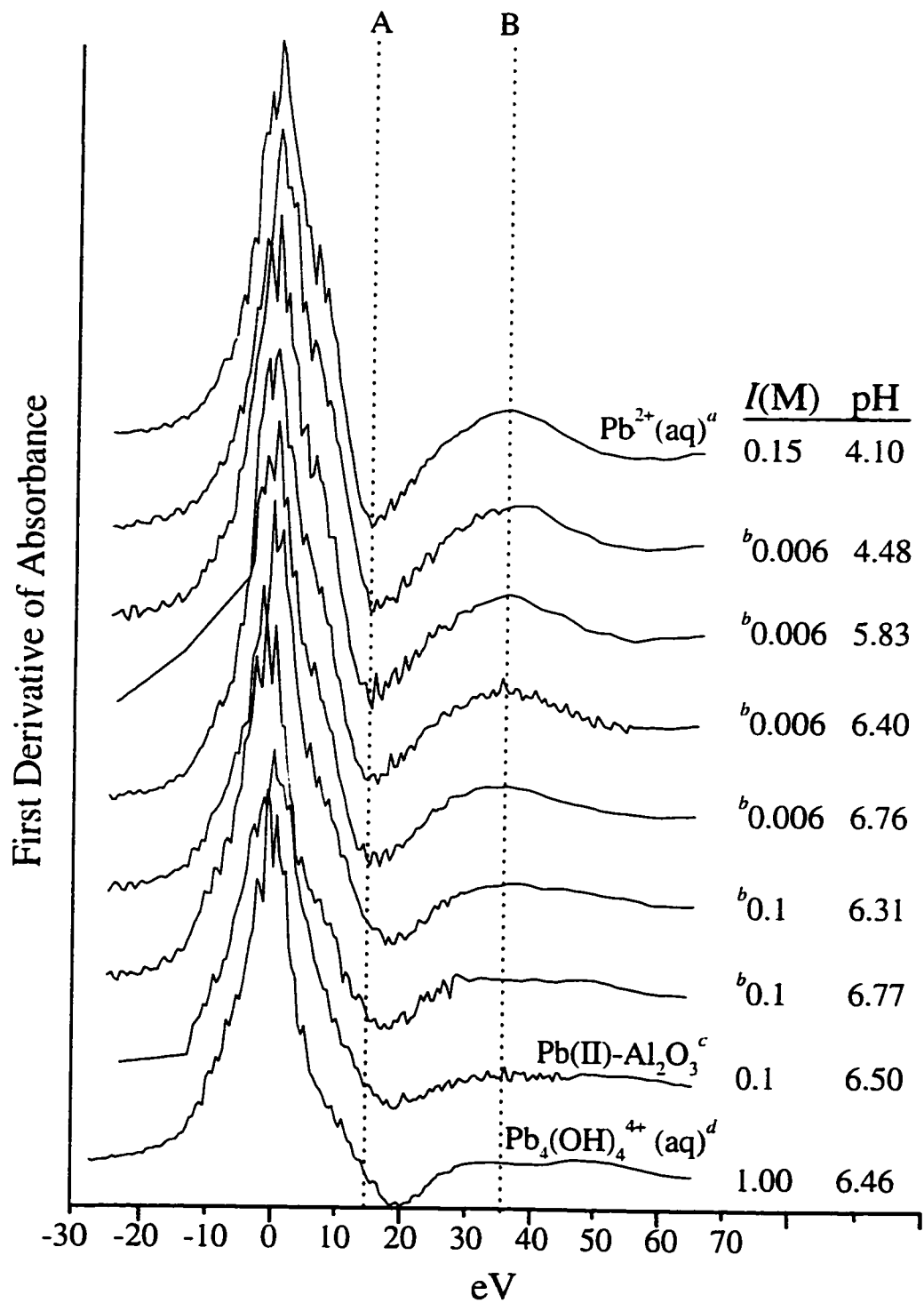


Figure 3.4 Derivative of the XANES from Figure 3.3.

For the low ionic strength samples, all of the spectra look similar to Pb^{2+} (aq), except for the sample equilibrated at $\text{pH}=6.76$. This suggests that in these samples Pb is forming outer-sphere complexes with the montmorillonite surface. In the sample equilibrated at $I=0.006$ M, $\text{pH}=6.76$ there are indications that Pb is adsorbing as both inner-and outer-sphere complexes. In the Pb-montmorillonite sample equilibrated at $I=0.1$ M, $\text{pH}=6.31$ the spectral features also show that Pb is adsorbing via both mechanisms. The differences between the XANES spectra of the Pb-montmorillonite samples equilibrated at $I=0.006$ M, $\text{pH}=6.76$ and $I=0.1$ M, $\text{pH}=6.31$, indicate that the sample equilibrated at the higher ionic strength has more contributions to the XANES from inner-sphere adsorbed Pb than in the sample equilibrated at the lower ionic strength.

From the analysis of the XANES three important points can be made: 1) Pb adsorbed on montmorillonite at high ionic strength and high pH is forming inner-sphere complexes; 2) Pb adsorbed on montmorillonite at low ionic strength and low pH is forming outer-sphere complexes; and 3) inner-and outer-sphere complexes can occur simultaneously on the surfaces of montmorillonite; their occurrence is a factor of not only ionic strength, but also pH.

3.5.3 EXAFS Analysis

Figure 3.5 shows the background subtracted k^3 weighted χ functions for the Pb-montmorillonite samples and the Pb reference compounds. All of the spectra exhibit a sinusoidal beat pattern that is typical of O-shell backscattering. The complex χ structure of the β -PbO is due to the development of shoulders, and dampening or additive effects

resulting from contributions from second shell Pb atoms. The χ structures of the Pb-montmorillonite samples show a distinct change in the phase and amplitude as ionic strength and/or pH increases. The samples incubated at $I=0.006$ M, pH=4.48 and $I=0.1$ M, pH=6.76 have χ structures similar to the χ structures of Pb^{2+} (aq) and $\text{Pb}_4(\text{OH})_4^{+}$ (aq), respectively. In the low ionic strength samples there is a large decrease in the amplitude of the signal at $k > 8 \text{ \AA}^{-1}$. This is a result of dampening of the XAFS signal due to a large amount of structural and thermal disorder, and the lack of heavy backscatter atoms in the LAS of the samples (Yu et al., 1989). The samples equilibrated at $I=0.1$ M, pH=6.31-6.76 have some structure at higher k suggesting that a change in the mechanism of surface complexation is occurring. Qualitative analysis of the similarities and differences that exist between the Pb-montmorillonite samples and the reference compounds suggest similar results as were observed for the XANES analysis (Figure 3.3 and 3.4).

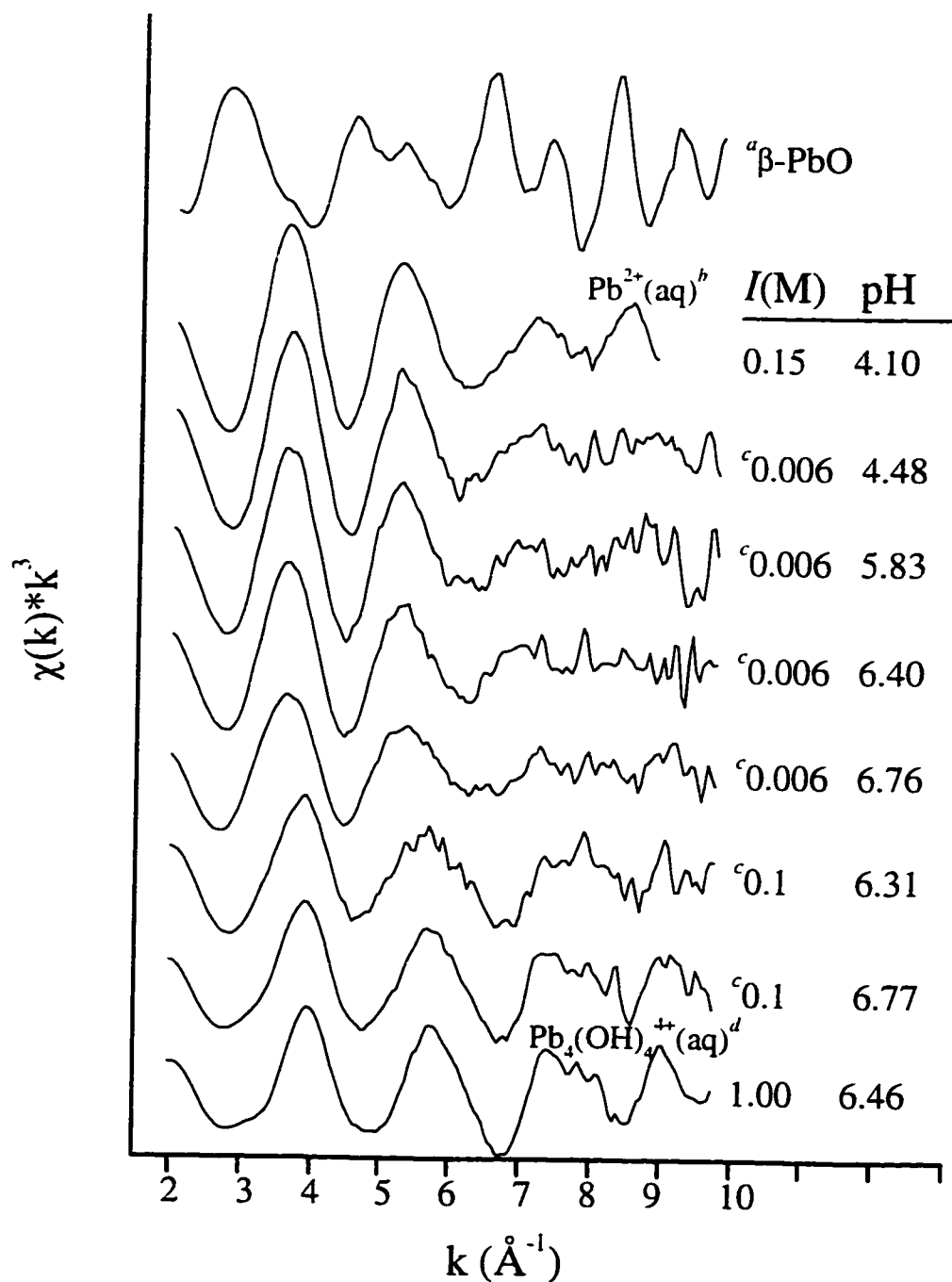


Figure 3.5 k^3 weighted normalized χ -functions for Pb-montmorillonite samples equilibrated at various ionic strengths and pH, and the reference samples. ^aFrom Hesterberg et al. (1997). ^b[Pb]=50 mM. ^cPb-montmorillonite samples. ^d[Pb]=84 mM.

In order to isolate the characteristic frequencies that exist in the χ structure the EXAFS data were Fourier transformed to yield radial structure functions (RSF). Figure 3.6 shows the RSF (uncorrected for phase shift) for the Pb-montmorillonite samples and the Pb reference compounds, along with the best fits obtained from multiple shell fitting. In all of the samples equilibrated at $I=0.006$ M with $\text{pH} \leq 6.40$, and the Pb^{2+} (aq) sample, only a single broad peak centered at ~ 1.9 Å is observed. This peak results from O backscattering in the first coordination shell of the Pb atoms. The large width of these peaks indicates that a high degree of disorder exists. In the sample equilibrated at $I=0.1$ M, $\text{pH}=6.77$ backscattering from the first shell O atoms is dominated by a single peak with a center at ~ 1.7 Å. This indicates that the bond distance between the Pb and O ($R_{\text{Pb-O}}$) is shorter than in the samples in which the center occurs at ~ 1.9 Å. In the sample equilibrated at $I=0.006$ M, $\text{pH}=6.76$ the center of the major peak occurs at ~ 1.7 Å, however, there exists a significant shoulder on the peak. This suggests that there are two distinct Pb-O distances present in this sample. Similar bimodal first shell peaks exist in the sample equilibrated at $I=0.1$ M and $\text{pH}=6.31$. In all of the samples with peaks in the RSF centered at ~ 1.7 Å there exists small peaks at higher R indicating the presence of backscatterer second shell atoms residing at longer distances, such as Pb, Si and/or Al. The identity of these atoms can be determined by fitting the data. The peak occurring at ~ 3.8 Å in the RSF is indicative of Pb backscattering and suggest that the sorption mechanism in these samples involves the formation of some Pb-polymer complexes; likely due to edge site saturation.

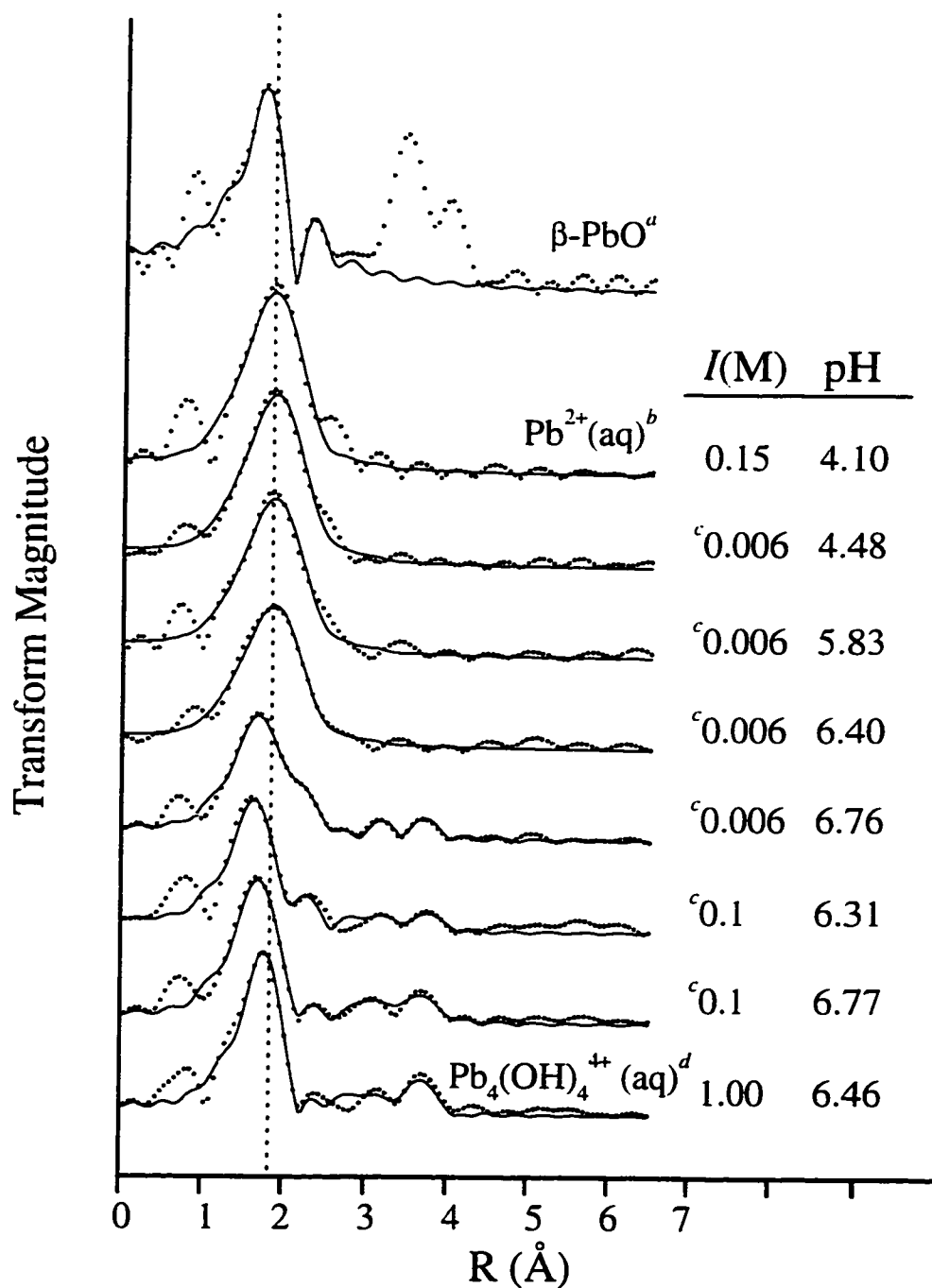


Figure 3.6 Fourier transforms (RSF) of the χ -functions in Figure 3, $\Delta k=2.3\text{-}9.6 \text{ \AA}^{-1}$. The solid line is the theoretical multishell fit to the data; the dotted line represents the experimental data. ^aFrom Hesterberg et al. (1997). ^b[Pb]=50 mM. ^cPb-montmorillonite samples. ^d[Pb]=84 mM.

Quantitative information about the LAS of Pb in the Pb-montmorillonite samples and the Pb reference compounds was obtained by fitting the data using theoretical backscattering paths obtained from α -PbO. The fit results are presented in Tables 3.3 and 3.4. In order to assess the predictive capabilities of the data fitting routine the results from fitting β -PbO and the Pb-montmorillonite sample equilibrated at $I=0.006$ M and $\text{pH}=6.77$ using different fitting strategies were compared (Table 3.3). The β -PbO sample was used since it is well characterized (Hesterberg et al., 1997) and has a distorted first shell of O atoms (Hill, 1985). The Pb-montmorillonite sample equilibrated at $I=0.006$ M and $\text{pH}=6.76$ was used because its RSF shows features suggesting that the LAS of adsorbed Pb consist of Pb-O bond distances characteristic of both inner- and outer-sphere adsorption. In the first fitting strategy the O backscatterers were fit without any constraints on these shells. In the second fitting strategy the $R_{\text{Pb-O}}$ of the second O shell was fixed at 2.47 Å (the fitted distance in the Pb^{2+} (aq) sample, uncorrected). In the third fitting strategy only a single O shell was fit. Fitting of the Pb-montmorillonite sample using the first fitting strategy resulted in bond distances for the first O shell of 2.31 Å, and 2.50 Å for the second O shell. The coordination numbers were $N=1.27$ and $N=5.55$ for the first and second shells, respectively. The errors associated with both coordination numbers and bond distances were relatively large. Fitting the sample using the second fitting strategy resulted in a bond distance for the first shell of 2.30 Å and coordination numbers for the first and second shell of 0.93 and 5.94, respectively. These results are very similar to the results obtained using the first strategy, but the errors associated with the coordination numbers and bond distances were smaller. The fit of the

Pb-montmorillonite sample using the third fitting strategy did not represent the two peaks that are present in the RSF, and had a poor residual. Fitting the β -PbO using the different fitting strategies gave similar results. In both samples, regardless of fitting strategy, the bond distances of the first and second O-shells are highly correlated. The results presented in Table 3.3 indicate that the bond distances obtained when fitting two O-shells are reliable. In addition, the results suggest that fixing the second O shell (the second fitting strategy) increases the fitting accuracy by decreasing the number of free variables in the fitting routine. This last point is important because in other Pb-montmorillonite samples the contribution from O atoms at longer distances was not as distinct as it was for these two samples.

The fit results for the Pb-montmorillonite sample and the reference compounds are presented in Table 3.4. For all of the montmorillonite samples equilibrated at $I=0.006$ M, except for the pH=6.76 sample, only a single shell was fit. This resulted in bond distances of 2.50 Å. Fitting of the Pb^{2+} (aq) EXAFS data resulted in a bond distance of 2.49 Å, which is close to the bond distances found by Bargar et al. (1996) for Pb^{2+} (aq) ($R_{\text{Pb-O}}=2.47$ Å). The bond distance derived from the Pb^{2+} (aq) sample is very close to the bond distances obtained for the Pb-montmorillonite samples equilibrated at $I=0.006$ M, pH=4.48-6.40. In addition coordination numbers were all very close ($N=8-9.8$) for these samples. The exact LAS for hydrated Pb^{2+} ions has not been determined. It has been estimated that the usual number of H_2O molecules that exist in the first solvation sphere is somewhere between 4-7.5 (Bockeris et al., 1954). Shimoni-Livny et al. (1998) suggested that the number of Pb-bound water molecules is far fewer,

and used ab initio molecular orbital optimization procedures to predict that the waters were coordinated to the Pb atoms with bond distances between 2.356 and 2.460 Å (average $R_{\text{Pb-O}}=2.408$ Å). The higher coordination numbers and longer bond distances obtained in our samples may be due to contributions from O backscatterers residing in the secondary solvation shell. However, as mentioned in the “Materials and Methods” section, bond distances obtained from these samples are not necessarily absolute, and estimates of coordination numbers can be particularly unreliable when there exists a large degree of distortion (Manceau et al., 1996; Sarret et al., 1998), as is the case in these samples. Nevertheless, the bond distances and coordination numbers obtained are useful for qualitative comparisons.

Table 3.3 Structural parameters and least squares precision (italicized in parenthesis) obtained using different fitting schemes (see text) for β -PbO and Pb(II) adsorption on montmorillonite at pH = 6.76, $I = 0.006$ M.

Sample	Pb-O1 shell			Pb-O2 shell			Pb-Pb shell			E_0 (eV) ^d
	R (Å) ^a	N ^b	σ^2 (Å ²) ^c	R (Å)	N	σ^2 (Å ²)	R (Å)	N	σ^2 (Å ²)	
Pb-Montmorillonite										
pH = 6.76, $I = 0.006$ M										
fit result 1 ^h	2.31 (0.04)	1.27 (2.99)	0.010 (0.012)	2.50 (0.10)	5.55 (3.58)	0.027 (0.016)	3.76 (0.01)	1.32 (0.54)	0.011 (0.003)	5.06
fit result 2 ⁱ	2.30 (0.01)	0.93 (0.30)	0.009 (0.003)	2.49 ^e	5.94 (0.59)	0.028 (0.003)	3.76 (0.01)	1.14 (0.19)	0.010 ^e	5.10
fit result 3 ^j	2.42 (0.02)	7.94 (1.11)	0.034 (0.003)				3.73 (0.02)	1.13 (1.09)	0.009 (0.008)	7.69
β-PbO^j										
fit result 1 ^h	2.27 (0.02)	2.81 (1.28)	0.007 (0.005)	2.52 (0.06)	1.81 (2.00)	0.009 (0.015)				-0.20
fit result 2 ⁱ	2.26 (0.01)	2.23 (0.39)	0.005 (0.001)	2.49 ^e	2.71 (1.06)	0.016 (0.006)				0.50
fit result 3 ^j	2.21 (0.02)	2.26 (0.37)	0.007 (0.002)							11.2
XRD ^f	2.24 ^k	2		2.48	2					

^a Interatomic distance (corrected by adding $2 * \sigma^2/R$, see text). ^b Coordination Number. ^c Debye-Waller factor. ^d

Phase shift. ^e Fixed. ^f Raw data from Hesterberg et al. (1997). ^g From Hill (1985). ^h All parameters allowed to vary. ⁱ R_{Pb-O2} fixed. ^j Only 1 O shell fit. ^k Mean bond distance.

Table 3.4 Structural parameters derived from the XAFS experimental data using theoretical phase shift and amplitude functions for Pb(II) solutions and Pb adsorption on montmorillonite samples reacted at different I and pH

Sample	Pb-O1 shell			Pb-O2 shell			Pb-Pb shell				
	R (Å) ^c	N ^b _f	σ ² (Å ²) ^c	R (Å) ^c	N ^b	σ ² (Å ²)	R (Å) ^c	N ^b	σ ² (Å ²) ^d	E ₀ (eV) ^d	
Pb(II)-Montmorillonite											
6.77	0.1	2.29	2.8	0.011	2.49 ^h	0.8 ^g	0.010	3.75	1.7	0.01 ^h	7.75
6.31	0.1	2.28	2.2	0.010	2.49 ^h	3.0	0.020	3.79	1.2	0.01 ^h	5.97
6.76	0.006	2.30	0.9	0.009	2.49 ^h	5.9	0.028	3.76	1.1	0.01 ^h	5.10
6.40	0.006				2.50	8.0	0.030				3.97
5.83	0.006				2.50	9.0	0.030				3.98
4.48	0.006				2.50	9.0	0.029				3.40
Pb(ClO₄)₂ Solutions											
[Pb]=50 mM	4.78	0.15			2.49	9.8	0.029				5.14
[Pb]=84 mM	6.46	1.00	2.30	2.6	0.010			3.77	1.6	0.01 ^h	6.70

^a Interatomic distance (corrected by adding 2* σ²/R, see text). ^b Coordination Number. ^c Debye-Waller factor. ^d Phase shift. Fit quality confidence limits: ^e 1%, ^f 30%, ^g 75%. ^h Fixed.

Based on the similarities between the EXAFS of the Pb^{2+} (aq) sample and the Pb-montmorillonite samples equilibrated at $I=0.006$ M, $\text{pH}=4.48-6.40$ the predominant LAS surrounding the adsorbed Pb atoms is very similar to the LAS surrounding hydrated Pb atoms. This suggests that Pb is adsorbing via outer-sphere mechanisms on the montmorillonite at this ionic strength and these pH values. These results agree with the results obtained by analyzing the XANES data. This type of adsorption most likely occurs on the basal planes where there exists an electrostatic charge resulting from isomorphic substitution in the octahedral layer (Figure 3.1). Whether the hydrated Pb atoms form weak hydrogen bonds with the basal O, or reside in the diffuse double layer above the basal O cannot be assessed since no second neighbor structural atoms (Si or Al) were detected. It is possible that both types of outer-sphere complexes are occurring. The bond distances observed for the outer-sphere adsorbed Pb ($R_{\text{Pb-O}}=2.50$ Å) are similar to the bond distances that Bargar et al. (1996) observed for outer-sphere Pb adsorbed on the 001 plane of $\alpha\text{-Al}_2\text{O}_3$ ($R_{\text{Pb-O}}=2.51$ Å).

The fit results for the samples equilibrated at the higher ionic strength, and the sample equilibrated at $I=0.006$ M, $\text{pH}=6.76$ have EXAFS contributions from two different O shells, as well as second shell Pb backscatterers. In these samples our fits indicate the presence of O atoms at $R_{\text{Pb-O}}=2.28-2.30$ Å and $R_{\text{Pb-O}}=2.49$ Å (fixed, see previous discussion). The coordination numbers for the O-shell fit at $R_{\text{Pb-O}}\sim 2.29$ Å ranged from 0.9-2.8, and for the second O-shell $N=0.8-6$. The two Pb-O bond distances in these samples suggest the presence of two different Pb populations with distinct LAS. As discussed above, adsorbed Pb atoms with $R_{\text{Pb-O}}=2.49$ Å are indicative of Pb adsorbed via

an outer-sphere complex. Bond distances for the O shell at $R_{\text{Pb-O}} \sim 2.29 \text{ \AA}$ are similar to those found for the $\text{Pb}_3(\text{OH})_3^{4+}$ (aq) sample ($R_{\text{Pb-O}} = 2.30$, see Table 3.4), where Pb is coordinated by three OH ligands. Bargar et al. (1997), and Strawn et al. (1998) found that inner-sphere Pb complexes adsorbed on aluminum hydroxide had Pb-O bond distances of approximately 2.25 \AA to 2.30 \AA long, and that these distances are consistent with the formation of covalent bonds between Pb atoms and hydroxide ligands. Thus, in the Pb-montmorillonite samples the Pb-O bond distances between 2.28 - 2.30 \AA are indicative of Pb adsorbing via an inner-sphere mechanism.

The presence of second shell Pb atoms in the montmorillonite samples equilibrated at $I=0.1 \text{ M}$, $\text{pH}=6.31$ - 6.77 , and $I=0.006 \text{ M}$, $\text{pH}=6.76$ suggest the presence of Pb polymer complexes in these samples. It is not likely that these complexes occur as precipitates since the solution is undersaturated with respect to PbO (s) . O'Day et al. (1994) and Scheidegger et al. (1998): have found that Co and Ni, respectively, form hydroxide like multinuclear complexes on mineral surfaces even when the solution is undersaturated with respect to these phases. However, in those studies second shell metal backscattering atoms had much larger contributions than the second shell Pb backscattering contributions present in the samples in this study. The small size of the Pb second shell backscattering peak in the RDF (Figure 3.6), and the small value of $N_{\text{Pb-Pb}}$ (1.1 - 1.7) obtained from the fitting suggest that the size and/or number of Pb-polymer complexes forming is small. Fitting the second shell Pb-backscatterers resulted in 1.1 - 1.7 Pb atoms at a distance of 3.75 - 3.79 \AA . This is the same Pb-Pb distance that occurs in

$\text{Pb}_4(\text{OH})_4^{4+}$ (aq) ($R_{\text{Pb-Pb}}=3.76 \text{ \AA}$, $N=1.6$, this study; $R_{\text{Pb-Pb}}=3.76 \text{ \AA}$ (Bargar et al., 1997); and $R=3.75 \text{ \AA}$ (Grimes et al., 1995)).

Bargar et al. (1997) also reported the formation of Pb polymeric complexes at the surfaces of $\alpha\text{-Al}_2\text{O}_3$. However, they proposed that the LAS of the polymer complexes is distinctly different than the LAS of $\text{Pb}_4(\text{OH})_4^{4+}$ (aq) complexes. In our samples the similarity in bond distances, coordination numbers, χ structure, and XANES spectra suggest that the complexes being formed are similar to $\text{Pb}_4(\text{OH})_4^{4+}$ (aq), which is a tetrahedrally shaped Pb cluster with each Pb coordinated to three hydroxide ligands (Grimes et al., 1995; Bargar et al., 1997). The formation of $\text{Pb}_4(\text{OH})_4^{4+}$ (aq) complexes prior to adsorption is not likely for the following reasons: 1) the pH of the Pb-montmorillonite was increased slowly causing a sharp decrease in available Pb as pH increased, and 2) even if none of the Pb were to adsorb most of the available Pb is Pb^{2+} (aq) (at pH=6.75, $I=0.1 \text{ M}$, ~87% Pb^{2+} (aq), ~6% $\text{Pb}_4(\text{OH})_4^{4+}$ (aq) and 7% other Pb-OH complexes (Baes et al., 1986)). The most probable reasons for the formation of Pb-polymers on montmorillonite is multilayer adsorption, and/or enhanced polymer formation due to nucleation from the clay.

In the montmorillonite samples, the relative distribution of Pb between inner- and outer-sphere complexes can be inferred from the coordination numbers obtained for the different O shells. In the samples equilibrated at $I=0.006 \text{ M}$, pH=4.48-6.40 the majority of Pb is adsorbed as outer-sphere complexes since Pb-O bonds with distances characteristic of inner-sphere coordination were not present, and the coordination numbers in all of the samples were ~9. At $I=0.1 \text{ M}$, pH=6.77 most of the Pb is adsorbed

as inner-sphere complexes. In the samples equilibrated at $I=0.1$ M and $\text{pH}=6.31$ and $I=0.006$ M, $\text{pH}=6.76$, the Pb distribution is mixed between inner-and outer-sphere complexes. The coordination numbers of these samples are strongly affected by destructive interference due to the fact that the EXAFS spectra are out of phase, as indicated in Figure 3.7. Thus, the coordination numbers reported in Table 3.4 do not represent a decrease in the number of O atoms surrounding the Pb atoms in the two different types of adsorption complexes. Instead, they represent the different degrees of destructive interference that occur as a result of *averaging* of the contributions from the two different adsorption complexes. In other words, in the systems in which both inner- and outer-sphere adsorption is occurring the actual coordination number of the adsorbed Pb is most likely the same as the coordination number as in the Pb-montmorillonite samples where a single type of adsorption complex dominates. The relative change in the coordination numbers in the systems with two types of adsorption complexes occurring can be used to determine the extent of adsorption via the different adsorption mechanism. Using this reasoning it follows that the amount of inner-sphere adsorption in these samples increases in the order $I=0.006$ M, $\text{pH}=6.76 < I=0.1$ M, $\text{pH}=6.31 < I=0.1$ M, $\text{pH}=6.77$. The same trends for inner-sphere complexation can also be inferred from the XANES spectra.

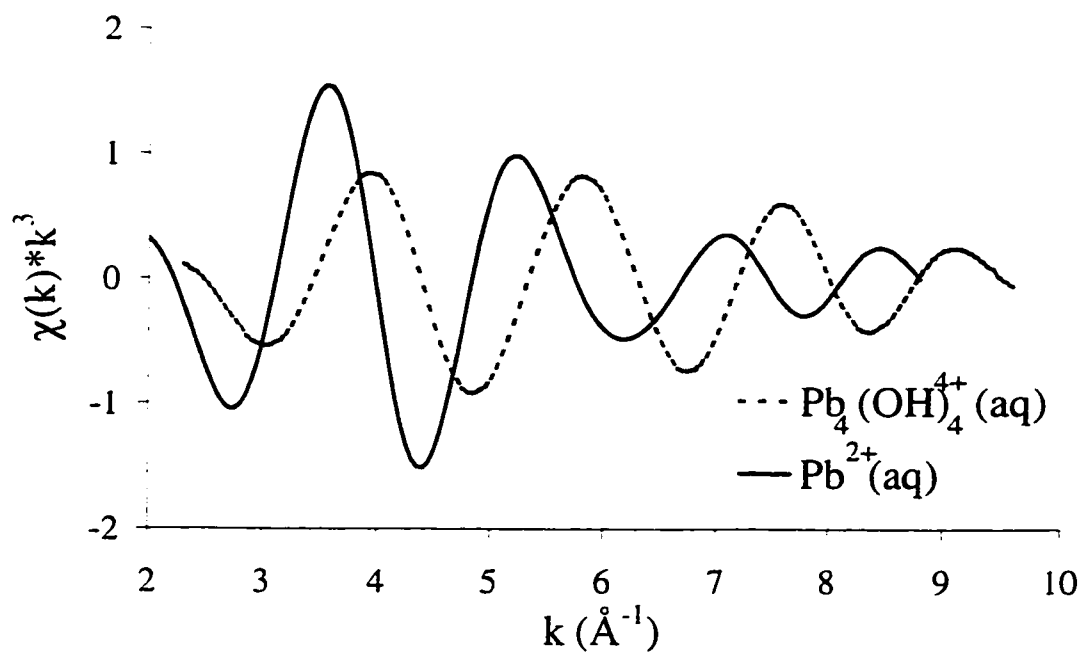


Figure 3.7 Back transformed $\text{Pb}^{2+}(\text{aq})$ ($\Delta R=1.03\text{-}2.95$ \AA) and $\text{Pb}_4(\text{OH})_4^{4+}(\text{aq})$ ($\Delta R=1.03\text{-}2.77$ \AA) samples.

The EXAFS data from this research shows qualitatively and quantitatively that Pb can adsorb as both inner- and outer-sphere adsorption complexes on montmorillonite. XAFS data presented in this paper support the theory that there are multiple types of adsorption sites on montmorillonite. The distribution of Pb between these sites is not only a function of the relative concentration of competing ions, but also pH. Thus, the pH-dependent behavior for Pb adsorption presented in Figure 3.2 can be explained as an increase in inner-sphere adsorption on the edges of the montmorillonite.

3.6 Summary

The results of the macroscopic and microscopic experiments conducted in this study show that Pb adsorption on montmorillonite consist of both inner- and outer-sphere complexes, depending on ionic strength and pH. These results are summarized in Table 3.2. At low ionic strength and pH adsorption is primarily outer-sphere, and most likely occurs on the basal planes existing in the interlayer regions of the montmorillonite. The bond distances between the Pb and the first shell of O atoms for the outer-sphere complexes is 2.50 Å and the coordination number is ~9. This bond distance and coordination number is similar to the Pb²⁺ (aq) sample, suggesting that there exists a layer of water molecules between the complexed Pb atoms and the mineral surface. As pH and ionic strength increase inner-sphere adsorption becomes more important. The bond distance between inner-sphere adsorbed Pb and O ligands was ~2.30 Å. This bond distance is consistent with Pb forming covalent bonds. Thus, it is most likely that in the samples equilibrated at the higher ionic strength, and/or the higher pH, adsorption is occurring on the edges of the montmorillonite, and includes the formation of Pb-

polymers. The data from this study also suggest that adsorbed Pb can exist as a mixture of inner-and outer-sphere complexes under the appropriate ionic strength and pH conditions. The exact distribution between these adsorption modes is a function of competing ion concentration (ionic strength), and the speciation of the functional groups existing on the edges of the montmorillonite.

The information presented in this study will allow scientists and engineers to develop better models that predict the interaction of Pb with clay minerals. The large amount of pH-dependent adsorption that occurs in the Pb-montmorillonite samples demonstrates the importance of edge sites in metal sorption on clay minerals, and that speciation of the metals is a function of ionic strength and pH. This study has also demonstrated the utility of XAFS to distinguish between different adsorption mechanisms on surfaces when they are occurring simultaneously.

3.7 Literature Cited

- Amonette, J. C. and L. W. Zelazny, Eds. 1994. Quantitative methods in soil mineralogy. Soil Science Society of America Special Publications. Soil Science Society of America, Madison, WI.
- Avena, M. J. and C. P. De Pauli. 1998. Proton adsorption and electrokinetics of an Argentinean montmorillonite. *J. Colloid Interface Sci.* 202: 195.
- Babcock, K. L. 1963. Theory of the chemical properties of soil colloidal systems at equilibrium. *Hilgardia* 34 (11): 471.
- Baes, C. F. and R. E. Mesmer. 1986. *The Hydrolysis of Cations. 2.* Krieger Publishing Co., Malabar, FL.
- Baeyens, B. and M. H. Bradbury. 1997. A mechanistic description of Ni and Zn sorption on Na-montmorillonite. Part I: Titration and sorption measurements. *J. Cont. Hyd.* 27: 199.

- Bargar, J. R., G. E. Brown, Jr. and G. A. Parks. 1997. Surface complexation of Pb(II) at oxide-water interfaces: I. XAFS and bond-valence determination of mono- and polynuclear Pb(II) sorption products on Al-oxides. *Geoch. Cosmochim. Acta* 61 (13): 2617.
- Bargar, J. R., S. N. Towle, G. E. Brown, Jr. and G. A. Parks. 1996. Outer-sphere Pb(II) adsorbed at specific surface sites on single crystal α -alumina. *Geoch. Cosmochim. Acta* 60 (18): 3541.
- Bockris, J. O. M. and B. E. Conway. 1954. *Modern aspects of electrochemistry*. Butterworths Scientific Publications, London, England.
- Borchardt, G. 1989. Smectites. p. 675. *In* J. B. Dixon and S. B. Weed (eds.) *Minerals in soil environments*. Vol. 1. Soil Science Society of America, Madison, WI.
- Bouldin, C., L. Furenlid and T. Elam. 1995. MacXAFS: An EXAFS analysis package for the Macintosh. *Phys. B* 208/209: 190.
- Bunker, G. 1984. The XAFS of disordered systems and the cumulant expansion. p. 268. *In* K. O. Hodgson, B. Hedman and J. E. Penner-Hahn (eds.) *EXAFS and near edge structure III*. Springer Verlag, New York, NY.
- Chang, F.-R. C. and G. Sposito. 1996. The electric double layer of a disk-shaped clay mineral particle: effects of electrolyte properties and surface charge density. *J. Colloid Interface Sci.* 178: 555.
- Chisholm-Brause, C. J., K. F. Hayes, A. L. Roe, G. E. Brown, Jr., G. A. Parks and J. O. Leckie. 1990. Spectroscopic investigation of Pb(II) complexes at the γ -Al₂O₃/water interface. *Geoch. Cosmochim. Acta* 54: 1897.
- Fendorf, S. E. and D. L. Sparks. 1996. X-Ray absorption fine structure spectroscopy. p. 377. *In* D. L. Sparks (ed.) *Methods of soil analysis*. Vol. 5. Soil Science Society of America, Madison, WI.
- Goldberg, S. and R. A. Glaubig. 1988. Anion sorption on a calcareous, montmorillonitic soil-arsenic. *Soil Sci. Soc. Am. J.* 52: 1297.
- Grimes, S. M., S. R. Johnston and I. Abrahams. 1995. Characterization of the predominant low-pH lead(II) hydroxo cation, [Pb₄(OH)₄]₄₊; crystal structure of [Pb₄(OH)₄][NO₃]₄ and the implications of basic salt formation on the transport of lead in the aqueous environment. *J. Chem. Soc.* 12: 2081.

- Helmy, A. K., E. A. Ferreiro and S. G. Debussetti. 1994. Cation exchange capacity and condition of zero charge of hydroxyl-Al montmorillonite. *Clays Clay Miner.* 42 (4): 444.
- Hem, J. D. 1976. Inorganic chemistry of Pb in water. U. S. Department of the Interior. Washington.
- Hesterberg, D., D. E. Sayers, W. Zhou, G. M. Plummer and W. P. Robarge. 1997. X-ray absorption spectroscopy of lead and zinc speciation in a contaminated groundwater aquifer. *Environ. Sci. Technol.* 31: 2840.
- Hill, R. 1985. Refinement of the structure of orthorhombic PbO (massicot) by rietveld analysis of neutron powder diffraction data. *Acta Crystallogr.* C41: 1281.
- Hingston, F. J., A. M. Atkinson, A. M. Posner and J. P. Quirk. 1967. Specific adsorption of anions. *Nature* 215: 1459.
- Huang, C. P. and W. Stumm. 1973. Specific adsorption of cations on hydrous γ -Al₂O₃. *J. Colloid Interface Sci.* 43 (2): 409.
- James, R. O. and T. W. Healy. 1972. Adsorption of hydrolyzable metal ions at the oxide water interface. III. A thermodynamic model of adsorption. *J. Colloid Interface Sci.* 45: 65.
- Keren, R. and D. L. Sparks. 1995. The role of edge surfaces in flocculation of 2:1 clay minerals. *Soil Sci. Soc. Am. J.* 59: 430.
- Kim, Y., R. J. Kirkpatrick and R. T. Cygan. 1996. ¹³³Cs NMR study of cesium on the surfaces of kaolinite and illite. *Geoch. Cosmochim. Acta* 60 (21): 4059.
- Leciejewicz, J. 1961. On the crystal structure of tetragonal (red) PbO. *Acta Crystallogr.* 14 (12): 1304.
- Lytle, F. W., R. B. Gregor, D. R. Sandstorm, E. C. Marques, J. Wong, C. L. Spiro, G. P. Huffman and F. E. Huggins. 1984. Measurement of soft X-ray absorption spectra with a fluorescent ion chamber detector. *Nucl. Instrum. Methods Phys. Res.* 226: 542.
- Manceau, A., M.-C. Bosset, G. Sarret, J.-L. Hazemann, M. Mench, P. Cambier and R. Prost. 1996. Direct determination of lead speciation in contaminated soils by EXAFS spectroscopy. *Environ. Sci. Technol.* 30 (5): 1540.

- Marshal, C. E. 1935. Layer lattices and the base exchange clays. *Z. Kristallogr. Mineral.* 91: 443.
- McKinley, J. P., J. M. Zachara, S. C. Smith and G. D. Turner. 1995. The influence of uranyl hydrolysis and multiple site-binding reactions on adsorption of U(VI) to montmorillonite. *Clays Clay Miner.* 43 (5): 586.
- O'Day, P., G. E. Brown, Jr. and G. A. Parks. 1994. X-ray absorption spectroscopy of cobalt (II) multinuclear surface complexes and surface precipitates on kaolinite. *J. Colloid Interface Sci.* 165: 269.
- Papelis, C. and K. F. Hayes. 1996. Distinguishing between interlayer and external sorption sites of clay minerals using X-ray absorption spectroscopy. *Colloids and Surfaces* 107: 89.
- Person, P., J. Nordin, J. Rosenqvist, L. Lovgren, L.-O. Ohman and S. Sjoberg. 1998. Comparison of the adsorption of o-phthalate on boehmite (γ -AlOOH), aged γ -Al₂O₃, and goethite (γ -FeOOH). *J. Colloid Interface Sci.* 206: 252.
- Rao, K. L. and J. Wong. 1984. A XANES investigation of the bonding of divalent lead in solids. *J. Chem. Phys.* 81 (11): 4832.
- Reed, B. E., P. C. Carriere and R. Moore. 1996. Flushing of Pb(II) contaminated soils using HCl, EDTA, and CaCl₂. *J. Env. Eng.* 122: 48.
- Richens, D. T. 1997. *The chemistry of aqua ions.* John Wiley and Sons, Chinchester, England.
- Sarret, G., A. Manceau, L. Spadini, J.-C. Roux, J.-L. Hazemann, Y. Soldo, L. Eybert-Bernard and J.-J. Menthonnex. 1998. Structural determinations of Zn and Pb binding sites in penicillium chrysogenum cell walls by EXAFS spectroscopy. *Environ. Sci. Technol.* 32: 1648.
- Scheidegger, A. M., D. G. Strawn, G. M. Lambie and D. L. Sparks. 1998. The kinetics of mixed Ni-Al hydroxide formation on clays and aluminum oxides: A time-resolved XAFS study. *Geoch. Cosmochim. Acta* 62 (13): 2233.
- Schindler, P. W., P. Liechti and J. C. Westall. 1987. Adsorption of copper, cadmium and lead from aqueous solution to the kaolinite/water interface. *Neth. J. Ag. Sci.* 35: 219.

- Schoefield, R. K. and H. R. Samson. 1953. The deflocculation of kaolinite suspension and the accompanying change-over from positive to negative chloride adsorption. *Clay Miner. Bull.* 2: 45.
- Schulthess, C. P. and C. P. Huang. 1990. Adsorption of heavy metals by silicon and aluminum oxide surfaces on clay minerals. *Soil Sci. Soc. Am. J.* 54: 679.
- Shimoni Livny, L., J. P. Glusker and C. W. Bock. 1998. Lone pair functionality in divalent Pb compounds. *Inorg. Chem.* 37: 1853.
- Sparks, D. L. 1995. *Environmental soil chemistry*. Academic Press, San Diego, CA.
- Sposito, G. 1989. *The chemistry of soils*. Oxford University Press, New York, NY.
- Stern, E. A. 1988. Theory of EXAFS. p. 3. *In* D. C. Koningsberger and R. Prins (eds.) *X-ray absorption: Principles, applications, and techniques of EXAFS, SEXAFS, and XANES*. Wiley, New York, NY.
- Strawn, D. G., A. M. Scheidegger and D. L. Sparks. 1998. Kinetics and mechanisms of Pb(II) sorption and desorption at the aluminum oxide-water interface. *Environ. Sci. Technol.* 32 (7): 2596.
- Stumm, W. and J. J. Morgan. 1996. *Aquatic chemistry, chemical equilibria and rates in natural waters*. John Wiley & Sons, Inc., New York, NY.
- Teo, B. K. and D. C. Joy. 1981. *EXAFS spectroscopy: Techniques and applications*. Plenum, New York, NY.
- Thomas, G. W. 1977. Historical developments in soil chemistry: Ion exchange. *Soil Sci. Soc. Am. J.* 41 (2): 230.
- Wang, Z. and W. Stumm. 1987. Heavy metal complexation by surfaces and humic acids: A brief discourse on assessment by acidimetric titration. *Neth. J. Ag. Sci.* 35: 231.
- Westall, J. C. 1986. Reactions at the oxide-solution interface: Chemical and electrostatic models. p. 54. *In* J. A. Davis and K. F. Hayes (eds.) *Geochemical processes at mineral surfaces*. Vol. 323. American Chemical Society, Washington DC.
- White, G. N. and L. W. Zelazny. 1988. Analysis and implications of the edge structure of dioctahedral phyllosilicates. *Clays Clay Miner.* 36 (2): 141.

- Yu, Y. H., T. Tyliczszak and A. P. Hitchcock. 1989. Pb L₁ EXAFS and near edge-studies of lead metal and lead oxides. *J. Phy. Chem. Solids* 51 (5): 445.
- Zabinski, S. I., J. J. Rehr and A. Ankudinov. 1997. Multiple-scattering calculations of X-ray absorption spectra. *Phys. Rev. B* 52: 2995.
- Zachara, J. M., S. C. Smith, J. P. McKinley and C. T. Resch. 1993. Cadmium sorption on specimen and soil smectites in sodium and calcium electrolytes. *Soil Sci. Soc. Am. J.* 57: 1491.
- Zimdahl, R. L. and R. K. Skogerboe. 1977. Behavior of Pb in soil. *Environ. Sci. Technol.* 11: 1202.

Chapter 4

Effects of Soil Organic Matter on the Kinetics and Mechanisms of Pb(II) Sorption and Desorption in Soil

4.1 Abstract

To improve predictions of the toxicity and threat from Pb contaminated soil it is critical that time-dependent sorption and desorption behavior be understood. In this chapter the sorption and desorption behavior (pH=5.50, $I=0.05$ M) of Pb in a Matapeake silt loam soil (Typic Hapludult) were studied using stirred-flow and batch experiments. In addition we studied the effects of soil organic matter (SOM) on sorption and desorption behavior by treating the soil with sodium hypochlorite to remove the SOM fraction, and using a soil with six times as much SOM (St. Johns loamy sand [Typic Haplaquods]) as the Matapeake soil. Lead sorption consisted of a fast initial reaction in which all of the Pb added to the stirred-flow chamber was sorbed. Following this initial fast reaction, sorption continued and appears to be rate-limited (indicated by a decrease in the outflow concentration when the flow rate was decreased, or when the flow was stopped). The total amount of Pb sorbed was 102, 44 and 27 mmol kg⁻¹ for the St. Johns soil and the untreated and treated Matapeake soils, respectively. Desorption experiments were conducted on the soils using the background electrolyte as the eluent in the stirred-flow chamber. In the St. Johns soil only 32% of the total sorbed Pb was desorbed

(desorption time=sorption time). while 47 and 32% of the sorbed Pb was released from the untreated and treated Matapeake soil, respectively. The correlation between SOM in the soils, and the percent Pb desorbed from the soils suggests that SOM plays an important role in slow desorption reactions of Pb from soil materials. Aging experiments in which sorbed Pb was incubated for 1, 10 and 32 days showed that sorption incubation time had no effect on Pb desorption behavior. Analysis of the treated and untreated Matapeake soils by X-ray absorption fine structure (XAFS) spectroscopy revealed that the the local atomic structure of sorbed Pb is distinctly different in the two samples. In the soil treated to remove SOM the data were well represented by theoretical models using O, Si, and Pb backscattering atoms. In the untreated soil the XAFS data were best described by O and C backscatterers. These XAFS results confirm that the sorption mechanisms in the two systems are different.

4.2 Introduction

To predict the fate and transport of contaminants such as Pb in the environment scientists and engineers commonly rely on distribution coefficients and maximum adsorption levels that are obtained from experiments in which it is assumed that the reaction is at equilibrium. However, reactions in the environment are rarely at equilibrium, but instead are in a state of continuous change due to the dynamic processes occurring (Sposito, 1989; Sparks, 1995). Another discrepancy that causes errors in predicting the potential toxicity of a contaminant is that researchers often neglect desorption behavior, which is an important process controlling metal bioavailability in the environment. Thus, in order to improve remediation strategies, risk assessments, and

make better predictions about the mobility of contaminants it is critical that time-dependent metal sorption and desorption behavior on soil be understood, as well as the reaction mechanism of the sorption/desorption reactions.

Lead sorption behavior is often initially fast, followed by a slow reaction (Benjamin et al., 1981; Hayes et al., 1986; Strawn et al., 1998). The fast reaction is most likely adsorption via electrostatic attraction, and/or inner-sphere complexation with functional groups present on the soil components. There are several possible reasons for the slow sorption steps, such as: slow diffusion to interior sites existing on minerals and organic matter, formation of precipitates on surfaces which can sometimes be slower than typical sorption, and adsorption onto sites that have relatively large activation energies (Fuller et al., 1993; Papelis et al., 1995; Loehr et al., 1996; Scheidegger et al., 1998). Due to the heterogeneity of soils, and the presence of many different types of sorption sites, sorption reactions can take several days to reach steady state. It is possible that multiple slow reaction mechanisms are responsible for the slow sorption reactions in soils.

There are three main processes that control the fate and bioavailability of metals in soils: 1) removal of metals from the soil solution by sorption onto soil particles, 2) release of the metal from the soil particle to the soil solution (desorption), and 3) precipitation of the metal as an independent phase in the soil matrix. Less is known about the desorption behavior of metals from soils than the other two processes. This is unfortunate since once a soil is contaminated desorption is an important process that controls the bioavailability of the contaminant. There are several reasons for the lack of data on desorption behavior, for example: desorption experiments are more difficult to

conduct than adsorption experiments, the choice of solution used to desorb the sorbed metal can have dramatic effects on the results obtained, and desorption kinetics are often considered to be either the same as sorption, or insignificant. However, if accurate assessments on the fate of metals in soils are to be gained it is critical that desorption behavior be studied as well as sorption behavior.

It is often observed that desorption reactions are slower than sorption reactions. Smith and Comans (1996) predicted that adsorption half-lives for Cs sorption on sediments were between 50 and 125 days, while desorption half-lives were on the order of 10 years. Failure to include the slow desorption reaction in transport models severely underestimated the remobilization potential of Cs.

Slow desorption reactions have also been observed for metals (Kuo et al., 1980; McKenzie, 1980; Schultz et al., 1987; Ainsworth et al., 1994; Scheidegger et al., 1996). The mechanisms of slow desorption are likely the same as those for slow sorption. A possible reason that desorption reactions are slower than sorption reactions is because the sorbate undergoes a transformation from one phase to another, for example: conversion from an adsorbed species to a surface precipitate. In addition, desorption reactions often require large activation energies, which cause the reaction to proceed slowly (McBride, 1994).

Lead sorption and desorption rates on mineral surfaces are often similar (Ainsworth et al., 1994; Gunneriusson et al., 1994; Strawn et al., 1998). However, in some cases desorption from soils may be much slower than sorption. This could be due to the presence of SOM and/or the formation of Pb multinuclear complexes with

carbonates, phosphates and sulfates present in the soil. Bunzl et al. (1976) found that the desorption rate of Pb from SOM was significantly slower than the adsorption rate.

Similar trends were found for Pb adsorption and desorption on activated carbon (Wilczak et al., 1993).

Soil organic matter is an important component of the soil since it has a high surface area, and has functional groups that are Lewis bases (e.g., carboxyl and phenol groups) that metals can form chemical bonds with (Sparks, 1995). It has been observed that Pb forms strong complexes with SOM, and that it can out-compete most other metals for adsorption sites on SOM (Kendorff et al., 1980; Elliot et al., 1986; Jin et al., 1996; Suave et al., 1998). Since SOM is an important sink for Pb in soils, a better understanding of Pb desorption behavior from the SOM fraction would be useful.

Kinetic studies are most often conducted using batch reactors. While valuable information has been obtained from these experiments, the batch technique is not ideal in desorption studies since readsorption of the sorbate and accumulation in solution can hinder desorption (Sparks, 1989). One of the most beneficial uses of stirred-flow reactors is to study desorption reactions since the desorbed products are continuously removed from solution. There are several other reasons that stirred-flow reactors are advantageous for studying sorption and desorption reactions: relatively fast reactions can be measured compared to batch methods; carbon dioxide can be easily removed from the system; sorption and desorption kinetics can be measured in a single experiment; and the system is well mixed, which aids in elimination of film diffusion and calculation of the

dilution occurring in the reaction chamber (Sparks, 1989; Amacher, 1991; Yin et al., 1997).

The objectives of this study are to characterize sorption and desorption behavior of Pb on soil, and to determine the importance of SOM on sorption and desorption. To accomplish these objectives we used both batch and stirred-flow studies, and soils with three different SOM contents. Information obtained from this study will allow scientists and engineers to improve remediation strategies, disposal practices and risk assessments. Such information is critical since Pb is used in a variety of industrial and manufacturing processes, but is one of the most common contaminants found at hazardous waste sites (Reed et al., 1996).

4.3 Methods and Materials

The A horizons (~0-20 cm) of the Matapeake silt loam (Typic Hapludult) and the St. Johns loamy sand (Typic Haplaquods) from Delaware were used in this study. The physicochemical and mineralogical properties of the soils were determined using standard methods (Sparks, 1996) (Table 4.1). Studies were also conducted on a Matapeake soil that was treated to remove organic matter using an adapted method described in Amonette and Zelazny (1994). Thirty grams of soil were suspended in ~50 mL of sodium hypochlorite (pH=9.5) (Na-hypochlorite is an effective oxidant for SOM, and is less invasive than other SOM removal procedures (Lavkulich et al., 1970)). The suspension was heated to 338 K and allowed to react for 20 minutes. The samples were then centrifuged, decanted, and treated with additional Na-hypochlorite. This procedure was repeated four times. Following oxidation of the organic matter the soil was washed

repeatedly with a 1 M NaNO₃ solution to Na saturate it. The Na-saturated soil was then washed with deionized water to remove excess NaNO₃. The resulting soil had 0.1% SOM remaining, as determined by the Walkley Black method (Nelson et al., 1996). Analysis of the soils for total carbon by loss on emissions resulted in 1.38% for the untreated Matapeake soil, and 0.18% for the treated Matapeake soil.

In all of the soils the < 2 mm fraction was separated by sieving. In order to eliminate fine colloids that can pass through the filter used in the stirred-flow experiments the soils were preconditioned using the following procedure: the soils were suspended in 0.01 M NaNO₃ and shaken at 160 rpm for 16 hours, and the samples were centrifuged at 10,000 rpm for 10 min and the supernatant was discarded, thus eliminating any fine colloids that did not settle during centrifugation. This procedure was repeated three times; in the third treatment deionized water was used to resuspend the soil rather than NaNO₃. The final paste was washed with deionized water and filtered to separate the soil.

All solutions were made with ACS reagent grade chemicals and distilled deionized water. Carbon dioxide was eliminated from all experiments by working under an N₂ atmosphere. The temperature of all experiments was maintained at 298 K.

Table 4.1 Physicochemical and mineralogical characteristics of the soils used in this study.

Soil type	Subgroup	pH	Cation exchange capacity (cmol + kg ⁻¹) ^a	Organic matter (%) ^b	Sand/silt/clay fractions (%)	Mineralogy of <2µm clay fraction
Matapeake silt loam	Typic Hapludult	5.3	2.86	2.1	42/54/5	kaolinite~vermiculite>quartz>mica
Treated Matapeake silt loam	-	-	-	0.1	-	-
St. Johns loamy sand	Typic Haplaquods	3.6	13.32	13	70/24/5	mica>kaolinite>montmorillonite>gibbsite>quartz

^a Based on Mg saturation, Ca exchange. ^b Walkley-Black method (Nelson, 1986).

4.3.1 Batch Experiments

In order to gain insight into the overall sorption behavior, and make comparisons to the results from the stirred-flow experiments, batch isotherm and kinetic studies were conducted on the Matapeake soil. One gram of soil was preequilibrated for 24 h in background solution adjusted to pH=5.50. The background solution consisted of a mixture of NaNO₃ and 0.05 M MES (buffer). The buffer was necessary to control pH during the adsorption experiments since initial experiments revealed that Pb sorption and desorption involve proton exchange reactions. Titration experiments with this buffer in solutions of Pb confirmed the results of others (Good et al., 1966; Baeyens et al., 1997); no detectable complexation reactions occur between Pb and the MES buffer. The concentration of NaNO₃ used in the experiments was adjusted to make total $I=0.05$ M (including the MES and the Pb solution).

In the isotherm experiments the initial Pb concentrations ranged from 1 to 12 mM. Samples with no soil present were prepared using identical procedures as the sorption samples to determine the exact initial concentration of the sorption samples. The solid concentration of the samples was 100 g L⁻¹. Following the addition of the Pb solution the pH of the samples was adjusted to pH=5.50. After 24 h of incubation the pH of the samples was checked again; only minor adjustments for the samples incubated at the highest concentrations were required. The samples were incubated for a total of 48 h on an end-over-end shaker operating at 20 rpm. At the end of the incubation period the samples were centrifuged at 10,000 rpm for 10 minutes. The supernatant was filtered

through a 0.2 μm filter and diluted 2:3 with 1 M HNO_3 . The solution was then analyzed for total Pb using an ICP spectrometer.

At the start of the kinetic experiment 1.5 ml of a Pb stock solution $[\text{Pb}]=12.25$ mM. was added to 3.5 ml of suspension (0.50 g soil). The pH of the suspension was maintained at 5.50 throughout the experiment using the MES buffer, and pH adjustments were made throughout the experiment by addition of NaOH. Periodically (8 min to 800 h) samples were removed from incubation and processed using the same procedures as mentioned above. The total amount of Pb adsorbed in the kinetic and the isotherm experiments was calculated from the difference between the initial and final Pb concentrations.

4.3.2 Stirred-flow Experiments

The reaction chamber used for these experiments was similar in design to the reaction chamber used in the experiments of Bar-Tal et al. (1990). The setup of the stirred-flow experiment is illustrated in Figure 4.1. The pump used in these experiments was a piston displacement pump designed for use in an HPLC system. The experiment was started by placing 0.75 g of pretreated soil in the reaction chamber and filling the chamber with background electrolyte ($I=0.05$ M [MES and NaNO_3] and $\text{pH}=5.50$). A 25 mm 0.2 μm filter was used in the reaction chamber. Upon sealing the reaction chamber, CO_2 free background electrolyte solution was flowed through the chamber for 10 min at 1 ml min^{-1} and the suspension was allowed to sit (no flow) for 20 min to preequilibrate. The reactor had an approximate volume of 8 ml, the exact volume was determined by

fitting the outflow concentration from an experiment in which soil was not present in the chamber. The suspension in the reaction chamber was stirred by a magnetic stir bar (12.7 mm long and 3 mm in diameter) at 400 rpm. To initiate the experiment a Pb solution ($[Pb]=2.32$ mM, $I=0.05$ M) was pumped into the chamber. The effluent was collected using a fraction collector set to collect 2 ml of solution per tube. The fraction collector was started when the first drop of solution exited the outflow tube. The flow rate in the experiments was either 0.4 ml min^{-1} or 4 ml min^{-1} . The flow rate was monitored and found to be stable within $\pm 3\%$ throughout the experiment.

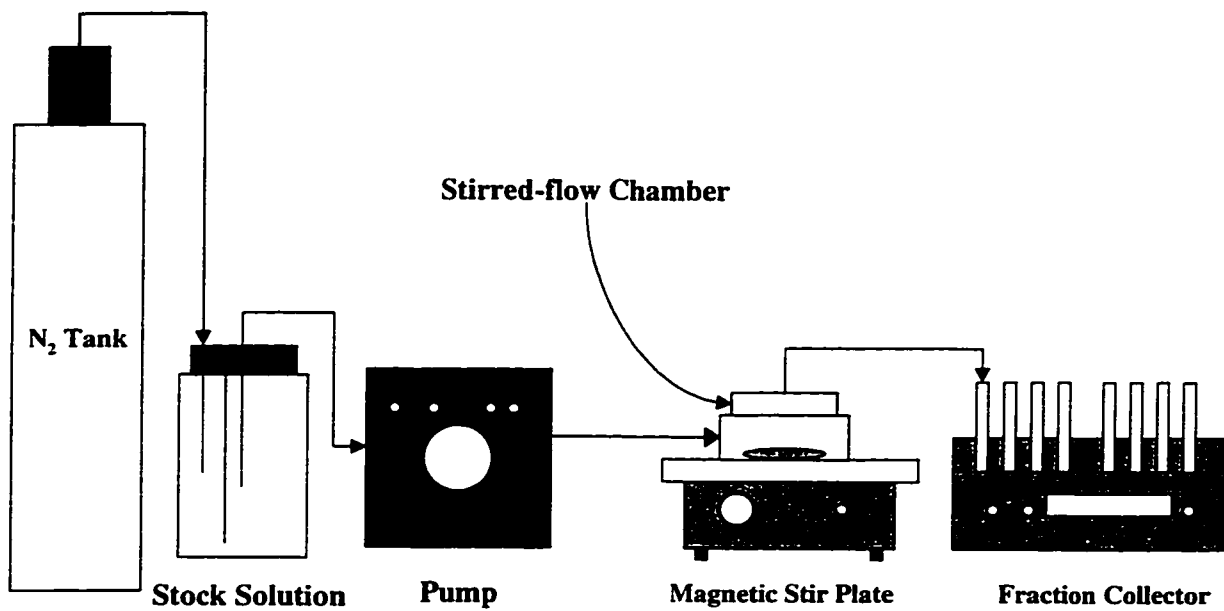


Figure 4.1 Schematic illustrating the experimental design of the stirred-flow experiments.

When the [Pb] in the outflow was the same as the inflow the adsorption experiment was ended. The tubes were then purged with background electrolyte, and the desorption experiment was initiated. In all of the desorption experiments the pH and ionic strength of the inflow solution was the same as in the sorption experiments; in other words, the desorption and sorption solutions were identical except for the presence of Pb.

To determine if the sorption and desorption reactions were rate-limited the flow was stopped during the experiment for 30 min. If the reaction is not at equilibrium when the flow is stopped then sorption will continue (Bar-Tal et al., 1990). This results in a drop in the [Pb] in the chamber, which will be detected in the outflow when the flow is resumed.

The effects of aging on desorption were measured on the Matapeake soil by first adsorbing Pb using batch incubation procedures as described above, and then transferring the soil to the stirred-flow chamber for desorption. In these experiments the initial sorptive in the chamber was a 2.32 mM Pb solution, the same concentration present in the chamber at the start of the desorption experiments conducted directly after the stirred-flow sorption experiments. The outflow from all of the experiments was acidified and analyzed with an ICP spectrometer for total Pb.

The data from the stirred-flow experiments are plotted as a function of chamber volumes (CV), which is calculated by multiplying the flow rate and the time and dividing by the volume of the chamber. This is useful for comparisons of data obtained from experiments conducted at different flow rates since it normalizes the data relative to the flow rate. Thus, any differences between the data obtained at the different flow rates

are the result of either changes in the surface reactions, or in the physical flow and mixing dynamics (hydrodynamics) of the system.

To accurately analyze the results from stirred-flow experiments, it is necessary to account for hydrodynamic effects such as diffusion and dispersion. To accomplish this, tracer experiments at several different flow rates were conducted. From these data the effective volume of the chamber (V_{ce}) was calculated. Using the effective chamber volume instead of the actual volume to calculate CV allows data obtained at different flow rates to be compared. Thus, in all of the adsorption and desorption experiments presented in this study the flow rate dependent value of V_{ce} was used to calculate CV.

4.3.4 Data Analysis

One of the limitations of stirred-flow analysis is that the amount of sorbate being sorbed at any given time cannot be measured directly; instead it is necessary to use models to derive the adsorption behavior. A common approach to modeling reactions in a stirred-flow system utilizes a mass balance equation (Bar-Tal et al., 1990). The mass balance equation for a stirred-flow reactor is as follows:

$$\frac{dC_{chamber}}{dt} * V_c = ((C_{in} - C_{out}) * Q) - (m * \frac{dq}{dt}) \quad (4.1)$$

Where $C_{chamber}$ is the [Pb] in the chamber (mmol L^{-1}), t is time (min), V_c is the volume of solution in the chamber (L), C_{in} is the [Pb] that is being pumped into the chamber (mmol L^{-1}), C_{out} is the [Pb] leaving the chamber (mmol L^{-1}), Q is the flow rate (L min^{-1}), q is the

amount of Pb sorbed (mmol kg^{-1}), and m is the mass of soil (kg). Since in the stirred-flow chamber the solution is well mixed, the $[\text{Pb}]$ in the chamber equals $[\text{Pb}]$ leaving the chamber ($C_{\text{chamber}}=C_{\text{out}}$). If there is no soil in the chamber, or there is no reaction occurring, then $dq/dt=0$, and the equation can be integrated to find C_{out} as a function of time, which is equivalent to the outflow concentration of a non-sorbing tracer.

The reaction term dq/dt represents the rate of adsorption or desorption occurring in the reaction chamber. Equation (4.1) is a first-order differential equation that can be solved analytically only for limited cases (Skopp et al., 1986; Sparks, 1989; Bar-Tal et al., 1990). To solve Equation (4.1) one defines the rate law for the sorption/desorption reaction (dq/dt), and the outflow concentration as a function of time ($C_{\text{out}}(t)$) can be calculated. In this study fitting of the stirred-flow sorption data was not attempted.

Several equations have been used to describe sorption behavior in a stirred-flow reactor such as first-order, fractional-order, Elovich, and parabolic diffusion (Skopp et al., 1986; Sparks, 1989; Bar-Tal et al., 1990). However, based on the Pb desorption behavior observed in this study, these equations are not appropriate since the sorption behavior of a fast and slow reaction phase. A better model to describe the Pb sorption data would include a fast equilibrium reaction, and a slow rate-limited secondary reaction. Several different multireaction models have been developed to describe metal sorption and desorption in soils (Amacher et al., 1988; Selim et al., 1989; Smith et al., 1996). These reactions usually have two or more variables to be fit. It is our experience that fitting Equation (4.1) using rate laws with more than one parameter to be optimized yields

non-robust results (i.e., the rate constants are correlated to each other, and the initial guesses). This indicates that Equation (4.1) is over-parameterized when equations with too many variables are used to describe the reaction rate term.

For the desorption study, in order to make relative comparisons it is useful to normalize the data by the total amount of Pb sorbed. To do this we estimated the amount of Pb desorbed at a given time from the difference in the areas under the curves of the tracer, and the outflow concentration when desorption is conducted. The total amount of Pb sorbed can be estimated using a similar approach; when the outflow concentration is the same as the inflow concentration the difference between the blank and the sorption curve represents the total amount of Pb removed from solution. The amount of Pb sorbed or desorbed is then calculated by multiplying the area by the flow rate and dividing by the mass of soil. To calculate the areas under the curves the integral of a cubic-spline interpolated from $C_{out}(t)$ was calculated. These calculations were made using the algorithms in the computer program Scientist (MicroMath Inc.).

4.3.5 XAFS Experiments

Treated (SOM removed) and untreated soil samples were analyzed using XAFS to determine the local atomic structure surrounding the sorbed Pb in the presence and absence of SOM. The samples were incubated using the same procedures described above. For XAFS analysis the wet pastes were loaded into Teflon sample cell holders in the glovebox and sealed with Kapton Tape (CHR Industries).

XAFS data acquisition of the L_{III} -edge (13055 eV) was conducted at beamline X-11A at the National Synchrotron Light Source (NSLS), Brookhaven National Laboratory, Upton, NY. Details of the XAFS data collection procedures and data analysis are described in Strawn et al. (1998). In this study fitting of the RSF was attempted using theoretical paths for Pb, O, Si, and C backscatterer atoms generated from model compounds using FEFF 6.0. Estimations of the errors associated with the coordination numbers (N), bond distances (R) and Debye-Waller factors (σ^2) were made from the confidence limits of the least squares non-linear fitting procedure. Previous data analysis (Strawn et al., 1998) has shown that these values are usually larger than the absolute errors associated with fitting model compounds.

4.4 Results and Discussion

4.4.1 Batch Experiments

The adsorption isotherm for the Matapeake soil is presented in Figure 4.2. The solid line in Figure 4.2 represents the best fit of the data to the Freundlich adsorption isotherm equation:

$$q = K_d * C^{1/n} \quad (4.2)$$

Where K_d is the Freundlich distribution coefficient and n is a correction factor (Sparks, 1995). For the Matapeake soil $K_d=53.83$, and $n=4.64$. When the initial concentration of Pb is low most of the Pb is sorbed by the soil. This is characteristic of a strong affinity of the soil for Pb. As the initial concentration of Pb increases, the slope of the sorption isotherm levels off, indicating that the soil is reaching a sorption maximum. The sorption

behavior displayed by the Matapeake soil is typical L-type sorption behavior which is commonly observed for metal sorption by soils (Sparks, 1995).

The results of the batch sorption kinetic experiments are presented in Figure 4.3. Within the first 8 min (first sampling time) a very fast reaction occurred, accounting for 78% of the total sorbed Pb. Following the initial fast reaction the sorption reaction continued for ~50 h. At times longer than 50 hours only a small amount of additional sorption occurred (~7%). After 800 h, ~79% of the Pb initially added to the suspension had been removed. The data were modeled using a reversible first-order reaction:

$$\frac{dq}{dt} = k * (q_{\max} - q) \quad (4.3)$$

Where q_{\max} is the maximum amount of sorption at equilibrium (mmol kg^{-1}), and k is the overall rate coefficient (t^{-1}). This equation was chosen since reactions in soils are often observed to follow apparent first-order reaction kinetics (Sparks, 1989; Amacher, 1991). The initial conditions used to fit the data were $t=0.13$ h, $q=50$ mmol kg^{-1} , and $q_{\max}=65.0$ mmol kg^{-1} . The overall apparent rate constant obtained from the fit of the data was $k=0.012$ min^{-1} . Using this value the half life for the slow reaction was calculated to be 58 h.

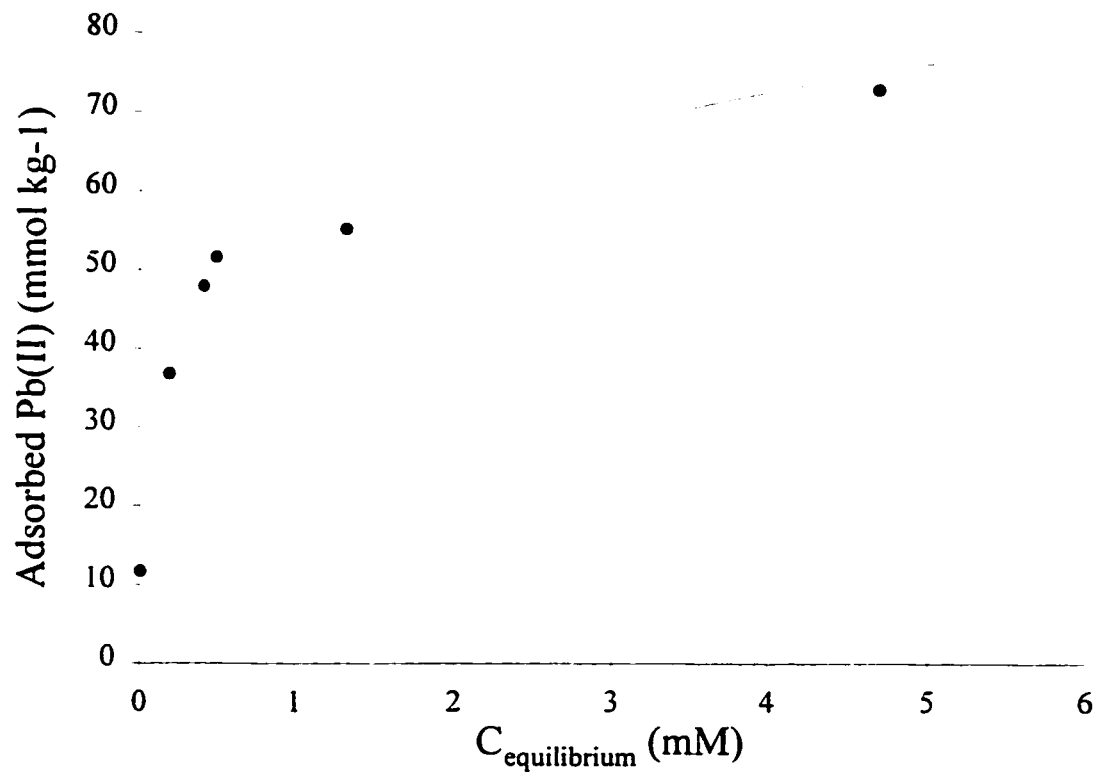


Figure 4.2 Sorption isotherm on the untreated Matapeake soil. The solid line is the best fit to the Freundlich equation (Equation (4.2)).

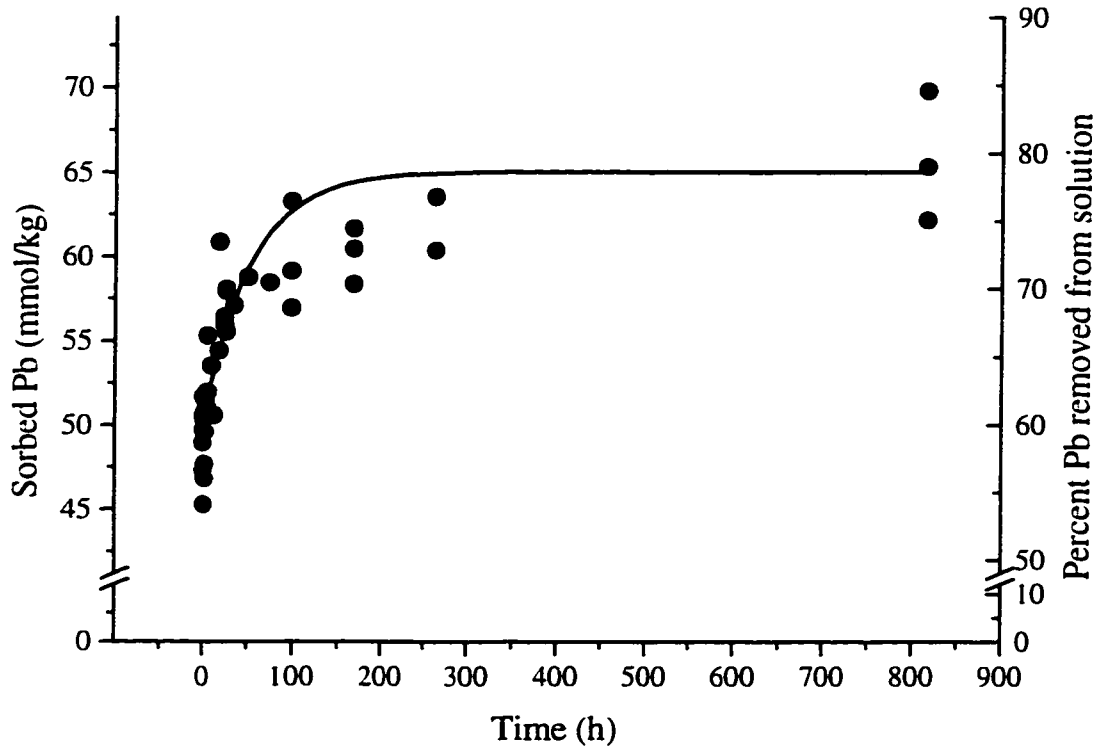


Figure 4.3 Sorption kinetics on Matapeake soil measured using the batch method. The solid line is the best fit to the first-order reversible equation, (Equation (4.3)).

The two stage time-dependent Pb sorption behavior is similar to the results observed on pure components and soils obtained by other researchers. Carriere et al. (1995) found that Pb sorption on soil was fast at low initial Pb concentrations, but at higher concentrations the reaction became much slower, taking several days to reach a steady state. From these results Carriere (1995) suggested that precipitation reactions were responsible for the slow sorption reaction since they were most noticeable at the higher [Pb]. Hayes and Leckie (1986), and Benjamin and Leckie (1981), found that sorption of Pb on iron hydroxides (common minerals in soils) was initially fast followed by a much slower reaction. Similar results were found by Strawn et al. (1998) for Pb adsorption on aluminum oxide. Slow Pb adsorption has also been observed on pure organic materials (Wilczak et al., 1993). Since soil is a mixture of organic and inorganic components, and it contains several different types of sorption sites, it is likely that several mechanisms are responsible for the slow sorption reactions. These may include diffusion, precipitation, and/or sorption reactions on sites that have a higher activation energy than the fast sorption sites.

4.4.2 Stirred-Flow Experiments

The results of the tracer experiments are presented in Figures 4.4 and 4.5. In Figure 4.4 the relative outflow concentration (C_{out}/C_{in}) is plotted as a function of the number of CV, assuming that $V_c=8.0$ ml at all flow rates. The data in Figure 4.4 reveal that as the flow rate changes from 0.4 to 4 ml min⁻¹, $C_{out}/C_{in}(CV)$ shifts to the right. These changes are particularly noticeable at higher CV. The most likely cause of this shift is

diffusion and/or dispersion-type effects that are occurring in the outflow tubing, as well as in transfer of the solution from the reaction chamber to the post-chamber (small volume after the filter, before the outflow tubing). Seyfried et al. (1989) suggested that any differences in C_{out}/C_{in} (CV) at different flow rates could be a result of inefficient mixing. However, since in this system the differences become more pronounced at longer times, or CV, and diffusion and dispersion are time-dependent (and flow rate dependent) processes, we propose that the differences are a result of diffusion and/or dispersion.

To account for the differences observed in Figure 4.4, Equation (4.1) was fit to the data with $dq/dt=0$ and V_c was allowed to vary. The model fit to the data resulted in effective chamber volumes (V_{ce}) of 7.98, 8.10 and 8.32 for $Q=0.4, 2.0$ and 4.0 ml min^{-1} , respectively (a maximum difference of ~4% difference). An alternative approach is to model the data using a coefficient that is analogous to the dispersion coefficient in the convective dispersion equation. However, since in this system using V_{ce} accomplishes the same thing as a dispersion coefficient would, and this model is simple and the data are well represented, we suggest that this approach is legitimate.

The data and the best fit for the tracer experiments as a function of the number of chamber volumes calculated using V_{ce} are presented in Figure 4.5. The data points nearly overlap, and the fit of the mass balance equation (Equation 4.1) represents the data very well ($r^2=1.00$). This suggests that using V_{ce} to calculate CV accounts for differences in diffusion and/or dispersion at the different flow rates.

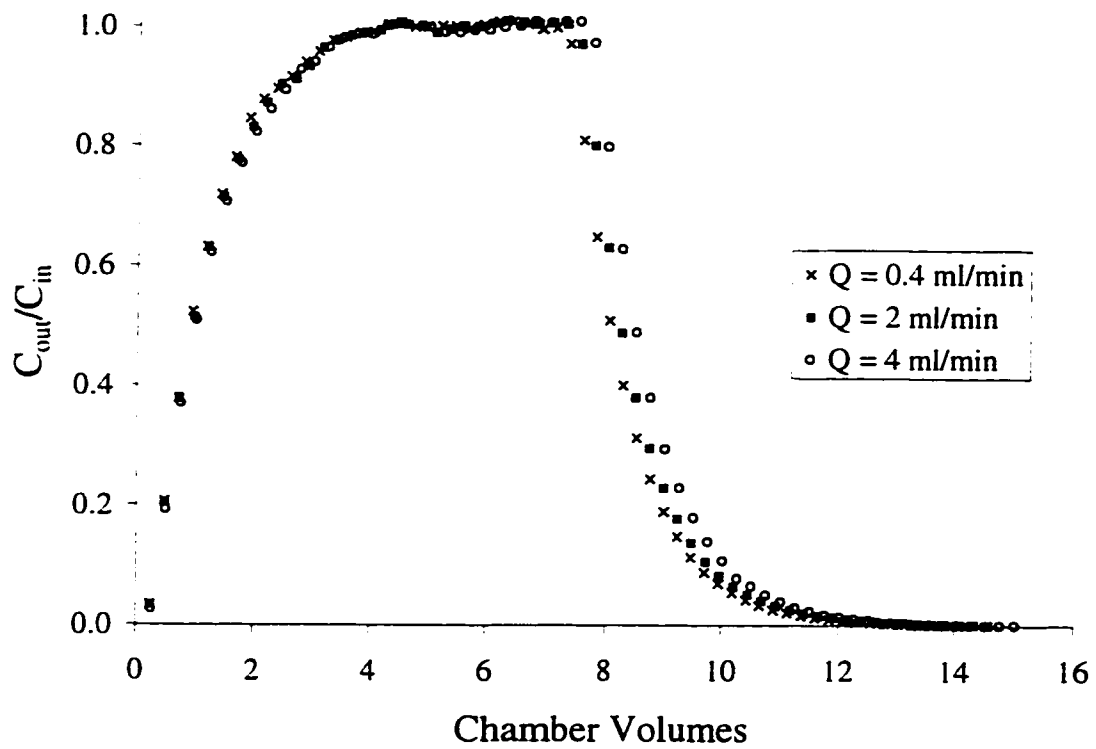


Figure 4.4 Results of tracer experiment conducted at different flow rates. Chamber volumes were calculated using $V_c=8$ ml.

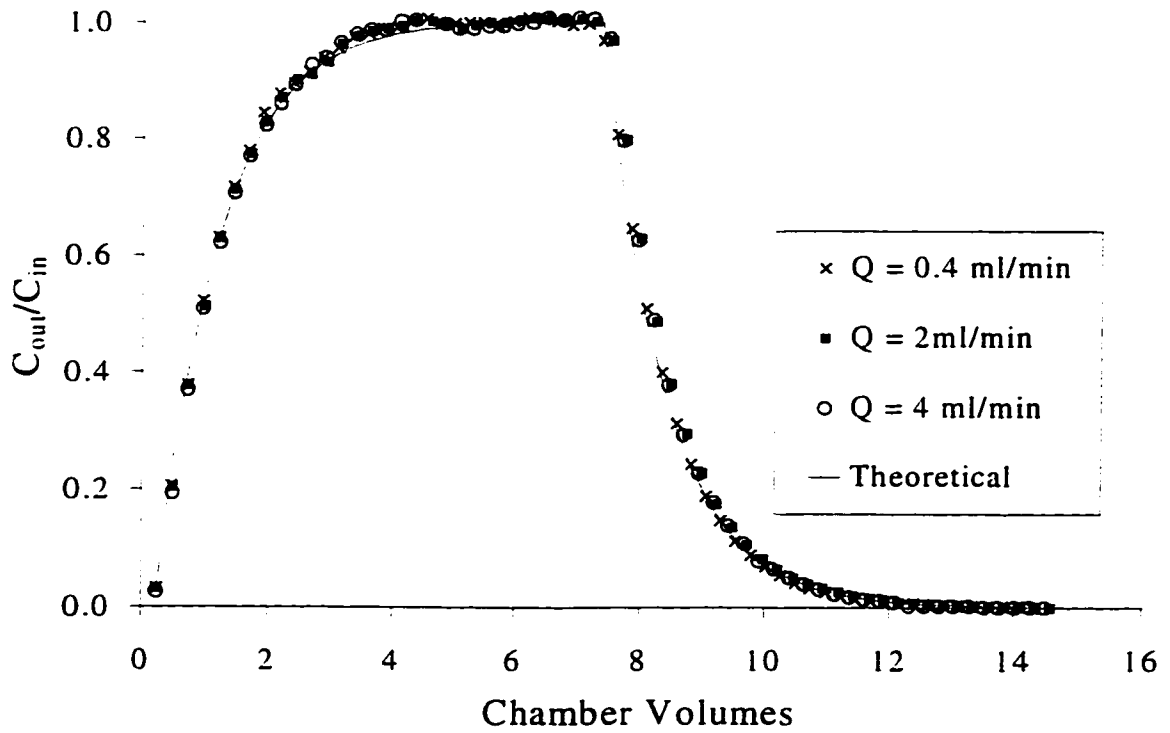


Figure 4.5 Results of tracer experiment conducted at different flow rates. Chamber volumes were calculated using the effective volume of the chamber derived from the best fit to Equation (4.1). The solid line is the fit to the data using Equation (4.1).

The data from the stirred-flow sorption experiments on the untreated Matapeake soil are presented in Figure 4.6. Five different data sets are presented in Figure 4.6: data from experiments conducted at two flow rates, data from a stopped-flow experiment, and two sets of theoretical tracer data. When the flow rate is increased from 0.4 to 4 ml min⁻¹ there is a shift in the midpoint ($\frac{1}{2} * C_{out} / C_{in}$) of the breakthrough from 2.7 to 2.4 chamber volumes, respectively. Since shifts resulting from hydrodynamic effects have been accounted for, this shift is a result of changes in the reaction occurring in the chamber. The average time the solute spends in the reactor vessel (τ) is a function of the chamber volume and the flow rate ($\tau = V_c / Q$) (Brezonik, 1994). For the experiment in which $Q = 4$ ml min⁻¹, $\tau = 2$ min, while for the experiment conducted at $Q = 0.4$ ml min⁻¹, $\tau = 21$ min. In a system where the reaction occurring is slower than the solute residence time (τ), the outflow concentration would be expected to increase as the flow rate increases. This is the behavior observed in Figure 4.6 for Pb sorption on the Matapeake soil, suggesting that sorption kinetics are being measured.

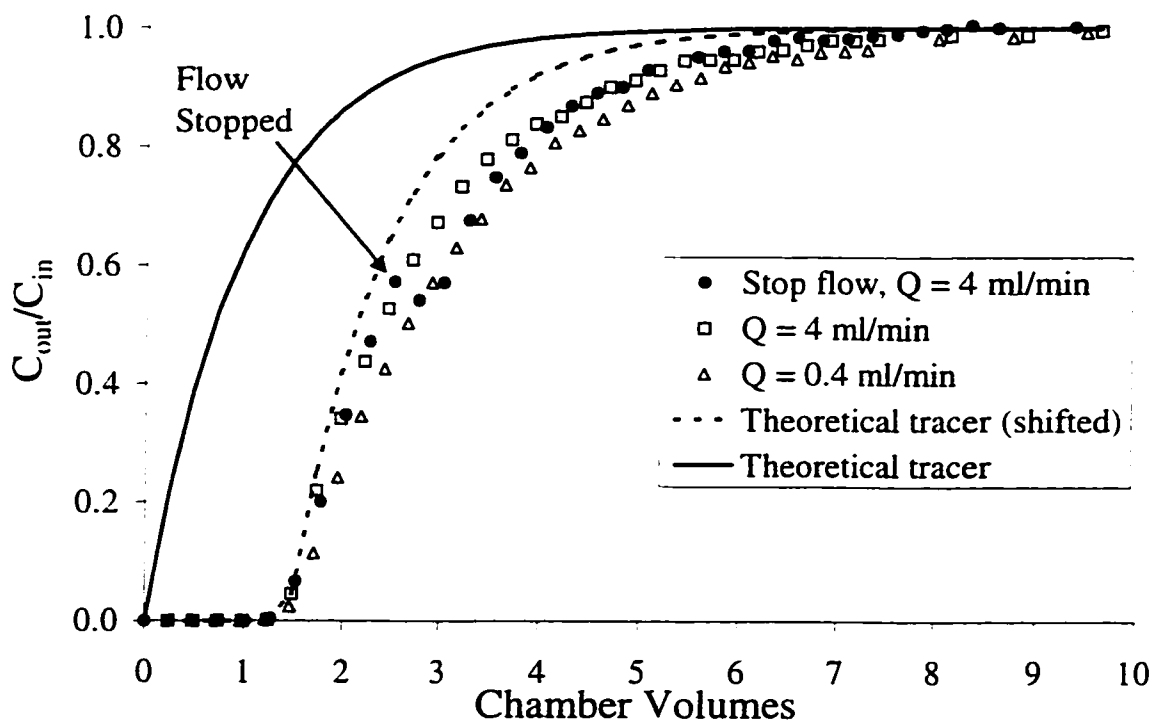


Figure 4.6 Results of sorption experiment conducted on Matapeake soil in the stirred-flow chamber, and theoretical tracers calculated using Equation (4.1).

The results of the stop flow experiment are presented in Figure 4.6. After 2.5 CV of Pb solution had flowed through the chamber the flow was stopped for 30 min. The [Pb] in the outflow solution dropped by ~6%. This is a significant drop giving additional evidence that the reaction is rate-limited. Thus, it can be concluded from the experiments in which the flow rate is changed, and the stopped-flow experiment, that the reactions in the stirred-flow reactor at 4 ml min⁻¹ are rate-limited. Although not shown, data from 2 ml min⁻¹ also show a shift in the outflow concentration that is intermediate between the 0.4 and 4 ml min⁻¹ experiments, suggesting that at this flow rate the reaction is also rate-limited.

The solid line in Figure 4.6 is the theoretical tracer calculated from Equation (4.1), when $dq/dt=0$. The midpoint of the breakthrough for this data is 0.75 chamber volumes. The midpoint for the sorption experiment conducted at 4 ml min⁻¹ occurs at 2.4 CV. This is shifted 1.65 chamber volumes from the midpoint of the breakthrough in the tracer. This retardation shows that the soil is adsorbing significant amounts of Pb. One of the distinctive characteristics present in the stirred-flow experiments is that initially all of the Pb input into the chamber is sorbed. This results in the outflow [Pb] being zero until ~1.2 CV. The initial adsorption accounts for ~65% of the total sorption that occurred on the soil. Since in this experiment $\tau=2$ min ($Q=4$ ml min⁻¹), the fast reaction occurring on the soil must have a half life < 2 min. Fast adsorption reactions for Pb on oxides have been studied using pressure-jump relaxation (Hayes et al., 1986; Yasunaga et al., 1986). Results from these studies suggest that the fast adsorption reaction is primarily due to the formation of bonds with functional groups that are readily available on

surfaces, and that the reaction occurs within seconds. These types of adsorption reactions are too fast to be measured using the stirred-flow reactor.

After ~1.2 CV the Pb concentration in the outflow becomes >0 (Figure 4.6). This suggests that Pb sorption is either slowing down, or that the soil has reached its maximum sorption capacity. If the soil were to sorb no additional Pb from solution then the breakthrough would follow the dashed line (a shifted theoretical tracer data set) in Figure 4.6. However, the [Pb] in the outflow is retarded compared to the tracer, indicating that sorption is continuing at these longer times. The stop flow and variable flow rate experiments indicate that the sorption reaction occurring after 1.2 CV is rate-limited. The slow reaction could be due to sorption on sites which are less readily available than those in which fast sorption occurred (diffusion limited), or a result of secondary sorption mechanisms such as precipitation or sorption on sites with larger activation energies.

Sorption on the Matapeake soil reaches a steady state after about 8 to 9 CV; indicated by $C_{out}/C_{in}=1$. At this point the total sorption on the soil was 44 mmol kg^{-1} . This value is only 68% of the total sorption that occurred in the batch kinetic experiment that was allowed to equilibrate for 800 h. Thus, even though additional sorption occurs, the reaction is too slow ($t_{1/2}=58 \text{ h}$) to detect any noticeable change in the [Pb] in the outflow solution in this series of experiments.

The effect of SOM on Pb sorption is shown in Figure 4.8. In the treated Matapeake soil (little SOM) the midpoint of the breakthrough arrives ~0.95 CV earlier than in the untreated soil. The total amount of Pb sorbed in the treated soil was 27 mmol

kg^{-1} . This is a 40% decrease compared to the untreated Matapeake soil. If the difference in Pb sorption between the treated and untreated soil is due to the presence of SOM then the amount of Pb sorbed on the SOM under these conditions is at least 810 mmol kg^{-1} ($1620 \text{ mmol charge (kg SOM)}^{-1}$). The range for SOM reported in the literature is $1500 - 3000 \text{ mmol charge (kg SOM)}^{-1}$, depending on the pH of the soil solution (Sparks, 1995). This is a very high sorption capacity and demonstrates the importance of SOM in Pb sorption in soils.

Changing the flow rate had only a small effect on $C_{\text{out}}/C_{\text{in}}$ (CV) for sorption in the treated soil (Figure 4.7), suggesting that the reaction being measured in these experiments is not necessarily rate-limited. In addition, following the initial fast reaction the shape of the breakthrough curve is nearly identical to the tracer (dashed line). The similarities between the tracer and the data indicate that very little additional sorption occurred following the initial fast reaction, which is contrary to what was observed for the untreated soil where a slower sorption reaction continued after the initial fast reaction. The lack of a slow reaction in the soil in which the SOM was removed suggests that the slow sorption reaction in the soil is a result of sorption on SOM. Since SOM consists of large polymers (Sparks, 1995) it is likely that slow diffusion to sites on the interior of the SOM molecule is the rate-limiting sorption process.

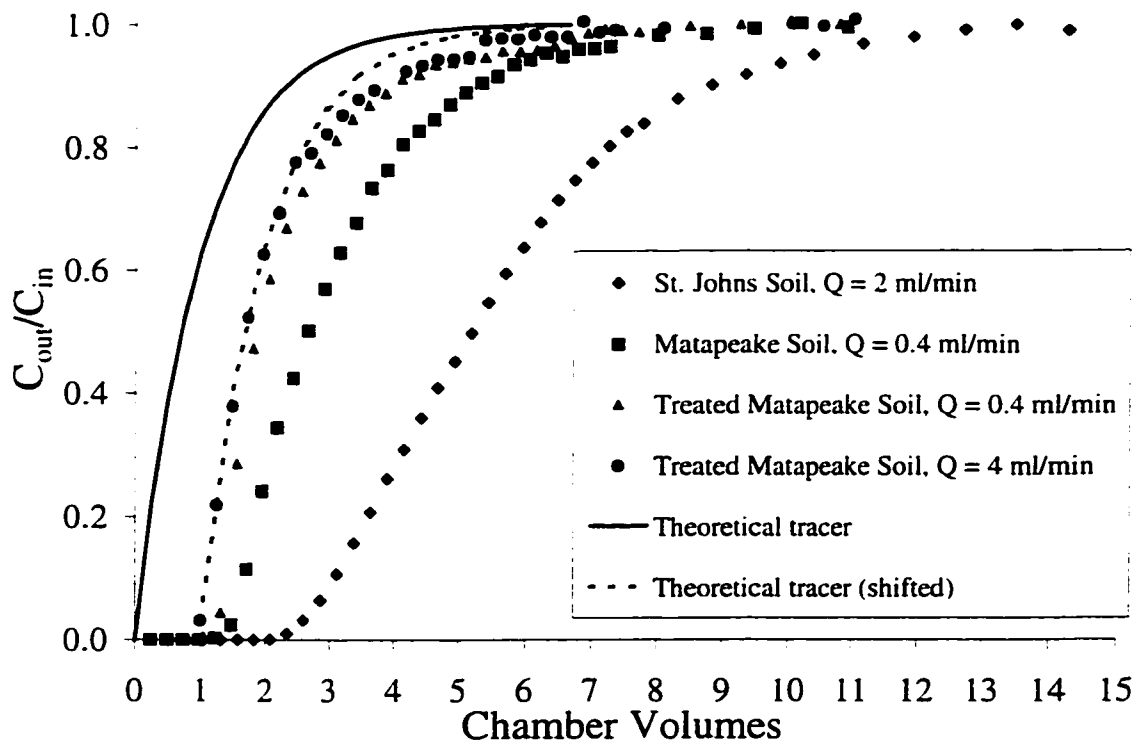


Figure 4.7 Breakthrough curves for sorption on treated and untreated Matapeake soils, the St. Johns soil, and theoretical tracers.

The midpoint of the breakthrough for the St. Johns soil occurred after 5.1 CV (Figure 4.7). This is 2.4 CV later than the breakthrough from the untreated Matapeake soil. In addition, the slope of $C_{out}/C_{in}(CV)$ is significantly smaller than it is for the Matapeake soil, and much different than the tracer. These differences imply that sorption is continuing after the initial fast reaction. The total sorption on the St. Johns soil is 102 mmol kg⁻¹. This is 2.3 times the sorption occurring in the Matapeake soil. Since the clay contents in the Matapeake and the St. Johns soils are similar (Table 4.1), but the St Johns soil has ~6 times more SOM, the most likely reason for the increased Pb sorption is the increase in sorption sites existing on the SOM. Using the sorption capacity calculated for the SOM in the Matapeake soil (810 mmol (kg SOM)⁻¹) the predicted amount of Pb sorbed on the SOM fraction (13% of total soil) in the St. Johns soil is 105 mmol (kg whole soil)⁻¹, which is close to the observed value of total Pb sorbed in the St. Johns soil (102 mmol kg⁻¹). Thus, from the stirred-flow experiments it is clear that SOM is an important factor for Pb sorption in the environment.

The results obtained from the desorption experiments on the untreated Matapeake soil are shown in Figure 4.8. Since a much smaller amount of Pb is recovered in the desorption experiment than was removed from solution in the sorption experiment the desorption reaction is not complete. This can be considered as an apparent hysteresis (DiVincenzo et al., 1997) since the reaction will most likely be reversible if given enough time. However, changing the flow rate from 0.4 to 4 ml min⁻¹ had insignificant effects on $C_{out}/C_{in}(CV)$. If desorption was fast and reversible within the time frame of the experiment then all of the sorbed Pb would be recovered from the soil, and there would

be no change in the desorption breakthrough curves. However, only a fraction of the total sorbed Pb was recovered, indicating that the reaction is not at equilibrium. Thus, since the breakthrough curves are nearly identical, the desorption kinetics must be too slow to measure using the stirred-flow reactor at flow rates of 0.4 ml min^{-1} .

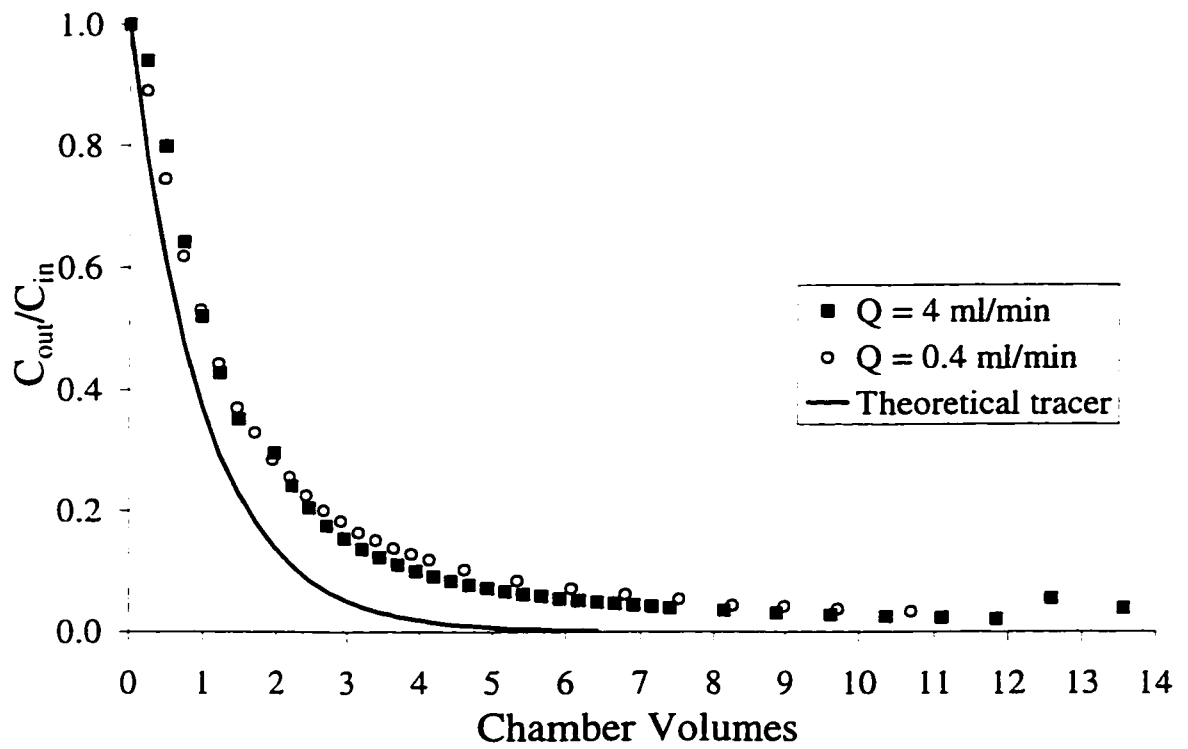


Figure 4.8 Breakthrough curves for desorption from the untreated Matapeake soil and theoretical tracer.

The total amount of Pb desorbed at the end of the desorption experiment can be determined from the difference in the areas under the breakthrough curves with and without soil in Figure 4.8. The total amount of Pb sorbed, and then desorbed for the treated and untreated Matapeake soil, as well as the St. Johns soil are listed in Table 4.2. In order to make comparisons the desorption data were converted to percent Pb desorbed by dividing by the total amount of Pb adsorbed. These data are presented in Figure 4.9. Since the area under the breakthrough curves does not include desorbed Pb that is present in the solution in the chamber, the values of the percent desorbed as a function of CV underestimate the percent desorption at the early times (when [Pb] is large). However, since the amount of Pb in the chamber towards the end of the experiment is small, the percent desorbed at later times is fairly accurate. In all soils desorption was incomplete within the time scales of these experiments (apparent hysteresis). In the treated and untreated Matapeake soils the total amount of Pb desorbed varied only slightly, even though there were dramatic differences in the amount of Pb sorbed. In the St. Johns soil only 35.6% of the sorbed Pb was desorbed. From these observations it appears that apparent hysteresis is becoming more significant as the amount of SOM increases, suggesting that the difference in sorption and desorption in the soils is due to slow desorption from the SOM fraction. This behavior agrees with the trend observed in the sorption experiments; as the percent SOM present in the soil increased, slow sorption was more noticeable. Yin et al. (1997) found similar results for sorption and desorption of Hg from soil.

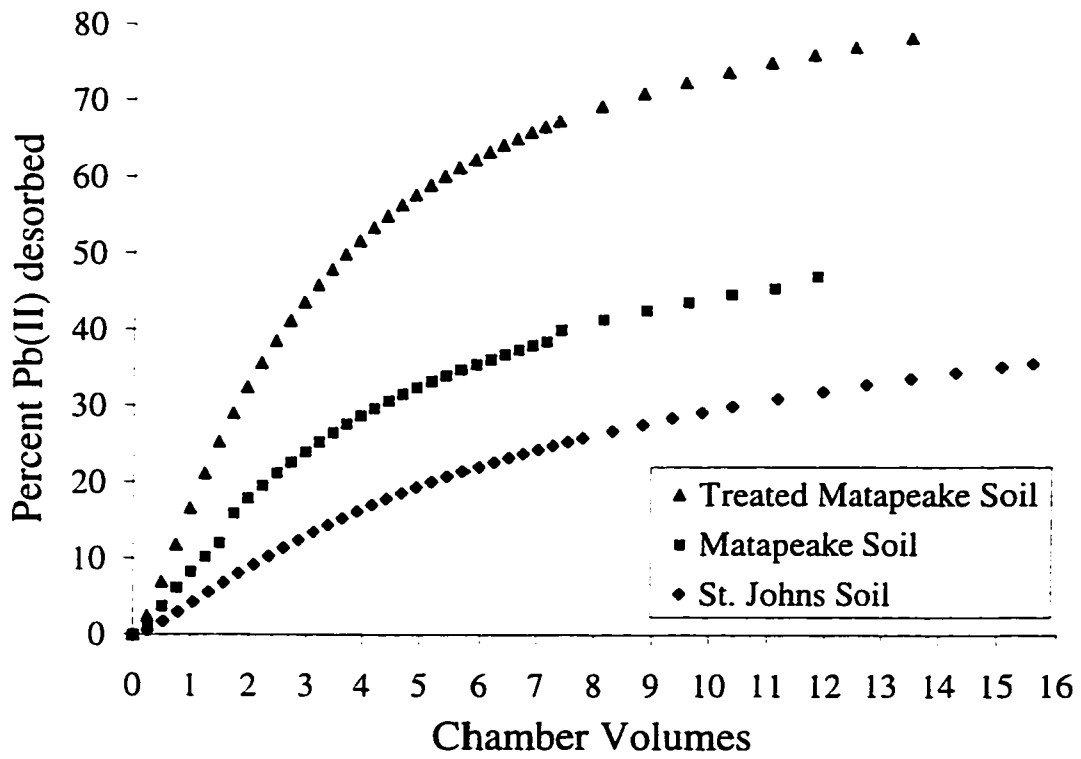


Figure 4.9 Percent Pb desorbed from treated and untreated Matapeake and St. Johns soil.

Table 4.2 Comparison of total Pb sorbed and desorbed in stirred-flow reactor for the soil samples after 12 CV.

Sample	Sorbed (mmol kg ⁻¹)	Desorbed after 12 CV (mmol kg ⁻¹)	Percent desorbed
Untreated Matapeake soil	44.0	20.7	47.0
Treated Matapeake soil	26.8	20.4	76.1
St. Johns soil	102	32.6	32.0

Strawn et al. (1998) found that desorption of Pb from Al_2O_3 is completely reversible within ~3 days. Similar results were found by Ainsworth et al. (1994) and Guneriusson et al. (1994) for Pb desorption on iron oxides. Desorption experiments conducted on montmorillonite (Strawn, 1998) have revealed that the time scales for Pb sorption and desorption are similar. Thus, it appears that Pb sorption on oxides and clays is reversible. However, based on the results of this study, desorption from whole soils is not completely reversible within the time scales of these experiments, and the amount of Pb desorbed is directly correlated to the percent SOM present in the soils. From these observations it can be concluded that Pb desorption from the SOM fraction of soils is slow. The most likely reason for this behavior is that the type of complex that forms between the Pb and the SOM is stronger than the complex forming on the surface of the mineral. On the surfaces of minerals the only type of Lewis bases for Pb to sorb are hydroxyls which are considered to be hard bases (low polarizability) (Sparks, 1995). The functional groups on SOM include carboxyls, phenols, amines and several sulphur containing functional groups which are soft bases (Sparks, 1995). Since soft acids prefer soft bases, the complexation of Pb by the functional groups on the SOM would be preferential to the hard acid hydroxyl ligands present on the mineral surface (Sparks, 1995). The possibility of the formation of other types of strong sorption products cannot be eliminated since soils are heterogeneous materials containing many different types of surfaces in which Pb can interact.

It is often observed that increasing incubation time leads to a decrease in the amount of sorbate that can be desorbed (Kuo et al., 1980; Schultz et al., 1987; Backes et

al., 1995). The effects of sorption incubation time on the total amount of Pb desorbed are presented in Table 4.3. Increasing the incubation time from one day to 32 days resulted in an increase in ~11% increase in adsorption. Despite increasing incubation time from 1 to 32 days the percent of Pb desorbed did not significantly change. This result shows that the complexes formed during Pb sorption are stable within 32 days of incubation, and do not convert into phases that are less readily desorbed.

Table 4.3 Effect of residence time on Pb desorption from the Matapeake soil using the stirred-flow reactor for desorption.

Sorption incubation time (days) ^a	Sorbed (mmol kg ⁻¹)	Desorbed (mmol kg ⁻¹)	Percent desorbed
1	54.9	27.9	50.8
10	60.0	28.7	47.8
32	66.1	30.5	46.1

^aSorption studies were conducted using a batch reactor

From the stirred-flow experiments five important conclusions can be made: 1) Pb sorption consists of a fast and a slow reaction, 2) Pb sorption increases with increasing SOM, 3) desorption is not reversible within the time frame of these experiments, 4) longer sorption incubation times have little impact on the amount of Pb that can be desorbed, and 5) apparent hysteresis increases as the percent SOM in the soil increases. In addition, the experiments discussed in this section have demonstrated the utility, and limitations, of using the stirred-flow reactor for studying reactions on surfaces. One of the unique aspects of this set of experiments was that desorption was studied using the same background as the sorption experiments. Often researchers conduct desorption experiments using organic chelators such as EDTA to prevent readsorption of the metal, however, in many cases, the chelate is actually promoting desorption by interacting with the sorbed metal, and the measured desorption rate is actually a ligand promoted desorption rate. Another method often used to study desorption is to lower the pH of the desorbing solution (proton promoted desorption). While both of these desorption methods provide important information, they do not describe the desorption behavior in terms of a single reversible reaction. The experiments presented in this study demonstrate the utility of the stirred-flow reactor for measuring desorption behavior without promoting the reaction by adding another reactant.

4.4.3 XAFS Experiments

Figure 4.10 shows the background subtracted k^3 weighted χ functions for the treated and untreated Matapeake soil samples. The χ structures are distinctly different in

phase, wavelength, and shape, particularly at higher k . The uniqueness of the χ structures is due to differences in backscattering from the atoms residing in the first and second coordination shells surrounding the sorbed Pb.

The radial structure functions for the two soil samples ($\Delta k=2.2-8.9 \text{ \AA}^{-1}$) are presented in Figure 4.11. The first major peaks that occur in the RSF are located at ~ 1.60 and 1.75 \AA in the untreated and treated Matapeake soil, respectively. These peaks are characteristic of backscattering from O atoms surrounding the sorbed Pb atoms. In the untreated Matapeake soil a large peak is observed at $\sim 2.4 \text{ \AA}$. This peak is noticeably smaller and shifted in the treated sample. At $R > 2.4 \text{ \AA}$ there exist other small peaks that arise from backscattering from either Pb or Si/Al atoms existing in the second shell of coordinating atoms.

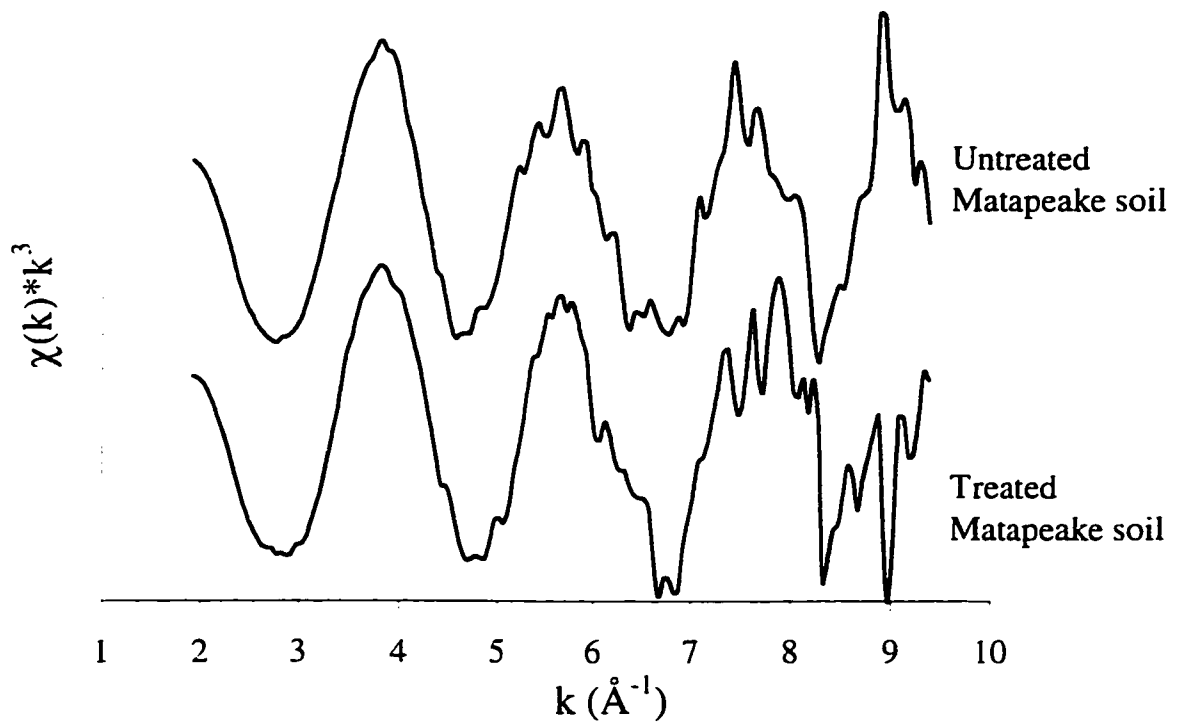


Figure 4.10 k^3 weighted normalized χ -functions from XAFS experiments for Pb sorption on the treated and untreated Matapeake soil.

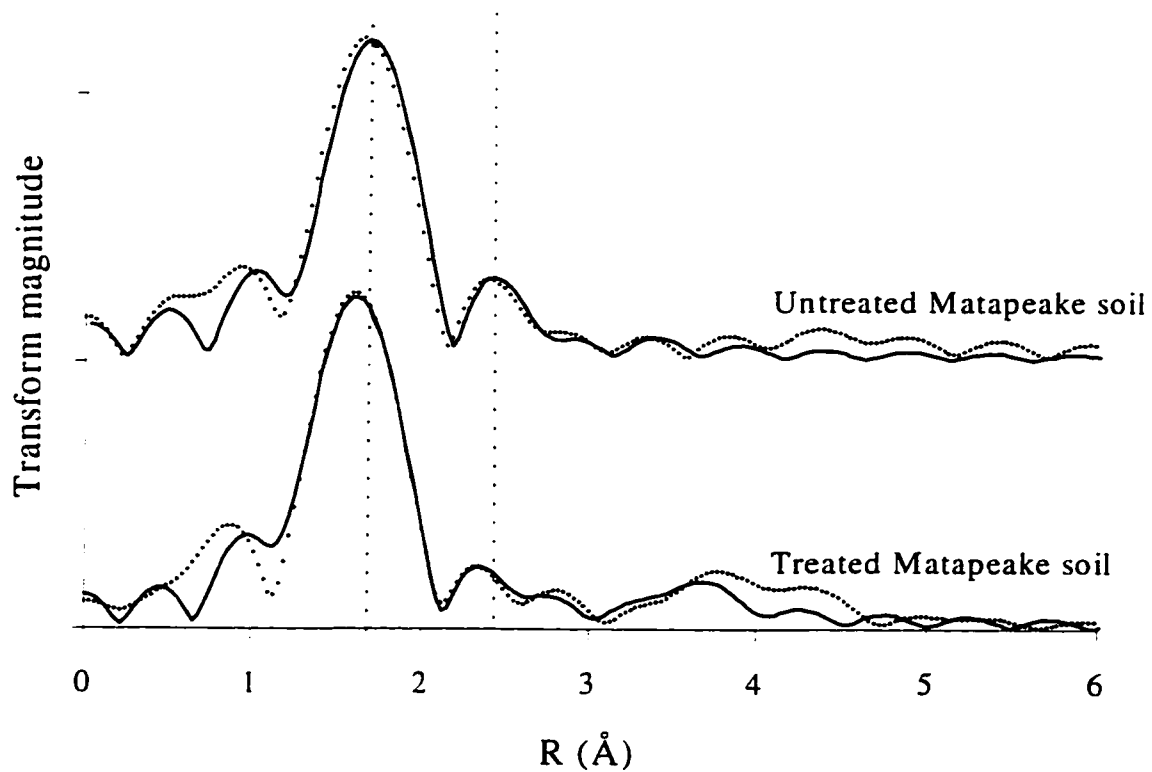


Figure 4.11 Fourier transforms (RSF) of the χ -functions in Figure 4.10 (dotted line), and results from multi-shell fits using theoretical backscattering phase and amplitude functions (solid line). Vertical dashed lines are aligned at the center of the two peaks used for fitting in the untreated Matapeake soil.

The identity of the atoms surrounding the sorbed Pb can be determined by fitting the data to the theoretical model created using the backscattering simulation program FEFF 6.0. As described in the “Methods and Materials” the fits of the samples were made using theoretical pathways from Pb, O, Si, and C as the backscattering atoms. In SOM there also exists N and S containing functional groups that can form complexes with Pb (Sparks, 1995). Analysis of the total N and S in the Matapeake soil revealed that in the untreated Matapeake soil there was only 0.016% total S, and 0.2% total N. In the treated Matapeake soil S and N were not detected. The total C in the untreated Matapeake soil was 1.38% (7 and 87 times the total N and S, respectively). Thus, contributions to the XAFS from N and S are not likely to be large unless the Pb is only forming complexes with these functional groups. Manceau et al. (1996) used XAFS to speciate Pb contaminated soil, they found that the XAFS from the soil was best modeled using a linear combination of Pb-salicylate and Pb-catechol reference compounds, suggesting that the Pb is complexed to these types of functional groups in the SOM. Xia et al. (1997) also found that Pb adsorption on humic acids isolated from SOM was best described by fitting first shell O atoms and second shell C atoms. Thus, in this study, S and N were not considered as second shell backscattering atoms (note: due to the similar atomic size of N and C, isolating the individual contributions from these atoms to the EXAFS is difficult). The best fits of the data are represented by the solid lines in Figure 4.11, and the resulting values for N, R, σ^2 are presented in Table 4.4. In both cases the fits represented the data very well.

Table 4.4 Structural parameters derived from the XAFS experimental data using theoretical phase shift and amplitude functions for Pb sorption on treated and untreated Matapeake soil samples.

Sample	Pb-O shell		Pb-C or -Si shell		Pb-Pb shell		E_0 (eV) ^d
	R (Å) ^{a,c}	N ^{b,f} σ^2 (Å ²) ^c	R (Å) ^c	N ^k σ^2 (Å ²)	R (Å) ^c	N ^k σ^2 (Å ²)	
Untreated Matapeake soil	2.29	1.55	0.006	3.06	1.21	0.004	11.5
Treated Matapeake soil	2.25	1.72	0.007	3.24	0.86	0.01 ^h	3.72
				C atom		1.28	0.01 ^h
				Si atom			16.1

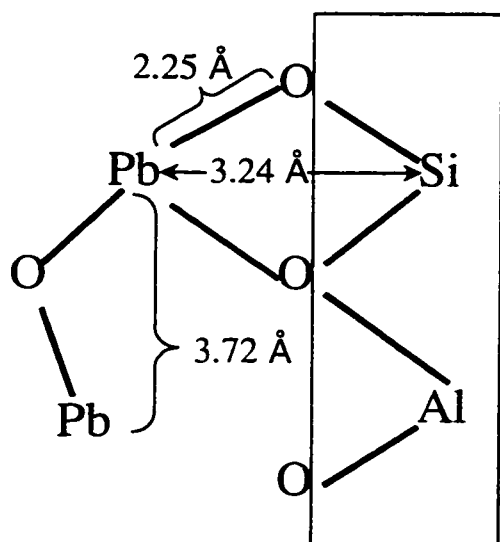
^a Interatomic distance. ^b Coordination Number. ^c Debye-Waller factor. ^d Phase shift. ^e Fit quality confidence limits: ^e 1%, ^f 10%, ^g 25%. ^h Fixed.

The bond distances and coordination numbers for the treated Matapeake soil are similar to those found by Strawn et al. (1998) and Bargar et al. (1997) for Pb adsorption on Al_2O_3 . In these cases Pb was adsorbed as inner-sphere complexes on the edges of octahedrally coordinated Al atoms. Based on $R_{\text{Pb-O}}$ and $R_{\text{Pb-Si}}$ in the treated Matapeake soil, it can be concluded that sorption on the soil consists of primarily inner-sphere complexes, similar to those that form on aluminum oxide. Significant Pb backscattering was also observed for this sample, suggesting that some multinuclear complexation is also occurring.

The EXAFS of the untreated Matapeake soil was best described by fitting O and C atoms as the backscattering atoms present in the local atomic structure of sorbed Pb. Attempts to fit Si and or Pb in the second shell of the sorbed Pb were unsuccessful. The predicted bond distance between the Pb and O (2.29 Å) is distinctly longer than the $R_{\text{Pb-O}}$ in the treated Matapeake soil ($R_{\text{Pb-O}}=2.24$ Å). The bond distance observed between the Pb and C atoms is 3.05 Å. This distance is shorter than the distance predicted by Xia et al. (1997) (3.26 Å) for Pb sorption on humic acid. The shorter bond distance may be due to a decrease in the Pb-O-C bond angle occurring in the sample, or coordination to different ligands than were present in the humic acid sample. Manceau et al. (1996) predicted that the speciation of Pb in a contaminated soil was 60% Pb-salicylate complexes and 40% Pb-catechol complexes. These complexes involve the formation of a five-membered chelate complex between the phenol functional groups of the catechol, and a six membered chelate complex formed between the phenol and carboxyl functional groups of the salicylate.

The differences in the RSF reveal that the local atomic structure surrounding the sorbed Pb atom is different in the two samples; in the treated soil C was not detected in the local atomic structure of the sorbed Pb, while in the untreated soil, the dominant backscatterers were O and C. Figure 4.12 illustrates the sorption mechanisms predicted from the XAFS results using a clay mineral surface and a phenol functional group from SOM as the sorbents for the Pb (these models are only examples of the bonding environments, the actual bonding environment in the soil involves several different types of sorbents). The XAFS results confirm that the sorption mechanisms in the two soils are different. Since in the untreated sample no Pb or Si backscatterers were detected, most of the Pb must be sorbed onto the SOM, suggesting that the SOM is outcompeting, or blocking, the mineral surfaces from sorbing available Pb.

Treated Matapeake soil



Untreated Matapeake soil

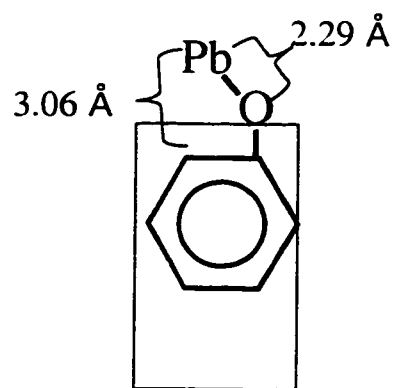


Figure 4.12 Examples of sorption complexes on the treated and untreated Matapeake soils based on the fit results of the XAFS data.

4.5 Summary

The results of this study provide evidence that Pb sorption and desorption behavior on soil cannot be characterized by batch equilibrium sorption isotherms alone, but factors such as reaction time, percent organic matter, and desorption behavior must also be considered to make accurate assessments of the fate of Pb in the soil. Results from the isotherm experiment showed that soil has a strong affinity for Pb. Batch sorption kinetic experiments revealed that Pb sorption behavior involves fast and slow sorption reactions. The fast reaction accounted for 78% of the total sorption within eight minutes (the first sampling time). The reaction was fit using a first-order reversible equation. Using the overall rate constant the half life for the slow reaction was estimated to be 58 h.

Measurement of sorption kinetics using the stirred-flow reactor revealed that the extent of the fast and slow reactions occurring in the soil is directly dependent on the amount of SOM present. Specifically, with increasing SOM content the rate of Pb sorption decreases. The Pb sorption capacity of the SOM is estimated to be at least 810 mmol kg^{-1} . Desorption experiments conducted using the stirred-flow reactor revealed that Pb desorption is hysteretic within the time frame of these experiments. The fraction of Pb that was desorbed from the soil decreased as the amount of SOM present in the soil increased. This indicates that the slow desorption reaction is primarily related to the SOM fraction of the soil. XAFS results from this study confirm that the types of

complexes forming in the soil with SOM and the soil without SOM are different, and help explain the macroscopic Pb sorption/desorption behavior.

In this study the advantages and limitations of using a stirred-flow reactor for measuring sorption and desorption reactions on soils have been demonstrated. It was shown that dilution occurring in a stirred-flow reactor can be accurately calculated using a mass balance equation, provided that diffusion and dispersion are taken into account.

The information presented in this study shows the importance of not only measuring sorption equilibrium to predict the behavior of Pb in soil, but also measuring time-dependent sorption and desorption reactions. This additional information will allow scientists and engineers to make better predictions about the transport, bioavailability, and sorption and desorption behavior of Pb in soil. Such information is critical for protecting natural resources, developing improved remediation strategies, and making better risk assessments, which will save money and resources.

4.6 References

- Ainsworth, C. C., J. L. Pilon, P. L. Gassman and W. G. Van Der Sluys. 1994. Cobalt, cadmium, and lead sorption to hydrous iron oxide: Residence time effect. *Soil Sci. Soc. Am. J.* 58: 1615.
- Amacher, M. C. 1991. Methods of obtaining and analyzing kinetic data. p. 19. *In* D. L. Sparks and D. L. Suarez (eds.) *Rates of soil chemical processes*. Vol. 27. Soil Science Society of America, Madison, WI.
- Amacher, M. C., H. M. Selim and I. K. Iskandar. 1988. Kinetics of chromium(VI) and cadmium retention in soils; A nonlinear multireaction model. *Soil Sci. Soc. Am. J.* 52 (2): 398.
- Amonette, J. C. and L. W. Zelazny, Eds. 1994. *Quantitative methods in soil mineralogy*. Soil Science Society of America Special Publications. Soil Science Society of America, Madison, WI.

- Backes, C. A., R. G. McLaren, A. W. Rate and R. S. Swift. 1995. Kinetics of cadmium and cobalt desorption from iron and manganese oxides. *Soil Sci. Soc. Am. J.* 59: 778.
- Baeyens, B. and M. H. Bradbury. 1997. A mechanistic description of Ni and Zn sorption on Na-montmorillonite. Part I: Titration and sorption measurements. *J. Cont. Hyd.* 27: 199.
- Bargar, J. R., G. E. Brown, Jr. and G. A. Parks. 1997. Surface complexation of Pb(II) at oxide-water interfaces: I. XAFS and bond-valence determination of mono- and polynuclear Pb(II) sorption products on Al-oxides. *Geoch. Cosmochim. Acta* 61 (13): 2617.
- Bar-Tal, A., D. L. Sparks, J. D. Pesek and S. Feigenbaum. 1990. Analyses of adsorption kinetics using a stirred-flow chamber: I. Theory and critical tests. *Soil Sci. Soc. Am. J.* 54: 1273.
- Benjamin, M. M. and J. O. Leckie. 1981. Multiple-site adsorption of Cd, Cu, Zn, and Pb on amorphous iron oxyhydroxides. *J. Colloid Interface Sci.* 79 (1): 209.
- Brezonik, P. L. 1994. *Chemical kinetics and process dynamics in aquatic systems*. Lewis Publishers, Boca Raton, FL.
- Bunzl, K., W. Schmidt and B. Sansoni. 1976. Kinetics of ion exchange in soil organic matter. IV. Adsorption and desorption of Pb^{2+} , Cu^{2+} , Cd^{2+} , Zn^{2+} and Ca^{2+} by peat. *J. Soil Sci.* 27: 32.
- Carriere, P. P. E., B. E. Reed and S. R. Cline. 1995. Retention and release of lead by a silty loam and a fine sandy loam. II. Kinetics. *Sep. Sci. Tech.* 30 (18): 3471.
- DiVincenzo, J. P. and D. L. Sparks. 1997. Slow sorption kinetics of pentachlorophenol on soil: Concentration effects. *Environ. Sci. Technol.* 31 (4): 977.
- Elliot, H. A., M. R. Liberati and C. P. Huang. 1986. Competitive adsorption of heavy metals by soils. *J. Environ. Qual.* 15 (3): 214.
- Fuller, C. C., J. A. Davis and G. A. Waychunas. 1993. Surface chemistry of ferrihydrite: Part 2. Kinetics of arsenate adsorption and coprecipitation. *Geoch. Cosmochim. Acta* 57: 2271.
- Good, M. E., G. D. Winget, W. Winter, T. N. Connolly, S. Izawa and R. M. M. Singh. 1966. Hydrogen ion buffers for biological research. *Biochemistry* 5 (2): 467.

- Gunneriusson, L., L. Lovgren and S. Sjoberg. 1994. Complexation of Pb(II) at the goethite (α -FeOOH)/water interface: The influence of chloride. *Geoch. Cosmochim. Acta* 58 (22): 4973.
- Hayes, K. F. and J. O. Leckie. 1986. Mechanism of lead ion adsorption at the goethite-water interface. p. 115. *In* J. A. Davis and K. F. Hayes (eds.) *Geochemical processes at mineral surfaces*. Vol. 323. American Chemical Society, Washington D.C.
- Jin, X., G. W. Bailey, Y. S. Yu and A. T. Lynch. 1996. Kinetics of single and multiple metal ion sorption processes on humic substances. *Soil Sci.* 1996 (8): 509.
- Kendorff, H. and M. Schnitzer. 1980. Sorption of metals on humic acid. *Geoch. Cosmochim. Acta* 44: 1701.
- Kuo, S. and D. S. Mikkelsen. 1980. Kinetics of zinc desorption from soils. *Plant and Soil* 56: 355.
- Lavkulich, L. M. and J. H. Wiens. 1970. Comparison of organic matter destruction by hydrogen peroxide and sodium hypochlorite and its effects on selected mineral constituents. *Soil Sci. Soc. Am. J.* 34 (1970): 755.
- Loehr, R. C. and M. T. Webster. 1996. Behavior of fresh vs. aged chemicals in soils. *J. Soil Cont.* 5 (4): 361.
- Manceau, A., M.-C. Bosset, G. Sarret, J.-L. Hazemann, M. Mench, P. Cambier and R. Prost. 1996. Direct determination of lead speciation in contaminated soils by EXAFS spectroscopy. *Environ. Sci. Technol.* 30 (5): 1540.
- McBride, M. M. 1994. *Environmental chemistry of soils*. Oxford University Press, New York, NY.
- McKenzie, R. M. 1980. The adsorption of lead and other heavy metals on oxides of manganese and iron. *Aust. J. Soil Res.* 18: 61.
- Nelson, D. W. and L. E. Sommers. 1996. Total carbon, organic carbon, and organic matter. p. 961. *In* D. L. Sparks (ed.) *Methods of soil analysis: Chemical methods*. Soil Science Society of America, Madison, WI.
- Papelis, C., P. V. Roberts and J. O. Leckie. 1995. Modeling the rate of cadmium and selenite adsorption on micro- and mesoporous transition aluminas. *Environ. Sci. Technol.* 29: 1099.

- Reed, B. E., P. C. Carriere and R. Moore. 1996. Flushing of Pb(II) contaminated soils using HCl, EDTA, and CaCl₂. *J. Env. Eng.* 122: 48.
- Scheidegger, A. M. and D. L. Sparks. 1996. Kinetics of the formation and the dissolution of nickel surface precipitates on pyrophyllite. *Chem. Geol.* 132 (1-4): 157.
- Scheidegger, A. M., D. G. Strawn, G. M. Lamble and D. L. Sparks. 1998. The kinetics of mixed Ni-Al hydroxide formation on clays and aluminum oxides: A time-resolved XAFS study. *Geoch. Cosmochim. Acta* 62 (13): 2233.
- Schultz, M. F., M. M. Benjamin and J. F. Ferguson. 1987. Adsorption and desorption of metals on ferrihydrite: Reversibility of the reaction and sorption properties of the regenerated solid. *Environ. Sci. Technol.* 21 (9): 863.
- Selim, H. M., M. C. Amacher and I. K. Iskandar. 1989. Modeling the transport of chromium (VI) in soil columns. *Soil Sci. Soc. Am. J.* 53 (4): 996.
- Seyfried, M. S., D. L. Sparks, A. Bar-Tal and S. Feigenbaum. 1989. Kinetics of Ca-Mg exchange on soil using a stirred-flow reaction chamber. *Soil Sci. Soc. Am. J.* 53: 406.
- Skopp, J. and D. McCallister. 1986. Chemical kinetics from a thin disc flow system: Theory. *Soil Sci. Soc. Am. J.* 50: 617.
- Smith, J. T. and R. N. J. Comans. 1996. Modeling the diffusive transport and remobilization of ¹³⁷Cs in sediments: The effects of sorption kinetics and reversibility. *Geoch. Cosmochim. Acta* 60 (6): 995.
- Sparks, D. L. 1989. *Kinetics of soil chemical processes*. Academic Press, Inc., San Diego, CA.
- Sparks, D. L. 1995. *Environmental soil chemistry*. Academic Press, San Diego, CA.
- Sparks, D. L., Ed. 1996. *Methods of Soil Analysis: Chemical methods*. Soil Science Society of America Book Series. Soil Science Society of America, Madison, WI.
- Sposito, G. 1989. *The chemistry of soils*. Oxford University Press, New York, NY.
- Strawn, D. G. 1998. *Kinetics and mechanisms of Pb(II) sorption and desorption in soils and soil minerals*. Ph.D. Dissertation. University of Delaware.

- Strawn, D. G., A. M. Scheidegger and D. L. Sparks. 1998. Kinetics and mechanisms of Pb(II) sorption and desorption at the aluminum oxide-water interface. *Environ. Sci. Technol.* 32 (7): 2596.
- Suave, S., M. McBride and W. Hendershot. 1998. Soil solution speciation of lead (II): Effects of organic matter and pH. *Soil Sci. Soc. Am. J.* 62 (1998): 618.
- Wilczak, A. and T. M. Keinath. 1993. Kinetics of sorption and desorption of copper (II) and lead (II) on activated carbon. *Water Env. Res.* 65 (3): 238.
- Xia, K., W. Bleam and P. A. Helmke. 1997. Studies of the nature of Cu²⁺ and Pb²⁺ binding sites in soil humic substances using X-ray absorption spectroscopy. *Geoch. Cosmochim. Acta* 61 (11): 2211.
- Yasunaga, T. and T. Ikeda. 1986. Adsorption-desorption kinetics at the metal-oxide-solution interface studied by relaxation kinetics. p. 231. *In* J. A. Davis and K. F. Hayes (eds.) *Geochemical processes at mineral surfaces*. Vol. 323. American Chemical Society, Washington D. C.
- Yin, Y., H. E. Allen, C. P. Huang, D. L. Sparks and P. F. Sanders. 1997. Kinetics of mercury(II) adsorption and desorption on soil. *Environ. Sci. Technol.* 31: 496.

Chapter 5

Conclusions

5.1 Summary of Research

The research presented in this dissertation deals with the interactions occurring between Pb(II) and soils. These interactions include both sorption and desorption processes. To isolate the types of reactions occurring on the surfaces of soil materials, kinetic and atomic level investigations of Pb reactions with pure minerals as well as whole soils were conducted. The minerals studied were Al_2O_3 , and montmorillonite. The effects of soil organic matter (SOM) on Pb sorption and desorption behavior were also investigated. Oxides, clay minerals and SOM comprise the majority of the reactive surfaces that exist in soils. Thus, the research in this dissertation has direct applicability to Pb reactions in soils and the environment.

To predict the behavior of contaminants such as Pb in the environment, a basic understanding of sorption and desorption reactions, both kinetic and equilibrium, is required. The research presented in this study combines a macroscopic technique to gain

insight into the rates and equilibrium behavior of Pb sorption and desorption, with a spectroscopic technique (XAFS) to gain atomic level information. The combination of spectroscopic and macroscopic data allows for more accurate predictions on the reaction processes in the environment to be made.

In Chapter 2 the kinetics and mechanisms of Pb sorption and desorption on Al_2O_3 were investigated. Adsorption was shown to involve a fast and slow reaction step. The results of the XAFS analyses showed no change in the sorption reaction occurring between 1.5 h to 23 days. The predominant sorption mechanism obtained from the XAFS analysis was an inner-sphere bidentate bond occurring between the Pb atoms and the edges of the structural aluminum octahedra. It was proposed from these data that the mechanism responsible for the slow sorption reaction is slow diffusion to sorption sites existing on the interior of the mineral. Desorption from the mineral was shown to be completely reversible within 3 days. This result was somewhat surprising since Pb sorption in soils is normally considered to be strong, and the attainment of equilibrium in desorption usually is slower than that for equilibrium in adsorption.

Chapter 3 investigates the effects of pH and ionic strength on Pb adsorption on the clay mineral montmorillonite. Macroscopic equilibrium experiments conducted on the montmorillonite show a distinct pH dependent behavior for Pb adsorption at high ionic strength. This behavior suggests adsorption on edge sites of the montmorillonite via covalent bonding to the hydroxide ligands (inner-sphere adsorption). At low ionic strength, adsorption was not pH dependent, suggesting that Pb is adsorbing on the planar sites existing in the interlayers of the montmorillonite via electrostatic attraction (outer-

sphere adsorption). XAFS results confirm that these two mechanisms are occurring. However, at high ionic strength and low pH, or at low ionic strength and high pH, the XAFS data indicate that a mixture of inner- and outer-sphere Pb complexes occur. This information could not be obtained from the macroscopic experiments alone.

The kinetics and mechanisms of Pb sorption and desorption on whole soils are presented in Chapter 4. One of the main goals of this chapter was to investigate the effects of SOM on Pb sorption and desorption behavior. From batch experiments it was observed that there is a fast initial sorption reaction followed by a much slower secondary reaction. The slow reaction had a half life of 58 h. Sorption experiments conducted using the stirred-flow reactor confirmed this sorption behavior, and indicated that the degree of slow sorption was strongly related to the amount of SOM present in the soil. These results indicate that sorption to the interior of the SOM is diffusion-limited. Contrary to the results on pure minerals described in Chapter 2 and Appendix 2, desorption from the soils was hysteretic within the time frame of the experiments (apparent hysteresis). The degree of apparent hysteresis was dependent on the percent SOM present. This behavior is most likely due to the formation of strong complexes with the ligand sites existing on the SOM. These complexes are probably stronger than the bonds formed between Pb and the hydroxyl groups of minerals, and require a large activation energy to be broken. Analysis of the extended portion of the XAFS (EXAFS) data from the soil confirm that most of the Pb in the soil is sorbed to the SOM. The XAFS data were successfully fit with C and O atoms as backscattering atoms.

5.2 Future Research

The research presented in this dissertation provides insight into Pb reactions occurring in the environment, utilizing the most cutting-edge tools for analyzing Pb reactions with soils. This information is only a small part of the whole picture... in fact, this research has spawned as many (or more) questions as it has answered. These are topics for future research. As the tools available to scientists are improved a better understanding of Pb behavior in the environment will be obtained.

One the most important questions about Pb behavior in the environment that deserves further research is the interaction between Pb and inorganic ligands present in the soil, e.g., sulphate, phosphate, and carbonate. While a great deal of research has been done on these topics, our present understanding of these reactions suffers from a lack of atomic level evidence to explain the reaction mechanisms, as well as information on the desorption and time dependency of the interactions.

Continued research on the speciation and availability of Pb in heterogeneous materials such as soils is an important area of research. As the tools available to soil scientists are improved, more accurate assessments of Pb speciation in the environment can be made.

In this dissertation it has been shown that Pb forms strong complexes with SOM. In soils a multitude of organic materials exists, such as: organic acids and chelates exuded by plants, organic chemicals applied to soils for agriculture or as waste from industry and municipal activities, and biological surfaces from organisms present in the

soil. For accurate assessment of Pb toxicity it is critical that the mechanisms occurring between Pb and these organic materials be understood. In addition, since uptake of Pb by plants often involves chelation of Pb by the organic chemicals exuded from plants, the mechanisms of Pb uptake by the plant roots should be studied.

The research discussed above represents only a few of the questions that need to be answered to obtain a better understanding of the behavior of Pb in the environment. If the models used by scientists to predict the fate of Pb in the environment are to be improved it is critical that information on the kinetics and mechanisms of Pb complexation in the soil be understood. This understanding will be greatly enhanced by conducting experiments that provide microscopic information.

Appendix A

Supplementary Material for Chapter 2

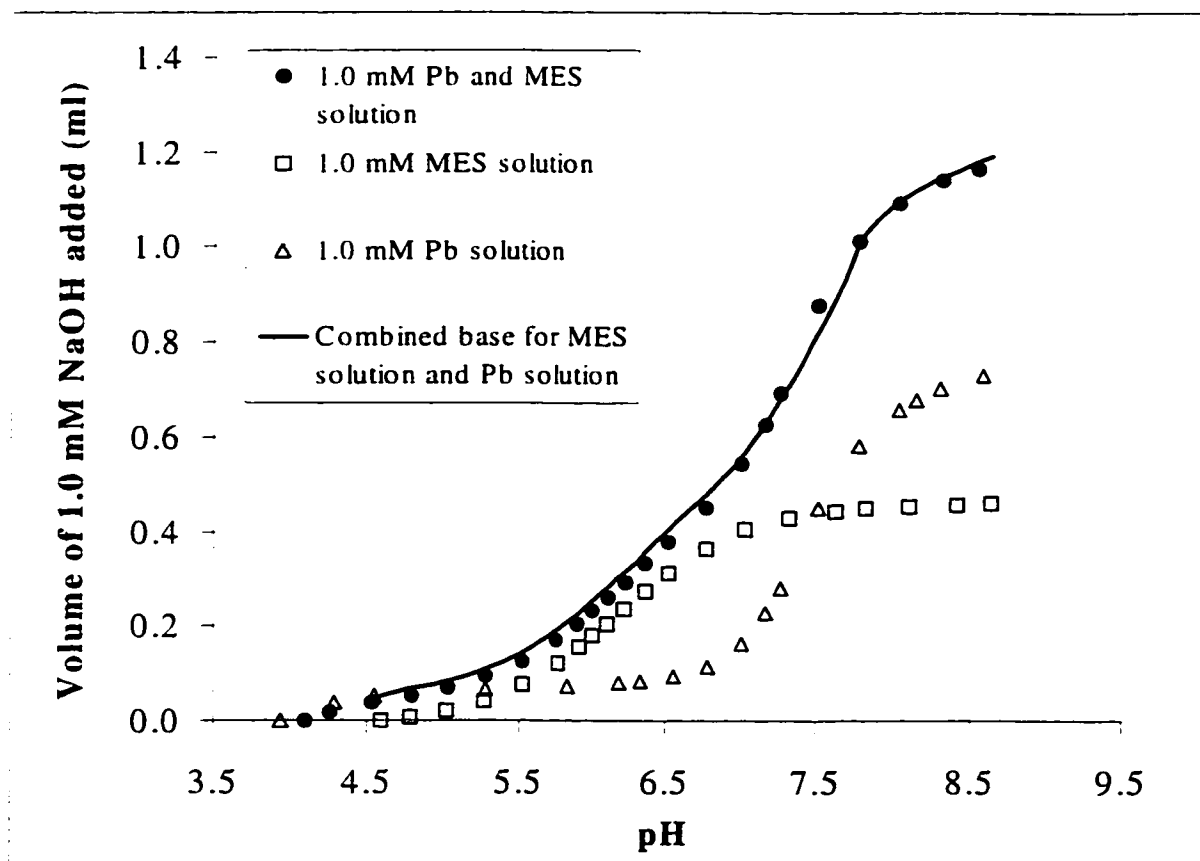


Figure A.1 Results from titrating Pb solution, MES (buffer) solution and a solution with both Pb and MES present. The solid line is the total base taken up by the independent Pb and MES solutions. The close match between the solid line and the Pb+MES solution indicates no change in pKa of solution when both chemicals are present in the same solution.

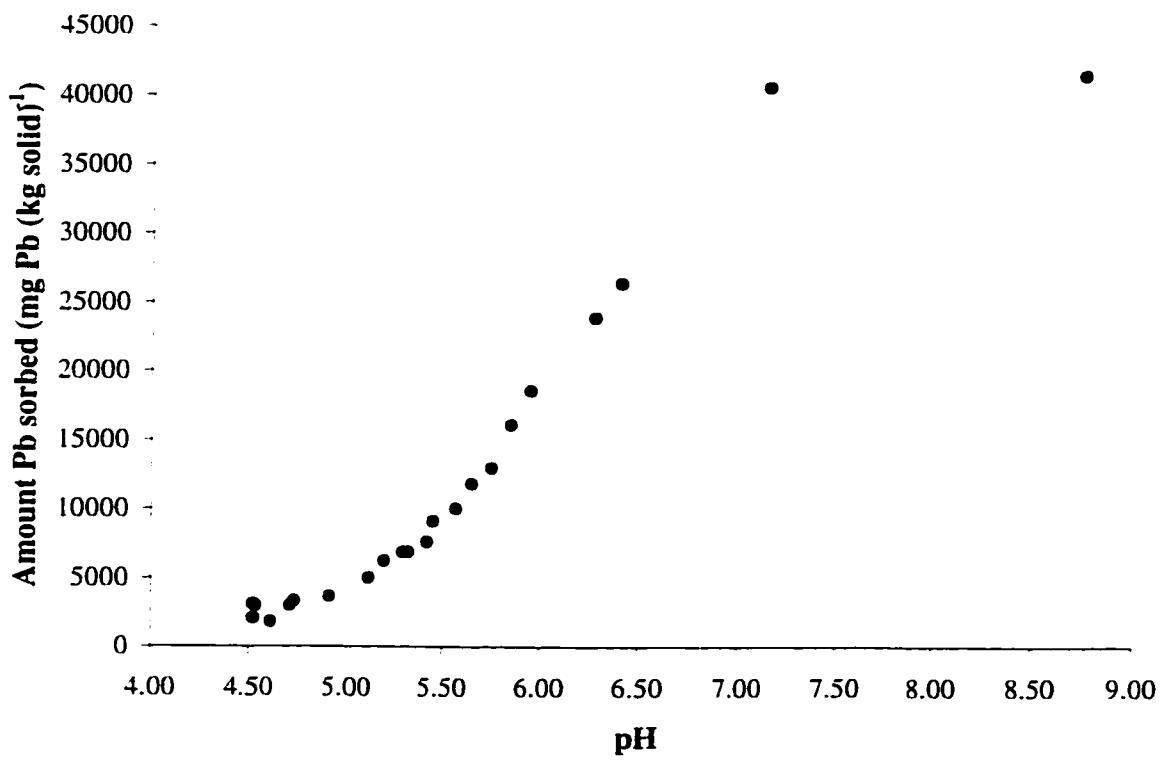


Figure A.2 pH edge for Pb adsorption on $\gamma\text{-Al}_2\text{O}_3$. $[\gamma\text{-Al}_2\text{O}_3]=10\text{ g L}^{-1}$, $I=0.1\text{ M}$, $[\text{Pb}]_{\text{initial}}=2.0\text{ mM}$.

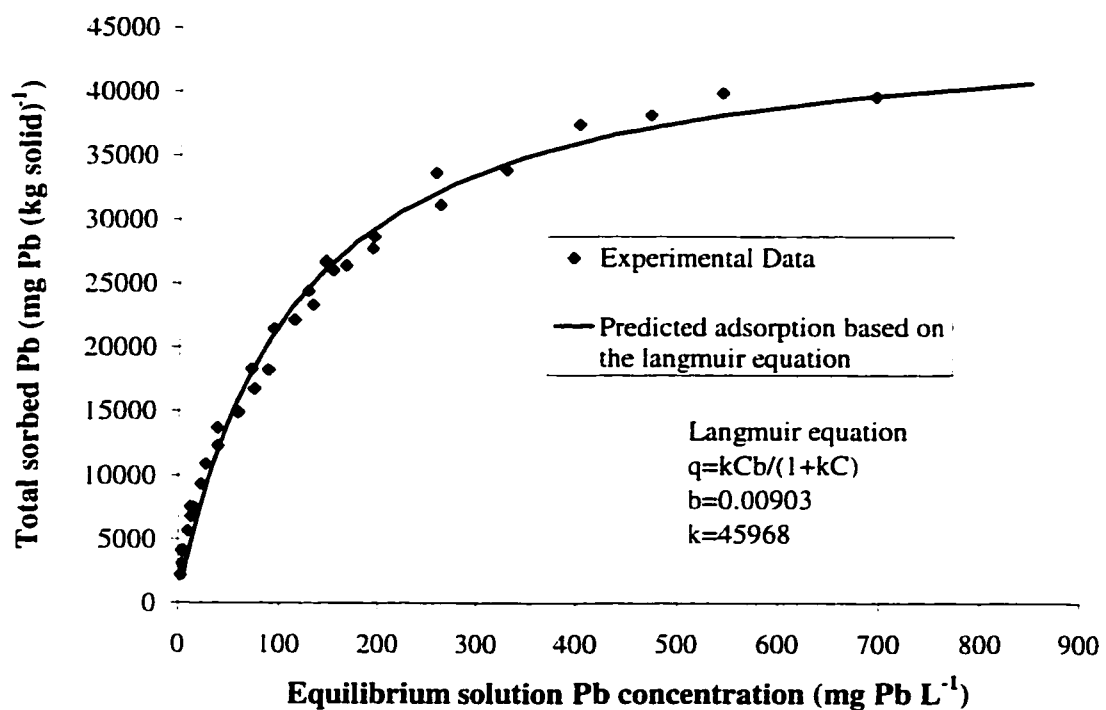


Figure A.3 Adsorption isotherm for Pb on $\gamma\text{-Al}_2\text{O}_3$. $[\gamma\text{-Al}_2\text{O}_3] = 10 \text{ g L}^{-1}$, $\text{pH}=6.50$, $I=0.1 \text{ M}$. In the Langmuir equation q is the total sorption, C is the equilibrium concentration, k is the maximum sorption, and b is an adsorption coefficient.

Table A.1 Test for efficiency of resin to remove Pb from solution and for Pb recovery from resin, as well as test to make sure washing does not desorb Pb from resin.

Sample	Mass of Pb initially (mg)	Mass of Pb in solution after resin (mg)	Mass of Pb in solution from resin wash (mg) ^a	Mass of Pb recovered (mg)	Percent of initial Pb recovered by resin
70N	2.07	0.00375	0	2.03	98
71N	2.07	0.00385	0	2.04	99
72N	2.07	0.0042	0	1.97	95

^a Values were below detection limits (~0.5 mg L⁻¹).

Table A.2 Atoms program input file containing crystallographic data to create file for FEFF 6.0 input file.

```
title name: PbO-red
title formula: PbO
title sites: Pb1, O1
title refer1: Leciejewicz (1961) Acta Cryst. 14, 1304.
title refer2: Dickenson and Friauf (1924) J Amer. Chem. Soc. 46, 2457.
title shoen: D74h
title notes 1: red lead oxide tetragonal
space P 4/n m m
a   = 3.96   c   = 5.01
rmax= 6.00
core = Pb1
atom
Pb   0.25000  0.25000  0.24000  Pb1
O    0.75000  0.25000  0.00000  O1
-----
```

Appendix B

Supplementary Material for Chapter 3

Table B.1 Results from X-ray diffraction characterization

Treatment	2θ	Interlayer Spacing
Untreated	6.8°	12.800 Å
Heated at 500° for 5 h	9.2°	9.604 Å
Glycolated at 50° for 24 h	5.8°	15.225 Å

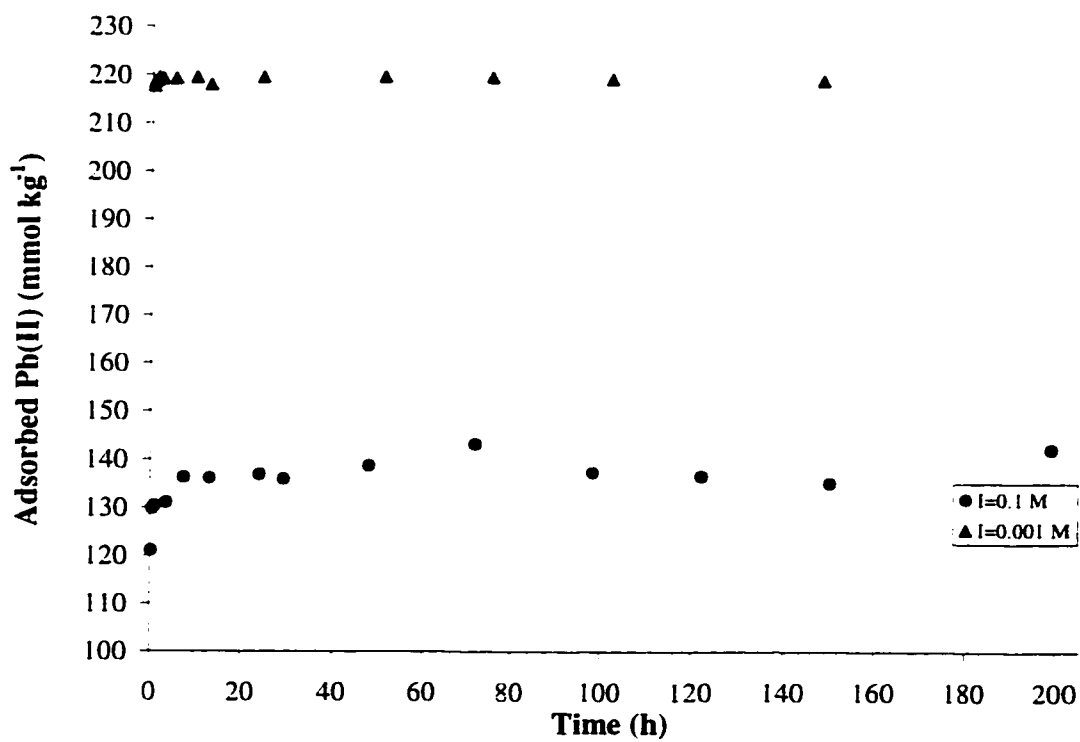


Figure B.1 Adsorption kinetics of Pb on montmorillonite at two ionic strengths. [montmorillonite]=10 g L⁻¹, [Pb]_{initial}=2 mM, pH=6.5.

Table B.2 Amount of Pb recovered from resin recovered from montmorillonite samples incubated for ~200 h of adsorption, and 45 min of desorption time. $I=0.1$ M, pH=6.5, initial amount of Pb adsorbed was ~140 mmol kg^{-1} .

Sample	Mass of Pb input into system (mg)	Mass of recovered Pb from resin (mg)	Percent Pb recovered (mg)
50M	2.07	1.91	92.3
51M	2.07	1.90	91.8
52M	2.07	1.89	91.3

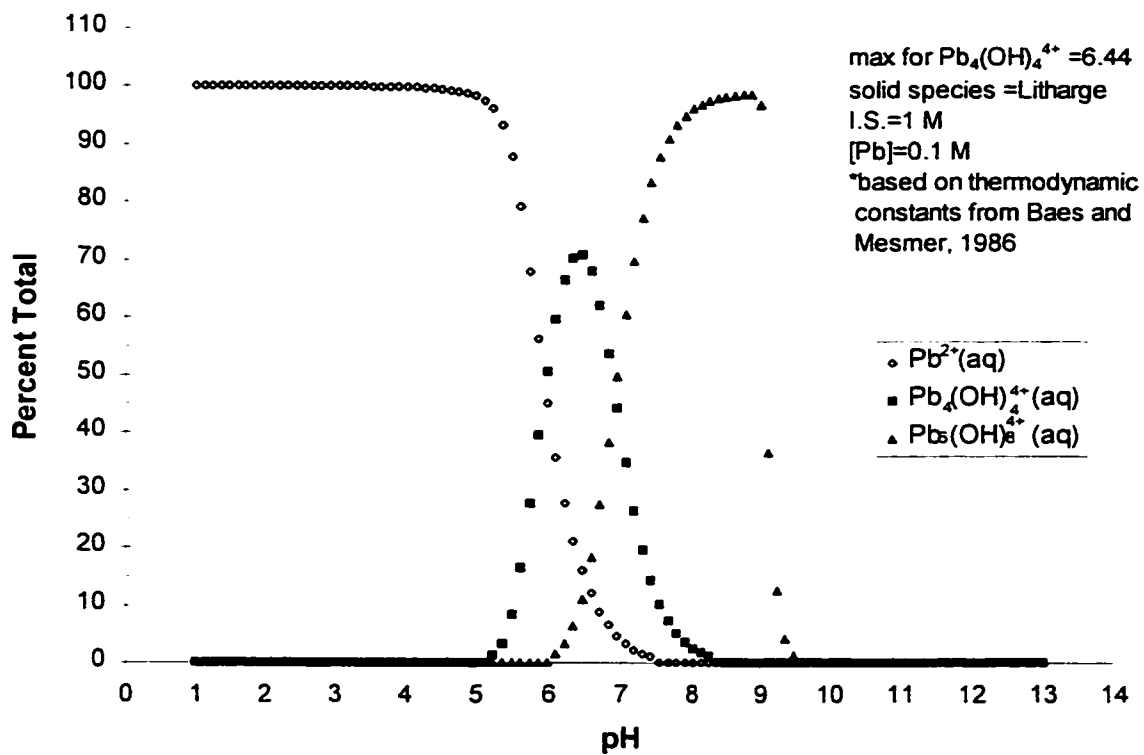


Figure B.2 Speciation diagram of Pb(II) in solution. These data were used to make standards for XAFS.

Appendix C

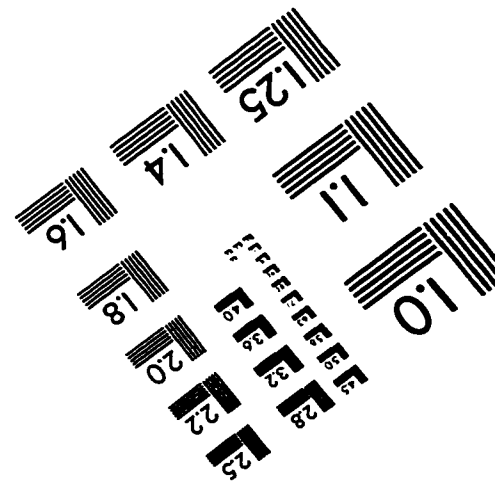
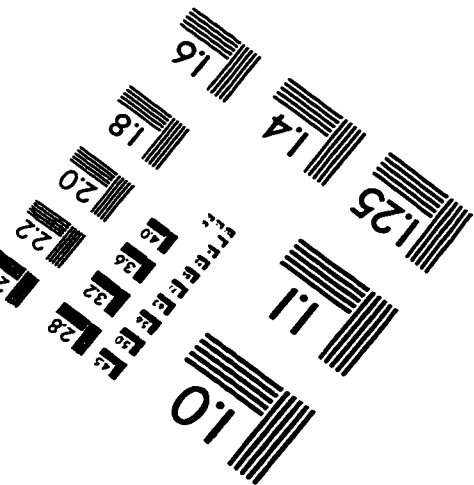
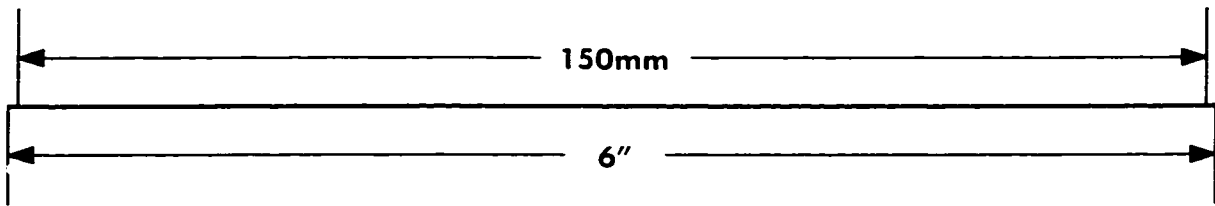
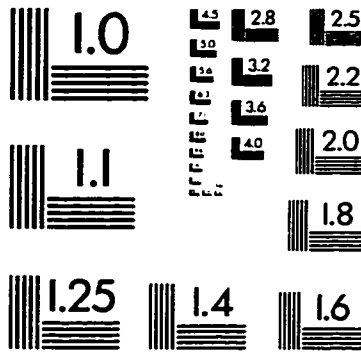
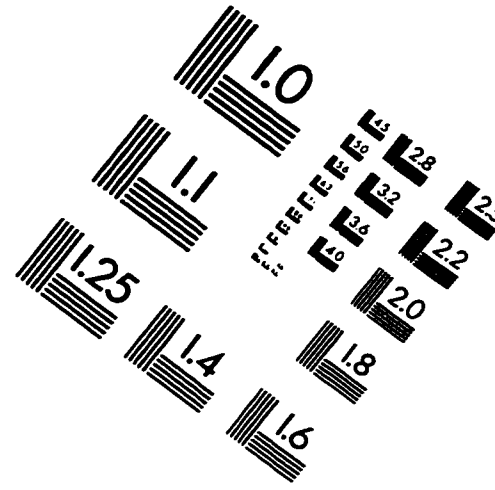
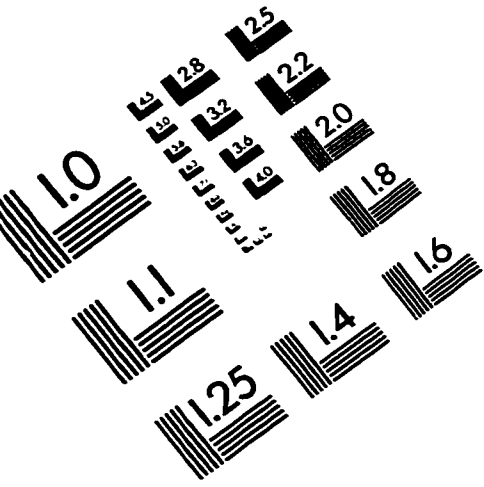
Supplementary Material for Chapter 4

Table C.1 Percentages of elements in treated and untreated Matapeake soils.

Properties	Matapeake soil	Treated Matapeake soil
Total C (%) ^a	1.38	0.18
Total S (%) ^a	0.016	0
Total N (%) ^a	0.20	0
Total P (%) ^b	0.010	0.011
Total miscellaneous exchangeable cations (K, Mg, Ca, Mn, Zn, Cu, K, Fe) (%) ^b	0.044	0.15

^a Based on loss on incineration at 1500° C. Based on Mehlich 1 extraction: 0.05 N HCl and 0.025 N H₂SO₄, 1:4 solid solution.

IMAGE EVALUATION TEST TARGET (QA-3)



APPLIED IMAGE, Inc
1653 East Main Street
Rochester, NY 14609 USA
Phone: 716/482-0300
Fax: 716/288-5989

© 1993, Applied Image, Inc., All Rights Reserved